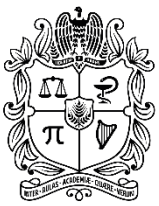

UNIVERSIDAD
NACIONAL
DE COLOMBIA

Accesibilidad de hidrocarburos en zeolitas y su efecto en el proceso de hydrocracking

José Mateo Martínez Saavedra

Universidad Nacional de Colombia
Facultad de Ingeniería, Departamento Ingeniería Química
Bogotá, Colombia
2021

Accesibilidad de hidrocarburos en zeolitas y su efecto en el proceso de hydrocracking

José Mateo Martínez Saavedra

Thesis is presented as a partial requirement to qualify for the title of:

Doctorado en Ingeniería Química

Director (a):

Prof. Ph.D, Ingeniero Químico, Gerardo Rodríguez Niño

Codirector (a):

Prof. Dr. Sc, Químico, Carlos Alexander Trujillo

Research Line:

Heterogeneous Catalysis

Research Group:

Laboratorio de Catálisis Heterogénea (LCH)

Universidad Nacional de Colombia

Facultad de Ingeniería, Departamento Ingeniería Química

Bogotá, Colombia

2021

A mi fuerza interior, mi mamá Yolanda y mis hermanas Mildreth y Mary.

Declaración de obra original

Yo declaro lo siguiente:

He leído el Acuerdo 035 de 2003 del Consejo Académico de la Universidad Nacional. «Reglamento sobre propiedad intelectual» y la Normatividad Nacional relacionada al respeto de los derechos de autor. Esta disertación representa mi trabajo original, excepto donde he reconocido las ideas, las palabras, o materiales de otros autores.

Cuando se han presentado ideas o palabras de otros autores en esta disertación, he realizado su respectivo reconocimiento aplicando correctamente los esquemas de citas y referencias bibliográficas en el estilo requerido.

He obtenido el permiso del autor o editor para incluir cualquier material con derechos de autor (por ejemplo, tablas, figuras, instrumentos de encuesta o grandes porciones de texto).

Por último, he sometido esta disertación a la herramienta de integridad académica, definida por la universidad.

Nombre: Jose Mateo Martinez Saavedra

c.c. 1.110.532.479 de Ibagué

Fecha 09/09/2021

Agradecimientos

A mis profesores Carlos Trujillo y Gerardo Rodríguez por compartir su sabiduría. A mis amigos Luis Ernesto Sandoval, José Alirio Mendoza, y Adrián Osorio por sus grandes enseñanzas. A mis amigos Jenny Julio y Rodrigo Pérez quienes no me dejaron caer en los momentos más difíciles. A mi amigo Alen Horvat quien, de manera inesperada, me dio el último empujón y la confianza para finalizar este proceso. Y a mi familia que siempre me llevaron en sus corazones; mi mama Yolanda Saavedra, mis hermanas Mildreth Martínez y Mary Martínez, y a mi abuelita Ofelia Cruz la persona que algún día espero alcanzar.

Resumen

Accesibilidad de hidrocarburos en zeolitas USY y su efecto en el proceso de hydrocracking

Descripción:

En este trabajo se estudió el impacto de las propiedades físicas y químicas de las zeolitas USY en el proceso de hydrocracking de hidrocarburos pesados orientado hacia su accesibilidad en zeolitas USY. Las propiedades texturales y morfológicas de las zeolitas USY fueron medidas usando fisisorción de N_2, Difracción de Rayos X (DRX), y Microscopía Electrónica de Transmisión (TEM). La acidez de las zeolitas USY fue caracterizada usando quimisorción de piridina medido por espectroscopía infrarroja (FTIR), y quimisorción de isopropilamina medida por análisis termogravimétrico (TGA). La actividad catalítica de catalizadores de platino soportados en zeolitas USY y en soportes no ácidos en el hydrocracking no isotérmico de fluoreno se estudió empleando un analizador térmico simultáneo de alta presión (STA-HP). El hydrocracking no isotérmico en un STA-HP permitió observar de forma cualitativa los pasos de la reacción del hydrocracking. Además, el test evidenció la necesidad de sitios ácidos Brønsted (BAS) en el hydrocracking, mostrando correlaciones positivas entre la entalpía de hydrocracking y la concentración de BAS. Un segundo test consistió en estudiar el hydrocracking de fenantreno usando un reactor Trickle-Bed a diferentes temperaturas. La participación de los BAS a distintas temperaturas fue calculada mediante el Turn-Over Frequency (TOF). El cálculo del TOF permitió correlacionar las propiedades estructurales de las zeolitas USY con su actividad catalítica hacia hydrocracking. Zeolitas con altos volúmenes de mesoporo reportaron más alto TOF de los BAS debido al mejor acceso del fenantreno al interior de las zeolitas. La accesibilidad del fenantreno en zeolitas USY se puede mejorar mediante el uso de agentes de lavado del aluminio amorfo. Mejorar la accesibilidad en las zeolitas USY favorece la

actividad catalítica hacia reacciones de hydrocracking y cracking considerablemente, además de favorecer las reacciones de hidrogenación.

Palabras clave: Hydrocracking, zeolitas USY, accesibilidad.

Abstract

Accessibility of hydrocarbons into USY zeolites and its effect in the hydrocracking reaction

Description

The present work is a comprehensive study of the effect of the physical and chemical properties of USY zeolites in the heavy hydrocarbons hydrocracking reaction. The study addresses USY zeolites accessibility for heavy hydrocarbons. Structural and morphological properties of USY zeolites were measured using nitrogen physisorption, X-Ray Diffraction (XRD), and Transmission Electron Microscopy (TEM). The acidity of USY zeolites was characterized using pyridine chemisorption recorded by FTIR, and isopropylamine chemisorption recorded by Thermogravimetric Analysis (TGA). The activity of platinum catalysts supported on USY zeolite and non-acidic support in non-isothermal fluorene hydrocracking was studied in a High-Pressure Simultaneous Thermal Analyzer (HP-STA). Non-isothermal hydrocracking of fluorene allows qualitative observation of the reaction paths over bifunctional catalysts. Besides, catalytic tests proved a positive correlation between hydrocracking enthalpy and BAS concentration. A second catalysis test studied phenanthrene hydrocracking using a Trickle-Bed Reactor (TBR) at different temperatures. BAS participation in the reaction was estimated by means of the Turn-Over Frequency (TOF). USY zeolites with high mesoporous volume showed high TOF of BAS indicating good accessibility of zeolite active sites for phenanthrene molecules. USY zeolites accessibility for phenanthrene can be improved by using chemical agents for amorphous aluminum oxides remotion. Improving the accessibility of USY zeolites favors catalytic activity towards hydrocracking and cracking reactions considerably. Moreover, improved accessibility benefits the hydrogenation reaction by shifting the chemical equilibrium towards the right direction.

Keywords: Hydrocracking, USY zeolites, Accessibility.

Table of Content

1. General introduction 5
1.1 Oil refining scenario 5
1.2 Hydrocracking process 6
1.2.1 Hydrocracking catalysts 8
1.2.2 Dealumination of Y zeolites 9
1.2.3 Mechanism of hydrocracking over bifunctional catalysts 11
1.2.4 The role of acid sites in Ultra-Stable Y (USY) zeolites aimed for hydrocracking reaction 13
1.3 Motivation of the thesis 13
1.4 Scope of the thesis 14
1.5 Organization of the thesis 14
1.6 References 15

2. Effect of USY zeolites on catalytic fluorene hydrocracking studied by a high-pressure simultaneous thermal analyzer 21
2.1 Introduction 22
2.2 Experimental. 24
2.2.1 Supports and materials used in the research 24
2.2.2 Platinum impregnation 24
2.2.3 Characterization 25
2.2.3.1. Powder X-Ray Diffraction (XRD) 25
2.2.3.2. Nitrogen physisorption 25
2.2.3.3. Transmission electronic microscopy (TEM) 25
2.2.3.4. Isopropyl-amine (i-PA) chemisorption 25
2.2.3.5. Pyridine (Py) chemisorption measured by IR spectroscopy 26
2.2.3.6. Hydrogen Chemisorption 27
2.2.4 Non-isothermal hydrocracking in an HP-STA 27
2.3 Results and discussion 28
2.3.1 Characterization 28
2.3.2 Non-isothermal hydrocracking test in HP-STA 34
2.4 Conclusions 40
2.5 References 40

3. Design, construction, and validation of a trickle-bed reactor to the study phenanthrene hydrocracking over USY zeolite-based catalyst 47
3.1 Introduction 48
3.2 Brief description of reaction and previous considerations 49
3.3 Tubing and fitting material 50
3.4 Engineering design of a trickle bed reactor 51
3.5 Description of reactor layouts considered 57

3.5.1 Liquid storage system 57
3.5.2 Pumping system 58
3.5.3 Gas feeding system 59
3.5.4 Reaction system 59
3.5.4.1. External section 60
3.5.4.2. Internal section 62
3.5.5 Phase separation systems 62
3.5.6 Pressure control and gas washing systems 63
3.5.7 Gas Mass Flow Control (GMFC) 63
3.6 Detailed design: Piping and fitting dimensions, schematic design of process instrumentation. 64
3.7 Experimental evaluation of the constructed TBR 66
3.7.1 Catalyst preparation 66
3.7.2 Characterization 67
3.7.3 Reaction test 67
3.7.4 Results and discussions 69
3.8 Conclusions 72
3.9 References 73

4. The effect of the USY zeolite properties on the phenanthrene hydrocracking performance 79
4.1 Introduction 80
4.2 Experimental 81
4.2.1 Catalyst preparation 81
4.2.2 Catalyst's characterization 82
4.2.3 Reaction test 82
4.3 Results and discussions 83
4.3.1 Catalyst Characterization 83
4.3.2 Reaction test 85
4.4 Conclusions 93
4.5 References 94

5. Effect of phenanthrene accessibility in USY zeolites during the hydrocracking reaction 98
5.1 Introduction 98
5.2 Experimental 101
5.2.1 Catalyst's preparation 101
5.2.2 Catalysts Characterization 101
5.2.3 Phenanthrene hydrocracking reaction 101
5.3 Results and discussion 102
5.4 Conclusions 108
5.5 References 109

6. Discussion 113
6.1 References 117

7. General Conclusions 119

List of Figures

Figure 1-1 Operation windows of hydroprocessing technologies with respect to the residue quality. 7
Figure 2-1 Characterization data of USY zeolites from Zeolyst ®. 29
Figure 2-2 FTIR spectra of representative USY zeolites, and CBV760 zeolite saturated of pyridine. 32
Figure 2-3 DSC curves of the fluorene hydrocracking on Pt supported on USY zeolite, Aerosil, and MCM-41. 35
Figure 2-4 DSC and DTG curves of the fluorene fusion, hydrogenation and hydrocracking on Pt supported on USY zeolites. A. DSC profiles; B. DTG profiles. 36
Figure 2-5 Effect of different acid sites measured by FTIR of pyridine on the perhydrofluorene hydrocracking enthalpy 39
Figure 3-1 Extended Charpentier and Favier diagram 52
Figure 3-2 Drop pressure of the gas as a function of liquid and gas flow rate. 53
Figure 3-3 Total liquid holdup of the TBR at different gas and liquid flow rates. 54
Figure 3-4 Bedwetting efficiency at different gas and liquid flow rates. 55
Figure 3-5 Process stages for hydrocracking in a TBR. 57
Figure 3-6 Arrangements for a liquid storage system. 58
Figure 3-7 Reactor arrangements for a) sampling, b) temperature control systems, and c) Temperature indicator 60
Figure 3-8 Packed bed holders. a) Tubing holder, b) tablet holder, c) Mesh support. 62
Figure 3-9 Arrangements of the gas-liquid separator. a) Flash separator, b) Cyclone separator, c) Mist eliminator, d) gas absorber. 63
Figure 3-10 P&ID diagram of a TBR for hydrocracking process. 65
Figure 3-11 Calibration curve FID response as a function of Phenanthrene/TiPB concentration. 68
Figure 3-12 TEM image of CBV600 USY zeolite with 40 %wt of γ-Al_2O_3. 69
Figure 3-13 Phenanthrene conversion efficiency as a function of residence time and the amount of catalyst, at 300°C and 70 bar. 70
Figure 3-14 Phenanthrene conversion efficiency in a hydrocracking reaction as a function of temperature and the type of catalyst. 71
Figure 4-1 TEM imaging of CBV600-USY(40%)/γ-Al_2O_3 composite. 84
Figure 4-2 Phenanthrene hydrocracking network over bifunctional Pt/USY catalysts. 86
Figure 4-3 Turn-Over Frequency of platinum with respect to the type of catalysts and the temperature of phenanthrene hydrocracking. 87
Figure 4-4 Product yields of phenanthrene hydrocracking over of Pt/USY based catalysts. 89

Figure 4-5 Hydrogen consumption as a function of catalyst type, temperatures, and type of reaction. 91
Figure 4-6 The effect of temperature on the ratio between Turn-Over Frequency of Bronsted Acid Sites (TOF_{BAS}) of phenanthrene hydrocracking..... 92
Figure 5-1 Characterization of USY zeolites after choline chloride treatment.....103
Figure 5-2 Graphical representation of phenanthrene distribution in the zeolite particles during hydrocracking concerning temperatures. 105
Figure 5-3 Turn Over Frequency (TOF) of different catalytic active sites. I. Platinum turn-over frequency (TOF_{Pt}), and II. BAS turn-over frequency (TOF_{BAS}), of CBV600 USY zeolite and treated zeolites.....106
Figure 5-4 Product yields of phenanthrene hydrocracking over treated and untreated Pt/CBV600 catalysts.....107
Figure 6-1 Graphical representation of hydrogen spillover over Pt/CVB600 USY zeolite, using the TEM picture from chapter 2.....115
Figure 6-2 Graphical representation of the role of the different catalytic active sites on the hydrocracking reaction. 115

List of Tables

Table 2-1 Structural properties of the USY zeolites measured by N_2 physisorption employing a sorptometer.....30
Table 2-2 Characterization of acid and metal sites in the USY zeolites and Pt/USY catalysts.....31
Table 2-3 Resume of DSC curves of the hydrocracking of fluorene over USY zeolites and nonacid supports.....37
Table 3-1 Pressure and temperature resistances of stainless steel (SS316) for different tubing diameters 51
Table 3-2 Reactor dimensions and bed configuration.....52
Table 4-1 Acidity and metal characterization of zeolite supports and associated Pt catalysts.....84
Table 5-1 Metal and acidic properties of treated Pt catalysts and untreated Pt catalysts as reference material. 102
Table 5-2 N_2 physisorption analysis of treated and untreated USY zeolites.....103
Table 5-3 Mass balance of choline chloride leaching of CBV600 USY zeolite.....104

List of Symbols and abbreviations

Symbols

Symbols	Term	Dimension IS	Definition
m	Mass of sample	g	
R	Waffer radius	1	
t	Wall tickness	inch	$\frac{P_i D_i}{2S - P_i}$
Pi	Working pressure	kPSI	
Di	Internal diameter	inch	
S	Maximum stress allowed for material	Ksi	
D_B	Bed diameter	mm	
L_B	Bed length	mm	
V_B	Bed volume	mm^3	
A_T	Transversal area	mm^2	
K_{GL}	Gas-Liquid mass transfer coefficient	m/s	
a_{GL}	Contact area between gas and liquid phases	m^2	
η_W	Wetting efficiency	-	
Sh	Sherwood number	-	$\frac{K_{LS} d_p}{D_B}$
Sc	Schmitt number	-	
K_{LS}	Liquid-solid mass transfer coefficient	m/s	
Re	Reynolds number	-	
Pe	Peclet number	-	

Symbol	Term	Dimensions SI	Definition
γ	Rate of reaction	1	$\frac{dC}{dt}$
ε	Integrated molar extinction coefficient	1	Section 2.2.3.5
π	Pi number	1	3.1416
ΔH_m	Hydrocracking mass enthalpy	J/g	$\Delta H/m_{reactant}$
ΔH	Hydrocracking enthalpy	J	Figure 2-4
ε_{BAS}	Integrated molar extinction coefficient of BAS	1	Section 2.2.3.5
ε_{LAS}	Integrated molar extinction coefficient of LAS	1	Section 2.2.3.5
C_{LAS}	LAS concentration on zeolites	$\frac{\mu mol\ Py}{g_{Zeolite}}$	$\frac{\pi R^2}{\varepsilon_{LAS}} \frac{IA(1470-1435\ cm^{-1})}{m}$
C_{BAS}	BAS concentration on zeolites	$\frac{\mu mol\ Py}{g_{Zeolite}}$	$\frac{\pi R^2}{\varepsilon_{BAS}} \frac{IA(1570-1510\ cm^{-1})}{m}$
Δm	Mass loss	g	Section 2.2.4
θ	Angle	°	Section 2.3.

Abreviaturas

Abreviatura	Término
USY	UltraStable Y zeolite
XRD	X-Ray Diffraction
TEM	Transmission Electron Microscopy
FTIR	Fourier Transform Infrarred Spectrocopy
TGA	Thermal Gravimetric Analysis

Abreviatura	Término
HP-STA	High-Pressure Simultaneous Thermal Analyzer
BAS	Brønsted Acid Sites
TOF	Turn-Over Frequency
EFAl	Extra-Framework Aluminum
TBR	Trickle-Bed Reactor
BPD	Barrels per Day
VGO	Vaccum Gas Oil
VR	Vaccum Residual
HDS	Hydrodesulfurization
FBR	Fixed Bed Reactor
EBR	Ebullated Bed Reactor
MBR	Moving Bed Reactor
SBR	Slurry Bed Reactor
ASA	Amorphous Silica Alumina
FAU	Faujasite
LAS	Lewis Acid Sites
H^+	Hydrogen deuterium atoms
SBAS	Strong Brønsted Acid Sites
SEM	Scanning Electron Microscopy
DSC	Differential Scanning Calorimetry
HC	Hydrocracking
PAH	Polyaromatic hydrocarbons
ASTM	American Society for Testing and Materials
NL-DFT	Non-Local Density Function Theory

Abreviatura	Término
HAADF	High-Angle Annular Dark-Field
TUM	Technische Universität München
i-PA	Isopropylamine
Py	Pyridine
IR	Infrarred
IA	Integrated peak area
Tm	Peak temperature
CFD	Computational Fluid Dynamics
PBD	Packed Bed Diameter
dP	Particle diameter
BL	Bed Length
HPHA	High-Pressure Hydrogen Attack

Introduction

Fuels derived from oil refining are the most common energy source in today's world. Gasoline, diesel, kerosene, jet fuel, gas, among others are the most common derivatives from crude oil. The demand for fuels increases each year with the growth of the population, and its continuous improvements in economic standards. Future predictions state that the world will depend on fossil fuels for the next 50 years. However, the oil refining industry is facing challenges due to growing pressures for the reduction of CO_2 emissions and the expected shortage of crude oil reserves. Moreover, remaining oil reserves contain a high concentration of impurities (i.e., O, S, N, and metals) and polyaromatic hydrocarbons making the refining processing more expensive.

In the last decades, the refining industry has invested in catalysis technologies to accomplish environmental regulations. Via hydrocracking technology using bifunctional catalysts, the low-quality oil is upgraded into high-quality fuels. The hydrocracking process conditions depend on the composition of the oil feedstock and the desired final products. Hydrocracking involves the cleavage of C-C bonds of hydrocarbons and the consecutive hydrogenation of unsaturated carbons. Depending on the type of catalysts, the mechanism of hydrocracking reaction changes, and the selectivity is modified. The refining industry favors bifunctional catalysts due to their high yields, stability, and low reaction temperature.

Bifunctional catalysts integrate two catalytic sites: Metals sites supported on a variety of acid solids. Metals conduct hydrogenation/dehydrogenation reactions. Noble metal and metal sulfides of the group VIIIB are usually employed as a hydrogenating phase. Acid sites perform isomerization, alkylation, dimerization, cracking, and hydrocracking reactions. Y zeolites are gaining popularity as catalysts support to accomplish hydrocracking processes. Y zeolites are crystalline aluminosilicates with a microporous structure. Microporosity extends the surface area able to accommodate acid sites. But Y zeolites are unstable to hydrocracking operational conditions. Y zeolites are chemically ultra-stabilized by removing tetrahedral aluminum from the crystalline structure. Tetrahedral aluminum incorporated into

the microporous structure of zeolite is principally responsible for hydrocracking reactions. Tetrahedral aluminum bound with oxygen atoms presents high electronic density able to attract protons such as sodium ions (Na+) or hydrogen ions (H+). Tetrahedral aluminum bonded to a hydrogen proton is also called Brønsted acid site (BAS) since tetrahedral aluminum can donate the proton to a Brønsted base. BAS and the tetrahedral aluminum amount usually no match due to the presence of tetrahedral aluminum bound to sodium ions. Researchers have tested post-synthesis treatments for partial removal of aluminum from Y zeolite while minimizing the destruction of crystalline structure.

Catalyst manufacturers utilize the steaming of NH_4-Y zeolite for aluminum remotion and produce commercial UltraStable Y (USY) zeolites. USY zeolites offer enhanced catalytic activities and sustain a low deactivation rate in an enriched hydrogen atmosphere. However, investigations demonstrated that USY zeolites lose catalytic activity at treating heavy hydrocarbons. Heavy hydrocarbons with molecular sizes larger than the micropore diameter in Y zeolite cannot reach the acid sites inside the crystalline structure. Micropore clogging by heavy hydrocarbons hinders hydrocracking catalytic activity of zeolite.

Removal of tetrahedral aluminum destroys crystal structure and generates empty spaces, which become mesoporous. These enlarged channels enable mass transport of oversized hydrocarbons into the zeolite. After the steaming process, tetrahedral aluminum is converted into amorphous aluminum oxides, also called Extra Framework-Aluminum (EFAl). EFAl occluded into the crystal structure, and mesoporous channels of the zeolite obstruct the access of hydrocarbons to the acid sites. This obstruction abates the hydrocracking catalytic activity of heavy hydrocarbons.

This investigation studied the accessibility of oversized hydrocarbons to the active sites of USY zeolites in the hydrocracking reaction. The objective of the study is to design new catalysts able to treat non-approachable oil.

The structural properties of USY zeolites employed in this work were characterized by: nitrogen physisorption, X-Ray Diffraction (XRD), and Transmission Electron Microscopy (TEM). Pyridine and isopropylamine chemisorption over USY zeolites recorded by FTIR and Thermogravimetric Analysis (TGA) allowed characterization of acid sites in zeolites.

The first chapter presents a literature review on the current situation in the oil refining industry, the role of hydrocracking technology in it, and the technical detail about the hydrocracking catalysts focused on USY zeolites. The second chapter deals with the non-isothermal hydrocracking of fluorene performed in a High-Pressure Simultaneous Thermal Analyzer (HP-STA) using USY zeolite-based catalysts and non-acidic supports. This comprehensive study reveals qualitative information about the hydrocracking pathways and the effect of BAS associated with those pathways.

Chapter three lays the design, construction, and evaluation of a Trickle-Bed Reactor (TBR) at a laboratory scale to study hydrocracking of phenanthrene using USY zeolites. Chapter four studies the effect of USY zeolites properties on the phenanthrene hydrocracking in the TBR. This study utilized the Turn-Over Frequency (TOF) of BAS as an indicator of its participation in the phenanthrene hydrocracking. Elevated temperature increases TOF of BAS in USY zeolites with high mesoporous volume. That was attributed to the improved accessibility of phenanthrene to the mesoporous channels in the USY zeolites.

In chapter five, EFAl in a USY zeolite with low mesoporous volume was removed by employing two washing treatments. Structural characterization showed that washing increases the mesoporous volume of USY zeolites. Washing treatment of zeolites resulted in higher TOF of BAS. This evidence demonstrates that mesoporous volume correlates with the accessibility of phenanthrene into the USY zeolite interior. Chapter six presents a general discussion and complementary aspects that may affect the accessibility, such as the molecular size of the hydrocarbon. Finally, chapter seven concludes this investigation.

1. General introduction

1.1 Oil refining scenario

Recent events of extreme weather are warning the authorities and public to declare urgency concerning climate change [1]. In this context, the oil and gas industry faces tough challenges in its role towards decarbonization of the world; to decrease its negative environmental impact [2]. Therefore, oil refining industries have sought to accomplish CO_2 net-zero emissions by financing programs committed to reforestation and CO_2 capture [3]. However, authorities and public opinion state that the refineries' efforts to mitigate carbon footprint are not enough [1] [2] [3].

Despite that, oil fuels are still a major source of energy in the world. Oil fuels are fuels produced from crude oil refining and distillation such as gasoline, diesel, kerosene, and jet fuel. The energy provided by fuel oils represented 33 % of the estimated total energy consumed in 2019 [4]. In 2016 the price dropped due to the entrance of new competitors into the market [5]. Even though oil fuels continued being an important supplier, owing to the fast development of new technologies [6] [3]. During the first semester of 2020, crude oil prices dropped further to a historical low of 17.6 $ per barrel as a consequence of the COVID-19 breakout [7] [8]. Since June 2020 Colombian production rate of crude oil has decreased from 900000 to 730000 barrels per day (BPD) [9]. These recent events point to the unpredictable and uncertain prospects for the oil industry.

Crude oil is a mixture of hydrocarbons and other organic and inorganic compounds. The distillation process separates different fractions of hydrocarbons on the basis of their boiling point properties. Oil fractions with boiling points below 250 °C (compounds between C6 to C14) make up light naphtha, kerosene, gasoline, and jet fuel. Distillates with a boiling point between 250 °C and 350 °C are part of the diesel cut (hydrocarbons between C14 and

C21). Fractions with boiling points between 350 °C and 550 °C (hydrocarbons between C21 and C45) are called Vacuum Gas Oil (VGO) and Vacuum Residual (VR) [10] [11].

Current crude oil reserves predominantly contain VGO and VR. This poses pressure on refineries to explore new technologies for transforming low-quality and heavy oil into fuels that comply with environmental standards. Contemporary researchers are on seeking new catalysts that would allow existing plants to efficiently refine different fractions of heavy oils [6]. Hydrocracking of heavy oils with metal dispersed catalysts is a proven technology for the production of low and middle boiling points (boiling point between 100 °C and 350 °C) distillates with a high commercial value [12] [13] [14].

In Hydrocracking, hydrocarbons are first cracked and then hydrogenated. This strategy helps to alleviate the CO_2 emissions by decreasing the number of unsaturated compounds in the fuel aimed for combustion [15]. In 2009, the Official Journal of the European reported that the concentration of atmospheric particulate matter derived from burning diesel fuel decreased by diminishing polyaromatic concentration from 11% to 8 % wt/wt [15] [16].

Catalysts in the hydrocracking process have dual functionality: Cracking and dehydrogenation/hydrogenation function. Cracking reactions are endothermic, while hydrogenation reactions are exothermic. Since, hydrogenation reaction releases more energy than cracking consumes, the overall hydrocracking thermodynamic character is exothermic [17]. Thus, the reactor design and the thermal/chemical stability of the catalysis are crucial factors for the hydrocracking process [18].

1.2 Hydrocracking process

Hydrocracking is a catalytic process used to convert heavy oil and VGO into a cleaner and lighter fraction [19]. Hydrocracking takes place at elevated hydrogen pressures (35 bar - 200 bar) and temperatures (260 °C - 425 °C) [20]. Depending on the severity of these operational conditions, hydrocracking is classified into two groups: mild and conventional. Mild hydrocracking occurs at lower temperatures and pressure than conventional hydrocracking. Hydrodesulfurization (HDS) of VGO normally takes place alongside [21]. Refineries perform hydrocracking in various reactor units such as Fixed-Bed (FBR),

Ebullated-Bed (EBR), Moving-Bed (MBR), and Slurry-Bed (EBR) reactors. Each of them consists of a distinct catalyst-bed setup [22]. Depending on the available feedstock and the desired end products, diverse reactor configurations might be used [23]. The most common hydrocracking reactor configurations are single stage and two-stage. In the single-stage, one reactor or a series of them are placed before a distillation unit. In the two-stage, the bottom residue in the distillation unit is introduced in a second hydrocracking reactor [24].

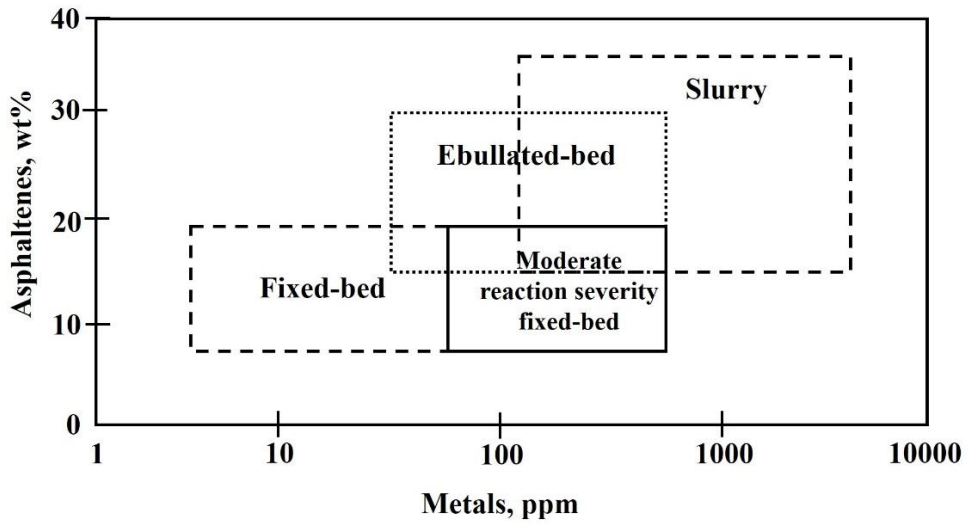

Figure 1-1 Operation windows of hydroprocessing technologies with respect to the residue quality [22].

The concentration of metals and asphaltenes in the raw feedstock is the key criteria for selecting the reactor configuration, based on the rate of catalyst deactivation [22]. Figure 1-1 shows the suitable reactor configuration as a function of the metal and asphaltenes content in the feedstock [22]. FBR is the most used hydrocracking reactor. This reactor is not suitable for feedstock with high metal content because metals can damage the reactor hardware. Despite that, refineries do employ FBR due to its relative simplicity, flexibility, and easy operation. The mass and heat transport inside the FBR is understood better than in the other reactor types (i.e., EBR, MBR, and EBR). This allows better control of the operating conditions and performance efficiency of the process [22]. FBR is a single or multilayer packed-bed of catalytic solids through which flows a stream of liquid and gas. The catalysts are composite materials appearing in various chemical and structural forms [25].

1.2.1 Hydrocracking catalysts

Metal catalysts on acid support are commonly used for hydrocracking of heavy oil fractions in FBR and EBR reactors [20]. Metal element catalyzes hydrogenation/dehydrogenation reactions. Acis support provides the surface area and acid activity responsible for cracking chemical bonds (i.e., C-C, C-S, C-O, C-M, and C-N) present in the feedstock [26].

The metal element can be a noble metal such as Pt, Pd, and Ir, or metal sulfide from the groups of periodic table VIA (Mo, W) and VIIIA (Co, Ni) [27]. The advantage of metal sulfides is their resistance to sulfur poisoning, but their hydrogenation capacity is lower with respect to the noble metals. Noble metals are used in sulfur-free systems and where a highly hydrogenated product is desired [14] [26].

The first refineries which implemented the hydrocracking process used acid solids based on Amorphous Silica Alumina (ASA) [17]. Around 1975, a new generation of zeolites with improved structural properties and superior acid function became available [17]. Today, zeolites are standard materials in oil refineries. Zeolites serve as a support of metal catalysts. Zeolites possess a well-organized microporous structure and tetrahedral aluminum, that facilitate the cracking and isomerization reactions. Besides, the crystalline network of the zeolite grant improves the catalyst's selectivity leading to the reaction to desirable products [13].

Different zeolites such as Beta (Micropore Diameter = 0.7 nm), ITQ (0.98 nm), and ZSM-5 (0.56 nm) have been applied successfully for the hydrocracking process [28]. However, Y zeolite (a.k.a. FAU zeolite) is receiving attention because of its relatively large microporous size (0.74 nm) and high content of tetrahedral aluminum [29]. The excess of tetrahedral aluminum makes this catalyst thermally unstable when exposed to hydrocracking operating conditions [30]. In order to improve stability, the Y zeolite structure is modified by dealumination methods [31]. Dealumination has demonstrated positive effects on hydrocracking reactions. It improves the thermal stability of zeolite, keeps low catalyst deactivation for coke formation, and enhances catalytic activity towards desired products [32]. Along with that, the dealumination process creates larger mesoporous channels in the crystalline network, which improves the diffusion of hydrocarbons larger than 0.74 nm. In the last decades, dealumination gained considerable attention among researchers due to the high industrial demand to upgrade heavy oil cuts [32].

1.2.2 Dealumination of Y zeolites

Y zeolites consist of tetravalent aluminum and silicon bound by oxygen atoms, forming a faujasite (FAU) crystal network [33]. Faujasite is an aluminum-rich form of the X zeolite with a silicon/aluminum (Si/Al) ratio superior to 1.5 [30]. Y zeolite is chemically unstable in water and at elevated temperatures. The presence of trivalent aluminum atoms in a tetrahedral network causes charge instability and weakens the crystalline structure [30]. Successful application of dealumination processes must employ Y zeolites with Si/Al ratios above 2.2. Dealumination treatments enable the production of Ultra-Stable Y (USY) zeolite. The advantage of USY is high thermal stability, hydrophobic properties, and enhanced catalytic activity for an exchange of crystallinity [33].

A simple dealumination treatment is carried out by submerging the Y zeolite into inorganic or organic acids. Acids hydrolyze Si-O-Al bonds in the crystalline structure producing $(OH)_2Al$- species. Then, in a second stage, these molecules are transformed into Extra-Framework Aluminum (EFAl) species trapped in the crystal structure [34] [35]. Acid treatments generate mesoporous in Y zeolites in exchange for a significant fraction of their crystallinity. Moreover, the USY zeolites obtained by this method contain structural defects along with an unbalanced charge. This charge is compensated with amorphous material which could be very detrimental for hydrocracking. The amorphous phase blocks the access of hydrocarbons to the acid sites inside the zeolite, preventing hydrocracking reactions to occur [35].

Hydrothermal treatment of NH_4NaY zeolite is another method to produce USY zeolites [36]. In the steaming, as is commonly called, a flow of steam at the pressure of 1 bar and temperature ranges from 250 °C to 700 °C passes through NH_4NaY zeolite. At temperatures below 250 °C, the dealumination process does not occur while at temperatures above 700 °C, the zeolite structure is severely damaged. Previous to the steaming process, Na^+ cations present in the sodalite cage of NaY zeolite are substituted with NH_4^+ ions [37]. Na^+ cations in the sodalite cage of zeolite do not allow the displacement of Al atom without destruction of zeolite structure. The reason lies in that Na^+ compensates for the unbalanced charge of the tetravalent aluminum. Then when Na^+ is exchanged with NH_4^+, this results in a lower temperature required for the dealumination. In summary, the steaming of Y zeolite is largely dependents on the degree of NH_4^+ substitution [30] [35] [36] [37].

Mesoporous USY zeolites in a wide range of Si/Al ratios can be synthetized by adjusting the steaming temperature or by consecutive steaming repetition. For each Al atom removed from the crystalline network, a mesoporous cavity is created. The creation of mesoporous channels in the zeolites has positive effects on their activity in relation to the hydrocracking of heavy oil fractions. These channels improve the accessibility of heavy hydrocarbons to acid sites [32]. However, for each aluminum removed, a crystalline portion of the zeolite is demolished and EFAl is produced. The EFAl overlay the crystalline external surface network as well as, the mesoporous channels [38], avoiding the access of hydrocarbons to the acid sites on the surface. Various strategies for the remotion of amorphous silicon and aluminum oxides have been investigated to find the optimal acid phase for the hydrocracking of heavy hydrocarbons [36].

The removal of amorphous material from zeolites is conducted by washing method using chemical agents such as mineral acids, organic acids, or hydroxides [35] [36] [39] [40] [41] [42]. The washing treatment also cleans mesoporous cavities; washing can cause a slight dealumination inside the USY zeolite, which interconnects the mesoporous channels and the outer surface. USY zeolites with an interconnected mesoporous network facilitate the diffusion of heavy hydrocarbons through the zeolite cavities. This results in a higher catalytic activity of zeolites.

Acid leaching treatment of steamed Y zeolites at mild conditions selectively dissolves amorphous EFAl species while preserving zeolite crystallinity. However, when the acid washing is performed under severe conditions, the zeolite undergoes a high loss of acidic properties [32] [43]. Desilication of USY zeolites is carried out by alkaline leaching. Like acid, alkaline leaching at severe conditions lead to a significant loss in the zeolite crystallinity, while new mesoporous channels are not formed [32] [38]. When alkaline leaching is performed under mild conditions, the authors reported a decrease in the Si/Al ratio. This was attributed to a realumination process; the reincorporation of Al into the crystalline network was found to be detrimental to the catalytic performance during hydrocracking reactions [44]. Other approaches, such as consecutive acid and alkaline leaching have successfully delivered USY zeolites with improved catalytic properties to hydrocarbons cracking reactions [45].

1.2.3 Mechanism of hydrocracking over bifunctional catalysts

Two different mechanisms have been proposed for hydrocracking over bifunctional catalysts: (i) the classic bifunctional model, and (ii) the hydrogen spillover model [14] [46]. The classic bifunctional model was originally proposed by Mills et. al. [47]. They suggested that catalytic cracking of hydrocarbons on the acid sites is mediated by the formation of olefinic species formed in the metal sites by dehydrogenation reactions. After, olefins are cracked on acid sites, and cracked products are hydrogenated on metal sites. The aforementioned considered that hydrocarbons have to migrate from the acidic to metal sites constantly to be cracked and hydrogenated/dehydrogenated. Weisz et. al [48] took Mills' proposal forward by investigating the ability of metal and acid sites to act independently as physically distinct catalysts. These studies are highly regarded in the literature and are used to explain the behavior of bifunctional catalysts [49] [50] [51] [52]. The primary role attributed to the metals is the dehydrogenation of saturated hydrocarbons to olefins. On the other hand, metals catalyze hydrogenation of cracked alkenes intermediates desorbed from the acid sites [53]. Alkenes desorb from the metal sites and diffuse to acid sites, where they are protonated to tertiary or secondary alkylcarbenium ions [54]. Carbenium ions are reactive intermediates generated on the acid sites, which can further undergo transformations such as skeletal rearrangements and carbon-carbon bond dissociation [14]. After chemical rearrangements, alkenes desorb from the acid sites and diffuse back to the metal sites where they are hydrogenated to the final products. The detection of olefinic gas intermediates has been outlined as the main proof of the classic bifunctional model [14] [48] [54].

Several authors have studied the effect of acid/metal ratio on the hydrocracking reaction selectivity [14] [26] [52] [53]. Metal catalysts with a low hydrogenation/dehydrogenation activity deposited on a relatively strong acid support (i.e., NiMo/HY, CoMo/β-zeolite) produce light hydrocarbons in hydrocracking. When both metal and acid sites have mild catalytic activities (i.e., NiMo/ASA, NiMo/γ-Al_2O_3), the hydrocracking reaction trends produce middle-size hydrocarbons. However, catalysts made of noble metals supported on strong acid support derive a wide range of products [14]. The latter is favorable and has been recognized as ideal hydrocracking [53].

Hydrogen spillover model assumes that hydrogen molecules dissociate on a metal site. Hydrogen ions then migrate to a metal oxide surface where they are adsorbed as

monoatomic hydrogen [46]. A mechanism based on the spillover phenomena supposes that hydrocarbons adsorbed on acid sites undergo hydrogenation with those hydrogen atoms/ions migrated from the metal phase. This hydrocracking mechanism proposed by Roessner and Roland in 1996 [55], suggested that the classic bifunctional model is not accurate due to its dependency on the hydrocarbon diffusion from one site to another. Roessner et. al. [55] studied the hydrocracking reaction of cyclohexane in a fixed-bed made of a metal phase separated from acid phase by a non-reactive bed layer. The intermediate olefins species were not detected. Despite that, Prins [56] stated that hydrogen spillover on defect-free supports such as Al_2O_3, SiO_2, MgO, and zeolites is energetically unfavorable. However, hydrogen spillover can arise when the support has defects or is covered by a carbonaceous layer [46] [57]. A recent work by Karim et al., [58] has shown that hydrogen spillover can take place on aluminum oxide, where hydrogen mobility is mediated by three-coordinated aluminum centers and water molecules. Water on the support/catalyst surface has been identified as a key player in hydrogen spillover. Water promotes hydrogen spillover by increasing the protons exchange rate between aqueous solution and catalysts surface [46] [57]. Hydrogen spillover effect in the benzene hydrogenation reaction was demonstrated by Choi et al., [59] encapsulating Pt clusters in acid zeolite A pores where the hydrocarbons cannot enter. The hydrogenation of benzene at 523 K showed that the catalyst was more active when blended with nonreducible supports like alumina [58] [60]. Probably, because alumina under hydrogenation reaction conditions performs hydrogen spillover more efficiently than zeolite. Ryo Ueda et al. [61] studied the pyridine hydrogenation over a noble Pd/SiO_2 – USY by using FTIR spectrometry. They observed that spillover hydrogen competes with the pyridine for adsorption on the Lewis Acid Sites (LAS). Spilled hydrogen adsorbed on LAS promotes the migration of pyridine to BAS of the zeolite, followed by diffusion to Pd clusters where hydrogenation is completed. Along with that, they show the exchange of deuterium atoms with the hydrogen interacting in the BAS. This proposal assumes the coexistence of deuterium atoms (H^+) with the H^- atoms in the BAS. The study of Ryo Ueda et. al. [61] showed that hydrogenation of aromatic hydrocarbons does not occur over BAS alone, although they can facilitate hydrogen spillover.

1.2.4 The role of acid sites in Ultra-Stable Y (USY) zeolites aimed for hydrocracking reaction

Tetravalent aluminum located in the Y zeolite framework has been claimed as responsible for cracking, isomerization, and alkylation reactions occurring during hydrocracking of heavy hydrocarbons [62] [63]. The conversion of hydrocarbons takes place when the unbalanced charge of the tetrahedrally coordinated Al^{3+} is compensated with a hydrogen-proton [62] [63]. At the specific reaction conditions, Al^{3+} conjugated in the framework can also donate the proton, the reason why they are called a Brønsted Acid Site (BAS). The dealumination process involves displacement of BAS towards the outer surface of catalysts, which has positive effects on the catalytic activity of Y zeolites [64]. Since cracking occurs on BAS, the observed activity enhancement is often attributed to the generation of Strong Brønsted Acid Sites (SBAS) during dealumination [63]. Various authors discuss the catalytic nature of SBAS [64]. Dempsey E. proposed that the acid strength of the BAS is inversely proportional to the concentration of aluminum atoms in a hexagonal prism or sodalite cage. On the contrary, other authors stated that the BAS distribution in the zeolite after dealumination has not a significant influence on the catalytic activity [38]. Beyerline et. al. [64] suggested that after the steaming treatment the EFAl remnants in the zeolite framework delocalize the charge in BAS, enhancing the cracking activity. However, the authors argued that the improvement in catalytic activity is due to a synergic effect between the EFAl and the BAS [64]. But they also stated that there is not enough evidence to relate the presence of EFAl to higher acid strength.

1.3 Motivation of the thesis

The accessibility of USY zeolites for relatively heavy hydrocarbons is a relevant topic in the petrochemical research field. The introduction of mesoporous channels in zeolite lattice does not always enhance the catalytic activity of zeolites. Although dealumination treatment improves the catalytic activity of USY zeolites, for hydrocracking of heavy hydrocarbons, the yield of the desired products remains low. Low yields are due to the dealumination process during which tetravalent aluminum is removed from the framework to EFAl species. This amorphous material limits the access of heavy hydrocarbons to BAS and SBAS in the zeolite, negatively affecting the product yields. Despite the numerous studies focused on the understanding of bifunctional catalysts, the mechanism of zeolite accessibility for heavy hydrocarbons, as well as hydrocracking reaction require further investigation. The present

thesis is a contribution to the understanding of the role of USY zeolites in the hydrocracking of heavy hydrocarbons. With the aim to advance catalytic hydrocracking towards its technological maturity.

1.4 Scope of the thesis

The main objective of this thesis is to study the effect of structural changes in the USY zeolites in the performance of heavy hydrocarbons hydrocracking. Two catalysis tests campaigns were carried out: i) non-isothermal fluorene hydrocracking in a High-Pressure Simultaneous Thermal Analyzer (HP-STA), and ii) phenanthrene hydrocracking in a Trickle-Bed Reactor (TBR). The former campaign investigated the catalytic activity to two active sites, (metal and acid), respectively. The heat of the reaction was then measured as a function of catalytic activity. In the second campaign, hydrocracking of phenanthrene under conditions close to industrial practice was studied. The role of acid and metal sites for three different temperatures was evaluated and associated with the structural properties of USY zeolites. Hydrocracking catalysts were prepared according to the test. For the test in HP-STA, USY zeolites were prepared by wet impregnation using $Pt(NH_3)_4Cl_2$. For the test in the TBR, USY zeolites were diluted in alumina prior to platinum wet impregnation. USY zeolites and their catalytic properties were investigated by using the following techniques: XRD, N_2 physisorption, TEM, SEM, FTIR spectroscopy, DSC-TG, and H_2 chemisorption.

1.5 Organization of the thesis

In chapter two, thermodynamic aspects of the hydrocracking reaction over bifunctional USY zeolites with different structural properties were studied. Chapter two focused on the understanding of fluorene hydrocracking reaction, discussed the role of acid sites, and proposed the reaction mechanism. Chapter three presented the engineering, design, construction, and evaluation of the TBR. Chapter four described the hydrocracking of phenanthrene over three USY zeolites with different Si/Al ratios and different reaction temperatures, to study the role of its structural properties in the reaction. In chapter five, a catalyst with a high number of acid sites clogged by EFAl material was treated with the aim to improve the accessibility for hydrocarbon reactants. To improve the catalyst accessibility, conventional treatment with EDTA and non-conventional treatment with choline chloride were utilized in this chapter. Chapter six discusses the effect of catalyst accessibility with

respect to the acid sites and the catalysts structural properties. The conclusions of this comprehensive research work are given in chapter seven.

1.6 References

[1] R. J. Johnston, R. Blakemore y R. Bell, «The role of oil and gas companies in the energy transition,» *Atlantic Council Policy Report,* 2020.

[2] K. Levin, D. Rich, K. Ross, T. Fransen y C. Elliott, «Designing and Communicating Net-Zero Targets,» *World resources institute,* 2020.

[3] British Petroleum Company, «Statistical Review of World Energy 2017,» 66, 2017.

[4] British Petroleum Company, «Statistical Review of World Energy 2018,» 67, 2018.

[5] British Petroleum Company, «Statistical Review of World Energy 2019,» 68, 2019.

[6] British Petroleum Company, «Statistical Review of World Energy 2020,» 69, 2020.

[7] D. ALOUI, K. GUESMI y R. HCHAICHI, «COVID 19's impact on crude oil and natural gasS&P GS Indexes,» *SSRN Electronic Journal,* 2020.

[8] K. Kingsly y H. Kouam, «COVID-19 and Oil Prices,» *SSRN Electronic Journal,* 2020.

[9] D. Castillo Camacho, «Diagnóstico del impacto de la pandemia y la crisis económica mundial en el sector de hidrocarburos en Colombia,,» 08 12 2020. [En línea]. Available: https://crudotransparente.com/2020/08/27/diagnostico-del-impacto-de-la-pandemia-y-la-crisis-económica-mundial-en-el-sector-de-hidrocarburos-en-colombia/. [Último acceso: 30 01 2021].

[10] J. Ancheyta, Modeling of Processes and Reactors for Upgrading of Heavy Petroleum, Ciudad de México: CRC/Taylor & Francis, 2013.

[11] D. Jones, S. J. Pujadó y P. Peter, Handbook of Petroleum Processing, Netherlands: Springer Netherlands, 2006.

[12] R. Sahu, B. Jin Song, J. S. Im, Y.-P. Jeon y C. W. Lee, «A review of recent advances in catalytic hydrocracking of heavy residues,» *Journal of Industrial and Engineering Chemistry,* 2015.

[13] A. Galadimaa y O. Murazaa, «Hydrocracking catalysts based on hierarchical zeolites: A recent progress,» *Journal of Industrial and Engineering Chemistry,* vol. 61, p. 265–280, 2018.

[14] J. Weitkamp, «Catalytic Hydrocracking—Mechanisms and Versatility of the Process,» *ChemCatChem,* vol. 4, p. 292 – 306, 2012.

[15] V. Calemma, M. Ferrari, S. Rabl y J. Weitkamp, «Selective ring opening of naphthenes: From mechanistic studies with a model feed to the upgrading of a hydrotreated light cycle oil,» *Fuel,* 2013.

[16] Directive 2009/30/EC of the European Parliament and of the Council, «Amending Directive 98/70/EC relating to the quality of petrol and diesel fuels,,» *Official Journal of the European Communities,* 2009.

[17] N. Choudhary y D. N. Saraf, «Hydrocracking: A Review,» *Ind. Eng. Chem. Prod. Res.,* vol. 14, nº 2, 1975.

[18] G. Bellussi, G. Rispolli y A. Carati, «Catalytic system and process for the hydroconversion of heavy oil products». U.S. Patente 0139677 A1, 16 Jun 2011.

[19] S. Zhang, D. Liu, W. Deng y G. Que, «A Review of Slurry-Phase Hydrocracking Heavy Oil Technology,» *Catal. Today,* vol. 98, p. 55–60, 2004.

[20] J. G. A. Scherzer, Hydrocracking Science and Technology, Marce Decker Inc, 1996.

[21] Akzo Nobel, «Hydroprocessing Course,» 2000.

[22] M. Angeles, C. Leyva, J. Ancheyta y S. Ramírez, «A review of experimental procedures for heavy oil hydrocracking withdispersed catalyst,» *Catalysis Today,* p. 220– 222, 2014.

[23] M. A. Fahim, T. Al-Sahhaf y A. Elkilani, Fundamentals of petroleum refining, Elsevier, 2009.

[24] J. G. Speight y W. Andrew, The refinery of the future, Elsevier, 2010.

[25] S. Mohanty, D. Kunzru y D. N. Saraf, «Hydrocracking: a review,» *Fuel,* vol. 69, 1990.

[26] A. Martínez, M. A. Arribas y S. B. C. Pergher, «Bifunctional noble metal/zeolite catalysts for upgrading low quality diesel fractions via selective opening of naphthenic rings,» *Catalysis Science & Technology,* 2016.

[27] G. Valavarasu, M. Bhaskar y K. S. Balaraman, «Mild Hydrocracking—A Review of the Process, Catalysts, Reactions, Kinetics, and Advantages,» *Petroleum Science and Technology,* vol. 21, nº 7-8, pp. 1185-1205, 2003.

[28] A. Primo y H. Garcia, «Zeolites as catalysts in oil refining,» *Chem Soc Rev,* 2014.

[29] Q. Cui, Y. Zhou, Q. Wei, X. Tao, G. Yu, Y. Wang y J. Yang, «Role of the Zeolite Crystallite Size on Hydrocracking of Vacuum Gas Oil over NiW/Y-ASA Catalysts,» *Energy Fuels,* vol. 26, p. 4664−4670, 2012.

[30] W. Lutz, «Zeolite Y: Synthesis, Modification, and Properties—A Case Revisited,» *Advances in Materials Science and Engineering,* p. 20, 2014.

[31] C. S. Triantafillidis, A. G. Vlessidis y N. P. Evmiridis, «Dealuminated H-Y Zeolites: Influence of the Degree and the Type of Dealumination Method on the Structural and Acidic Characteristics of H-Y Zeolites,» *Ind. Eng. Chem. Res,* vol. 20, nº 20, pp. 307-319, 2000.

[32] J. L. Agudelo, E. J. M. Hensen, S. A. Giraldo y L. J. Hoyos, «Influence of Steam-Calcination and Acid Leaching treatment on the VGO Hydrocracking Performance of Faujasite Zeolite,» *Fuel Processing Technology,* nº 133, pp. 89-96, 2015.

[33] M. Niwa, N. Katada y K. Okumura, Characterization and Design of Zeolite Catalysts, Tottori: Japan: Springer Series in Material Science, 2010.

[34] D. Verboekend, N. Nuttens, R. Locus, V. J. Aelst, P. Verolme, J. C. Groen, J. Perez-Ramirez y B. F. Sels, «Synthesis, Characterization, and catalytic evaluation of hierarchical faujasite zeolites: milestones, challenges and future directions,» *Chem. Soc. Rev.,* vol. 45, pp. 3331-3352, 2016.

[35] D. Verboekend y J. Perez-Ramirez, «Towards a Sustainable Manufacture of Hierarchical Zeolites,» *CHEMSUSCHEM,* nº 7, pp. 753-764, 2014.

[36] M. S. Maier, A. Jentys y A. J. Lercher, «Steaming of zeolite BEA and its Effect on Acidity: A comparative NMR and IR Spectroscopic Study.,» *J. Phys. Chem,* nº 115, pp. 8005-8013, 2011.

[37] J. A. Mendoza Mesa, *Estrategias para la formación de estructuras jerárquicas en zeolita Y por tratamiento con vapor de agua,* Bogotá: Universidad Nacional de Colombia, 2019.

[38] J. L. Agudelo Valderrama, *Effect of modification on USY zeolite properties and its hydrocracking performance,* Bucaramanga: Universidad Industrial de Santander, 2015.

[39] D. Verboekend, G. Vilé y J. Pérez-Ramírez, «Hierarchical Y and USY Zeolites Designed by Post-Synthetic Strategies,» *Advanced Functional Materials,* vol. 22, nº 5, p. 916–928, 2011.

[40] K. de Jong, J. Zečević, H. Friedrich, P. De Jongh, M. Bulut, S. Van Donk, R. Kenmogne, A. Finiels, V. Hulea y F. Fajula, «Zeolite Y crystals with trimodal porosity as ideal hydrocracking catalysts,» *Angewandte Chemie,* nº 122, p. 10272–10276, 2010.

[41] X.-w. Chang, L.-F. He, H.-n. Liang, X.-m. Liu y Z.-f. Yan, «Screening of optimum condition for combined modification of ultra-stable Y zeolites using multi-hydroxyl carboxylic acid and phosphate,» *Catalysis Today,* vol. 158, p. 198–204, 2010.

[42] A. Abramova, E. Slivinskii, Y. Goldfarb, A. Panin, E. Kulikova y G. Kliger, «Development of efficient zeolite-containing catalysts for petroleum refining and petrochemistry,» *Kinetics and Catalysis,* vol. 46, p. 758–769, 2005.

[43] D. Verboekend, G. Vilé y J. Pérez-Ramírez, «Mesopore Formation in USY and Beta Zeolites by Base Leaching: Selection Criteria and Optimization of Pore-Directing Agents,» *Cryst. Growth Des,* vol. 12, p. 3123−3132, 2012.

[44] M. J. Remy, D. Stanica, G. Poncelet, E. J. P. Feijen, P. J. Grobet, J. A. Martens y A. Jacobs P., « Dealuminated H-Y Zeolites: Relation Between Physicochemical Properties and Catalytic Activity in Heptane and Decane Isomerization.,» *J. Phys. Chem,* vol. 100, pp. 12440-12447, 1996.

[45] J. L. Agudelo, E. J. M. Hensen, S. A. Giraldo y L. J. Hoyos, «Effect of USY Zeolite Chemical Treatment with Ammonium Nitrate on Its VGO Hydrocracking Performance,» *Energy & Fuels,* vol. 30, nº 1, p. 616–625, 2015.

[46] R. Prins, «Hydrogen spillover. Facts and fiction,» *Chem. Rev.,* vol. 112, nº 5, p. 2714–2738, 2012.

[47] G. A. Mills, H. Heinemann, T. A. Milliken y A. G. Oblad, «Hydroforming reactions, studies with pure hydrocarbons,» *Ind. Eng. Chem,* vol. 45, 1953.

[48] P. B. .. S. E. W. Weisz, «Stepwise Reaction on Separate Catalytic Centers: Isomerization of Saturated Hydrocarbons,» *Science ,* vol. 126, p. 31, 1957.

[49] H. Coonradt y W. Garwood, «Mechanism of hydrocracking,» *Ind. Eng. Chem. Process,* vol. 3, pp. 38-45, 1964.

[50] H. W. Haynes, J. F. Parcher y N. E. Heimer, «Hydrocracking Polycyclic Hydrocarbons over a Dual-Functional Zeolite (Faujasite)-Based Catalyst,» *Ind. Eng. Chem. Process Des. Dev,* vol. 22, nº 3, p. 401–409, 1983.

[51] T. Isoda, S. Maemoto, K. Kusakabe y S. Morooka, «Hydrocracking of pyrenes over a nickel-supported Y-zeolite catalyst and an assessment of the reaction mechanism based on MD calculations,» *Energy and Fuels,* vol. 13, nº 3, p. 617–623, 1999.

[52] J. Zecevic, G. Vanbutsele, K. P. De Jong y J. A. Martens, «Nanoscale intimacy in bifunctional catalysts for selective conversion of hydrocarbons,» *Nature,* vol. 528, nº 7581, p. 245–254, 2015.

[53] M. Guisnet, «Ideal ' bifunctional catalysis over Pt-acid zeolites,» vol. 218–219, pp. 123-134, 2013.

[54] J. Weitkamp y H. Schulz, «Olefinic Intermediates in Catalytic Hydrocracking of Paraffins,» *J. Catal.,* vol. 29, p. 361–366, 1973.

[55] F. Roessner y U. Roland, «Hydrogen spillover in bifunctional catalysis,» *J. Mol. Catal. A Chem,* vol. 112, nº 3, p. 401–412, 1996.

[56] R. Prins, V. K. Palfi y M. Reiher, «Hydrogen spillover to nonreducible supports,» *J. Phys. Chem. C.,* vol. 116, nº 27, p. 14274–14283, 2012.

[57] A. M. Stumbo, P. Grange y B. Delmon, «Effect of spillover hydrogen on amorphous hydrocracking catalysts,» *Stud. Surf. Sci. Catal.,* vol. 101, p. 97–106, 1996.

[58] W. Karim, «Catalyst support effects on hydrogen spillover,» *Nature,* vol. 541, nº 7635, p. 68–71, 2017.

[59] M. Choi, S. Yook y H. Kim, «Hydrogen Spillover in Encapsulated Metal Catalysts: New Opportunities for Designing Advanced Hydroprocessing Catalysts,» *ChemCatChem,* vol. 7, nº 7, p. 1048–1057, 2015.

[60] M. Boudart, M. A. Vannice y J. E. Benson, «Adlineation, Portholes and Spillover,» *Zeitschrift fur Phys. Chemie,* vol. 64, nº 1-4, p. 171–177, 1969.

[61] R. Ueda, T. Kusakari, K. Tomishige y K. Fujimoto, «Nature of Spilt over Hydrogen on Acid Sites in Zeolites: Observation of the Behavior of Adsorbed Pyridine on Zeolite Catalysts by Means of FTIR,» *Journal of Catalysis,* vol. 194, p. 14–22, 2000.

[62] L. E. Sandoval Díaz, J. González Amaya y C. A. Trujillo, «General aspects of zeolite acidity characterization,» *Microporous Mesoporous Mater,* vol. 215, p. 229–243, 2015.

[63] Y. L. A. J. Zhang, «Promotion of protolytic pentane conversion on H-MFI zeolite by proximity of extra-framework aluminum oxide and BrØnsted acid sites,» *J. Catal.,* vol. 370, p. 424–433, 2019.

[64] R. A. Beyerlein, C. Choi-Feng, J. B. Hall, B. J. Huggins y G. J. Ray, «Effect of Steaming on the Defect Structure and Acid Catalysis of Protonated Zeolites.,» *Topics in Catalysis,* vol. 1, nº 4, pp. 227-42, 1997.

2. Effect of USY zeolites on catalytic fluorene hydrocracking studied by a high-pressure simultaneous thermal analyzer

Summary

Non-isothermal fluorene hydrocracking was studied employing a High-Pressure Simultaneous Thermal Analyzer (HP-STA) at pressure 50 bar. Two types of catalysts were tested. Platinum loaded on non-acid Aerosil, MCM-41 and platinum loaded on five acid USY zeolites with different Si/Al molar ratios. Pt/USY catalysts were characterized by nitrogen physisorption, X-Ray Diffraction (XRD), Transmission Electron Microscopy (TEM), isopropylamine decomposition recorded by TG, pyridine chemisorption recorded by FTIR, and hydrogen chemisorption. Two methodologies for the platinum reduction on the supports were compared in this study: reduced pressure method, and high hydrogen pressure method. Results showed that smaller platinum clusters are formed when reduced pressure method is applied. For all catalysts, complete hydrogenation of the two aromatic rings occurred before initiation of hydrocracking reaction. Platinum loaded on non-acid supports demonstrated lower catalytic activity towards fluorene hydrogenation. Non-acid catalysts required higher temperatures than acid catalysts for complete hydrogenation and showed null hydrocracking activity below 400 ºC. Higher density of acid sites reduced the onset temperature of hydrocracking reaction (HC). Hydrocracking mass enthalpy (ΔH_m) was given as an indicator of the catalytic activity. Acid catalysts presented a nearly linear relationship between ΔH_m and Brønsted acid sites (BAS) concentration. Linear relationship was also proven between ΔH_m and Strong BAS (SBAS) sites. This indicated that not all BAS participates in the hydrocracking with the same intensity. The non-isothermal hydrocracking reaction studied by a HP-STA technique is a novel approach. This study delivered qualitative information on reaction mechanism and contributed to the understanding of the catalytic activity of Pt/USY catalysts with different acidity and structural properties.

2.1 Introduction

Hydrocracking is a process applied to upgrade heavy oil fractions. Upgrade includes either removal of contaminants containing S, O, N, and metals or conversion of polycyclic aromatic hydrocarbons (PAHs) into aliphatic saturated chains [1]. PAHs are potent atmospheric pollutants emitted after fuel combustion. PAHs are also major constituents of oil, coal, and tar deposits. Their catalytic reforming involves hydrocracking process able to transform PAHs into high-value fuels and petrochemicals [2].

The hydrocracking (HC) of PAHs is achieved in two steps. In the first step, double bonds in aromatic rings get hydrogenated producing saturated rings. In the second, saturated rings are open by C-C bonds cleavage [3]. A hydrocracking catalyst consists of a metal phase loaded on acid supports such as alumina and zeolites. Steamed Y zeolites are extensively used as an acid support. Zeolites provide a wide range of catalysts by varying the conditions of steaming and extraction of residual amorphous material. This zeolite upgrade provides the catalysts that respond to the needs of the petrochemical industry [4] [5] [6]. Zeolites of mild acidity and large mesopores are required when the process is intended to convert heavy crude oil into middle size hydrocarbons. Such combination of zeolite properties facilitates diffusion of hydrocarbons and hinders coke formation on the surface of the catalyst [7] [8].

Brønsted Acid Sites (BAS) in the zeolite catalyze cracking, isomerization, and alkylation reactions [9] [10]. The removal of aluminum through steaming process provides additional chemical and thermal stability of zeolites. The steaming process forms extra-framework aluminum (EFAl) [8] [9] [11]. EFAl species could be favorable for hydrocracking, although their catalytic effect depends on the concentration, size, and dispersion [12] [13]. On the other hand, the excess of EFAl species clogs micro and mesoporous channels causing severe transport limitations [12].

(De-)hydrogenation reactions are attributed to the metal phase [14]. Noble metals of the VIIIB group and metal sulfides have been found as effective hydrogenation catalysts [15] [16] [17]. When the reaction is carried out with noble metals, complete hydrogenation of aromatic rings occurs before the scission of C-C bonds [17]. Metal sulfides promote ring opening reactions before hydrogenation reactions complete [15] [18] [19].

After hydrogenation of PAHs over metal sites, cyclic hydrocarbons are cracked over acid sites. The cleavage of C-C bonds in the cyclic hydrocarbons is followed by a series of skeletal rearrangements based on an exocyclic type A β-scission until a branched carbon chain is reached [3] [19]. Type A β-scission delivers olefins intermediates which are then hydrogenated over metal sites passing three adsorption/desorption steps. Several authors opposed to this reaction mechanism stating that the olefin diffusion between acid and metal sites at the reaction conditions seems unlikely [20] [21].

The alternative mechanism advanced by Roland et. al. [20] considers that the hydrogenation reaction takes place over acid sites [20]. The mechanism predicts that hydrogen molecules splits-off on metal sites and then migrate to the acid sites (a.k.a., hydrogen spillover) [22]. Monoatomic hydrogen interacts with hydrocarbon molecules adsorbed on the acid sites. Thus, alternative hydrocracking mechanism, suggest that activation, isomerization, cracking, and hydrogenation occur on the acid sites [20] [23]. In both classical and alternative mechanisms, the density of acid sites on the support plays an essential role in the hydrogenation efficiency [24].

Fluorene is a model compound with the molecular structure of typical PAH [25] [26]. Lapinas et. al. [25] studied fluorene hydrocracking over sulfided NiMo catalyst supported on Y zeolite. Catalyzed isomerization, and hydrocracking reactions initiate through the central five-carbon-membered ring of fluorene. They have measured equimolar product yields of saturated and aromatic single-ring compounds [25]. In contrast, Wang et. al. [26] tested platinum/USY catalysts for fluorene hydrocracking and evinced complete aromatic hydrogenation before the five-membered rings were broken.

The experimental campaign investigated the role of acid sites in USY zeolites in association with their catalytic activity in fluorene hydrocracking. To conduct experimental testing a novel High-Pressure Simultaneous Thermal Analyzer (HP-STA) has been utilized. The reaction energy of complete fluorene hydrogenation and hydrocracking was measured. Some aspects of the reaction mechanism are discussed in this chapter. Correlations between USY zeolite properties and the reaction temperature as well as correlation between USY properties and catalytic activity were proposed. These correlations contribute to the understanding of hydrocracking mechanisms using bifunctional catalysts based on USY zeolites.

2.2 Experimental.

2.2.1 Supports and materials used in the research

Standard USY zeolites with reference codes CBV600, CBV712, CBV720, CBV760, and CBV780 were purchased from Zeolyst International. As reported by Verboekend et al. [5], these USY zeolites are prepared by traditional procedures of steaming and exchange from a parental Na-Y zeolite (CBV100). Higher number of the USY zeolite means higher Si/Al ratio and mesoporous area, while the acid sites per gram of zeolite decrease. Aerosil was supplied by Evonik, and MCM-41 was prepared as reported in [27]. HY zeolite (CBV400) was used as reference zeolite for DRX measurements. Merck supplied the fluorene, and Linde the hydrogen

2.2.2 Platinum impregnation

Zeolites were enriched by wet impregnation using water solution of $Pt(NH_3)_4Cl_2$, kept at the pH 5.2. After wet impregnation platinum held 0.85% of the total catalyst mass (on a dry basis). To ensure the steady humidity content, zeolites containers were covered with cloth and stored in a room with constant relative humidity (approx. 40%). When water content reached equilibrium, it was determined by thermogravimetric analysis (TGA).

Wet impregnation was carried out using a rotary evaporator. Rotary evaporator set to 90 °C, 90 rpm, 0,2 bar, evaporated residual water within 30 min of operation [28]. Prior to hydrocracking test, the catalysts were activated by two different methods: (1) the in-situ auto-reduction method according to Oudenhuijzagen et al. [29], and (ii) heating up at atmospheric pressure of hydrogen. The auto-reduction method involved heating up the catalysts until 300 °C, at the rate 2 °C/min under a vacuum atmosphere (approx. 2.5 mbar). Subsequently, the catalysts kept under the hydrogen flow of 1L/min for 30 minutes, maintaining the temperature at 300 ºC and at atmospheric pressure. The second method follows the same procedure but at 1 bar of hydrogen pressure during all the experiment. The effects of these two activation methods were examined by TEM morphological imaging.

2.2.3 Characterization

2.2.3.1. Powder X-Ray Diffraction (XRD)

Powder XRD patterns were recorded for the angle 5° to 50°/2θ. Diffractometer PANalytical EMPYREAN operated with a Cu Kα radiation equal to 0.15418 nm coupled with a nickel filter. XRD patterns were evaluated by XpertPro software based on a standard test method ASTM D3942. Small-angle patterns were recorded from 1º to 10º/2θ in a BRUKER D8 ADVANCE diffractometer at 0.6 s/step of 0.02035º (2θ) in a DaVinci geometry.

2.2.3.2. Nitrogen physisorption

Isotherms and textural properties were obtained by nitrogen physisorption using a Quantachrome Autosorb 1C sorptometer. Nitrogen adsorption/desorption isotherms were recorded for 74 K and 0.753 bar (atmospheric pressure in Bogotá, Colombia). Prior to surface area analysis, catalysts were degassed for five hours under the vacuum and temperature 573 K. Textural properties were calculated by simulation of the experimental isotherm. Non-Local Density Functional Theory (NL-DFT) computational modeling was employed to determine adsorption properties assuming that pores have cylindrical and spherical shapes.

2.2.3.3. Transmission electronic microscopy (TEM)

Electronic imaging was conducted by Scanning Transmission Electron Microscopy (STEM) with High-Angle Annular Dark-Field (HAADF) in a Titan G2-300 from FEI. STEM enabled morphological characterization of catalysts. Images were taken at Max Plank Institute and the Technische Universität München (TUM) in Germany.

2.2.3.4. Isopropyl-amine (i-PA) chemisorption

Brønsted Acid Sites (BAS) in zeolites were quantified through the reaction with i-PA [30] [31] using HP-STA instrument from Linseis. Approximately 0.2 g of zeolite was weighted in a 3.4 mL capacity ceramic pan. Prior to chemisorption reaction, zeolite was calcined. Calcination temperature at 400 °C was reached via heating rate 3 ºC/min while maintaining reduced pressure ($1x10^{-2}$ mbar). Calcined zeolite was cooled down by a N_2 flow of 1 L/min.

Once cooled down, 2 mL of i-PA was added to the ceramic pan and the first heating ramp initiated with the heating rate 10°C/min until reaching 300 °C. The final temperature ramp reached 400 ºC with heating rate 5 ºC/min. During the first heating ramp, physisorbed i-PA desorbed from the zeolite and left the pan in the vapor form. In the second heating ramp, chemisorbed i-PA decomposed. BASs were quantified by the mass of chemisorbed i-PA assuming a 1:1 molar ratio between i-PA molecules and the BAS.

2.2.3.5. Pyridine (Py) chemisorption measured by IR spectroscopy

Nicolet FTIR 5700 spectrometer with a resolution of 4 cm^{-1} recorded IR spectra zeolites carrying adsorbed pyridine. IR spectra were recorded at 150 ºC. FTIR measurement method was adopted from [6] [9]. Zeolite samples were pressed into self-supported wafers. Samples were then activated in a vacuum atmosphere (1×10^{-6} mbar), at temperature 350 °C. Once samples reached 350 ºC, H_2 filled the system for an hour. After, samples were cooling down to 150 °C, and the remnant H_2 was evacuated, leaving the system in ultra-vacuum. Later, pyridine was administered at 0.5 mbar for one hour and evacuated for another hour to desorb the weakly bounded pyridine. The concentration of total BAS and LAS was determined by integrating the peak areas at the bands 1545 cm^{-1} and 1450 cm^{-1}, respectively, using equations 2.1 and 2.2. The integrated molar extinction coefficient (Ɛ) of bands of pyridine adsorbed on BAS and LAS are 0.73 and 0.96 cm μmol^{-1}, respectively [6]. The concentration of Strong Brønsted Acid Sites (SBAS) was obtained by integrating the areas of the sample bands after pyridine in the samples were evacuated for 0.5 h at 450 °C.

$$[C_{BAS}] = \frac{\pi R^2}{\varepsilon_{BAS}} \frac{IA(1570 - 1510\ cm^{-1})}{m} \quad [2.1]$$

$$[C_{LAS}] = \frac{\pi R^2}{\varepsilon_{LAS}} \frac{IA(1470 - 1435\ cm^{-1})}{m} \quad [2.2.]$$

where R is the wafer radius, IA the integrated peak area in that range, and m the mass of the wafer.

2.2.3.6. Hydrogen Chemisorption

Platinum dispersion was calculated by Hydrogen chemisorption using a Thermo Scientific Surfer Analyzer. Prior to chemisorption analysis, the catalysts were activated. Approximately 250 mg of catalyst reached activation temperature at 350 ºC via heating rate 3 ºC/min at while maintaining reduced pressure. Once achieved 350 ºC a hydrogen flow filled the system for a period of one hour. The chemisorption isotherm was measured at room temperature for the pressure range between 0 and 533 mbar. The dispersion was calculated assuming a molar relation 1:1 between the H and the platinum atoms, using the cero-extrapolation method.

2.2.4 Non-isothermal hydrocracking in an HP-STA

The hydrocracking of fluorene over USY zeolite supported Pt catalysts (Pt/USY) was studied by HP-STA instrument. HP-STA was calibrated against melting points and fusion enthalpies of indium, tin, and lead. Prior to hydrocracking reaction, catalysts were activated according to the description given in section 2.2.3.6. Hydrocracking reaction was carried out in an aluminum pan. A 15 mg layer of the catalyst was covered by a 15 mg layer of fluorene powder. HP-STA test conditions were adjusted to a constant flow of hydrogen 400 NmL/min and to a pressure 50 bar. Differential Scanning Calorimeter (DSC) curves were recorded from 25 °C to 400 °C with a heating rate 10 °C/min. The DSC curve of each reaction was corrected for the baseline response. That is subtracting the baseline response (i.e., catalysts alone) from the hydrocracking reaction curve. The specific heat of reactants changes during the experiment because of the temperature variation [9]. This leaves open-ended peaks at the end of the DSC curves. The experiments were repeated with CBV760 and HY catalysts; detailed results are consigned in appendix A. Measurement repeatability is presented as standard error. Standard error is calculated as standard deviation divided by the square root of the number of measurements. Error bars were drawn in the graphics with the results (fusion: ±7.5%; hydrogenation: ±2.2%, hydrocracking: ±4.7%).

Gaseous products of hydrocracking reaction were characterized by a Pfeiffer mass spectrometer. A sniffer probe placed over the crucible transferred product gases from HP-STA to the mass spectrometer for continuous gas analysis. In the HP-STA experiment, the amount of fluorene in aluminum pan is 15 mg. Such a small amount of fluorene generates

a small number of products which are additionally diluted in a 13 L volume of the HP-STA instrument. Thus, the mass spectrometer cannot detect the gaseous products sniffer probe. Therefore, hydrocracking reaction were repeated on Pt/CBV712, Pt/CBV780, and Pt/Aerosil catalysts in a big pan with 500 mg of catalyst and 500 mg of fluorene. The use of this pan disabled the option of recording the DSC but allowed following *in-operando* the mass loss. Larger sample also yielded enough gaseous products for direct detection by the mass spectrometer.

Activity index of reaction ΔH_m (J/g) was calculated to evaluate the activity of catalysts. ΔH_m was expressed as total heat of hydrocracking reaction (ΔH (mJ) - DSC signal) divided per the mass loss (Δm (mg) - TG signal). The total heat of reaction ΔH (mJ) is proportional to the rate of reaction as is expressed in equation 2.3. The mass loss is almost equivalent to the initial mass of fluorene suggesting its complete conversion.

$$r = \frac{dC}{dt} \propto \frac{dq}{dt} \quad [2.3]$$

2.3 Results and discussion

This section shows the results of the catalytic activity of Pt supported on USY zeolite catalysts and their respective characterization. Catalytic activity results recorded by calorimetric techniques were correlated with the properties of catalysts to explain the observations.

2.3.1 Characterization

Figure 2-1-I shows XRD patterns of USY zeolites [32]. Diffraction intensity (111) at 6.09 º increased when the Si/Al molar ratio increased. This was associated with the dealumination processes. That indicates that USY zeolites conserve its crystallinity despite dealumination processes. The evaluation of dealumination process considers CBV600 USY zeolite as the reference material [33]. When aluminum is removed from the crystalline structure of zeolite, Si-O bonds population increases. Si-O bonds are smaller than Al-O bonds which slightly affects the crystalline structure and the XRD pattern. Despite that, there is no apparent shift of the (111) reflection towards lower 2θ values with the decreasing amount of aluminum in the framework [32].

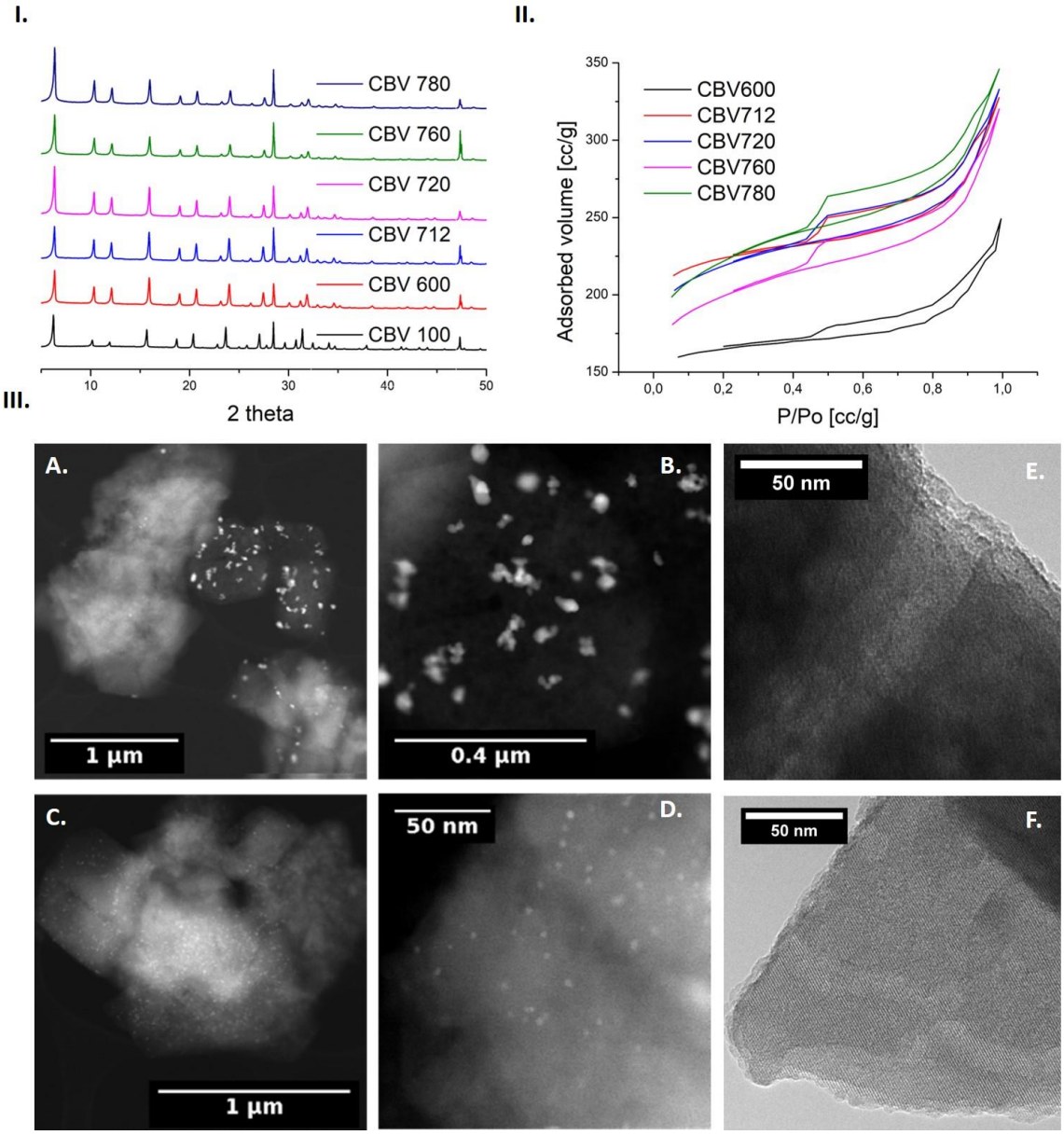

Figure 2-1 Characterization of USY zeolites from Zeolyst ®. I Powder XRD patterns, II. Collection of adsorptions N_2 isotherms, III. HAADF-STEM micrographs of CBV600 impregned with platinum by different methodologies: A. and activated at atmospheric pressure C. and D. activated at reduced pressure. D. and F. are HAADF-STEM micrographs of CBV600 and CBV712 respectively.

Figure 2-1-II shows adsorption/desorption isotherms of five USY zeolites with distinct structural properties. Figure 2-1-II curves were obtained by the nitrogen physisorption method. According to IUPAC classification, all USY zeolites acquired isotherms type IV(a) with hysteresis loops type H4. Type H4 hysteresis corresponds to materials that combine

micropores and mesopores [34]. Table 2-1 displays the structural properties of the USY zeolites and final catalyst measured by N_2 physisorption. The zeolite CBV600 presented the lowest adsorbed volume, indicating the presence of amorphous material occluded within the crystal structure [11]. Total volume as well as mesopore volume increase in USY zeolites with higher Si/Al ratio [35]. This is attributed to the dealumination treatments. With the aluminum removal, more mesopores are generated inside the crystalline structure of zeolites. The mesoporous surface area also presented similar trends with the Si/Al ratio of zeolites.

Table 2-1 Structural properties of the USY zeolites measured by N_2 physisorption employing a sorptometer

Zeolite	Vol_{Total} (cm^3/g)	Vol_{meso} (cm^3/g)	Vol_{micro} (cm^3/g)	A_{total} (m^2/g)	A_{meso} (m^2/g)	A_{micro} (m^2/g)
CBV 600	0.43	0.17	0.26	692	28.7	663.3
CBV 712	0.52	0.19	0.33	881	18.2	862.8
CBV 720	0.48	0.24	0.24	778	62.7	715.3
CBV 760	0.48	0.24	0.24	731	86.7	644.3
CBV 780	0.60	0.29	0.31	934	134.9	799
Pt 0,85%wt/CBV 600	0.42	0.22	0.20	511	23.2	487.8
Pt 0,85%wt/CBV 712	0.40	0.15	0.25	668	26.1	641.8
Pt 0,85%wt/CBV 720	0.42	0.19	0.23	684	82.49	601.5
Pt 0,85%wt/CBV 760	0.42	0.22	0.20	654	108.7	545.3
Pt 0,85%wt/CBV 780	0.46	0.24	0.22	711	105.2	605.8

* The values consigned in the table were calculated by the BET method.

* All USY zeolites used in this research are from commercial series of Zeolyst ®.

Figures 2-1-III-A, B, C, and D, shows electronic micrographs of activated Pt/USY(CBV600) catalyst, activated by the two different methods as described earlier. Pt clusters appear as bright dots with respect to darker areas associated with the zeolite support. This Z-contrast imaging is achieved when the STEM detector is positioned in a high dispersion angle from the optical axis. Images in Figures 2-1-III-A. and B show that platinum reduction at atmospheric pressure of hydrogen resulted in a poor platinum dispersion in comparison with the catalysts activated at reduced pressure [29]. Based on these findings, a reduced

pressure activation method was selected for catalysts activation prior to hydrocracking testing.

Figures 2-1-III-E. and F show HAADF-STEM of two USY zeolites: CBV600 and CBV712. CBV712 zeolite is prepared by removing the amorphous material of CBV600 by acid leaching. Figures 2-1-III-E and F show clearly mesoporous channels in both zeolites. Nevertheless, micropores are less visible for CBV600 than CBV712 because of amorphous material inside CBV600 USY zeolite.

Table 2-2 Characterization of acid and metal sites in the USY zeolites and Pt/USY catalysts

Zeolite/Catalysts	Si/Al	Acidity[1] i-Pa (µmol/g)	Acidity[2] Py BAS (µmol/g)	Acidity[2] Py LAS (µmol/g)	Acidity[2] Py SBAS (µmol/g)	Pt[3] Dispersion (%)	Cluster Size (nm)
CBV 600	9.8	783	251	139	114	-	-
CBV 712	12.4	959	314	112	154	-	-
CBV 720	15.3	556	263	54	179	-	-
CBV 760	28.4	265	142	19	88	-	-
CBV 780	54.3	130	86	6	22	-	-
Pt 0,85%wt/CBV 600	-	365	233	59	121	71	1.4
Pt 0,85%wt/CBV 712	-	-	310	51	278	69	1.5
Pt 0,85%wt/CBV 720	-	201	292	61	144	45	2.2
Pt 0,85%wt/CBV 760	-	-	84	15	74	91	1.1
Pt 0,85%wt/CBV 780	-	136	66	16	20	98	1.0

[1] Amount of i-Pa decomposed on the material measured in a DSC-TG

[2] Amount of pyridine adsorbed over the material surface at 150°C and 450°C by FTIR

[3] It is determined by H_2 chemisorption over metal surfaces calculated by extrapolation to zero of the resulting curve of the difference from the chemisorption and physisorption isotherms.

Structural properties of the catalyst were affected after the deposition of platinum over the zeolites. Mesopore volume of Pt/USY catalysts increased with respect to their USY zeolite analog whereas micropore volume decreased. Platinum clusters contribute to the total mesopore area, while blocking some microporous. Mean platinum cluster size in catalysts is around 1.5 nm (Table 2-2) which clogs the USY micropores (Table 2-2). Consequently, total volume slightly decreased in all Pt/USY catalysts except for of Pt/USY(CBV600),

attributed to micropores of this zeolite are already blocked. The N_2 adsorption isotherms after the platinum impregnation are consigned in appendix A.

Table 2-2 presents Si/Al ratio, molar concentration of acid sites, platinum dispersion, and platinum mean cluster size of USY zeolites and Pt/USY catalysts, activated under reduced pressure. The Si/Al ratio measured by XRD is an indirect indication of aluminum content in the crystalline network. On the other hand, almost linear relation exists between network aluminum content and acidity. Zeolites with higher amounts of network aluminum had a higher quantity of BAS measured by i-PA decomposition reaction. The USY zeolite CBV600 was the exception since it contained less BAS than CBV712 and CBV720. This is due to a significant fraction of the amorphous material that blocks the access of isopropylamine to the acid sites of USY zeolite CBV600.

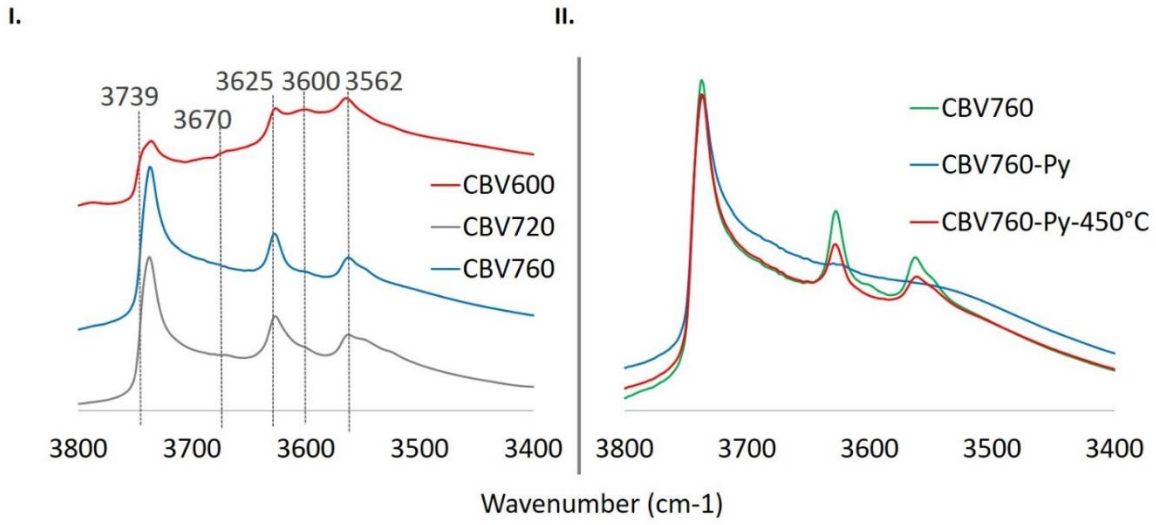

Figure 2-2 FTIR spectra of representative USY zeolites, and CBV760 zeolite saturated of pyridine. I. USY zeolites before absorption of pyridine, and II. CBV760 USY zeolite before adsorption of pyridine (green), after adsorption of pyridine (blue), and after degassing at 450 °C (red).

Figure 2-2-I shows the IR spectra of USY zeolites referenced as CBV600, CBV720, and CBV760. The IR spectra in the region from 3400 cm^{-1} to 3800 cm^{-1} shows five distinctive bands at 3562 cm^{-1}, 3600 cm^{-1}, 3625 cm_{-1}, 3670 cm^{-1}, and 3739 cm^{-1}. These bands are attributed to stretching vibrations of OH groups [11] [36]. The band at 3739 cm^{-1} is attributed to the terminal Si-OH groups [37]. The bands at 3562 and 3670 are related to BAS located in sodalite cages and supercages. The band at 3670 cm^{-1} is assigned to Al-OH groups in

EFAl [38]. The band at 3600 cm^{-1} refers to a high-frequency OH group perturbed by the interaction with LAS present in EFAl generated during steaming dealumination [38]. Several authors stated that LAS near to BAS acts as super-acid sites, which could promote the cracking reactions [12]. However, the effect of these super acid sites in the cracking reaction is not well understood. So, there is urgency for further investigation of zeolite assisted hydrocracking reactions [39] [40] [41]. Figure 2-2-II shows that some OH bands disappear with the addition of pyridine after degassing the system at 450 °C, which is a signal of the presence of some Strong Brønsted acid sites (SBAS).

The content of LAS, BAS and SBAS corresponds to the Si/Al ratio of the supports, as is shown in Table 2-2. With platinum deposition over the zeolite support the total amount of BAS measured by pyridine decreased. The exception was Pt/USY(CBV720) catalyst with a BAS increment of 11%. BAS content decreased for 7%, 1%, 41% and 23% in the Pt/USY catalyst referenced as CBV600, CBV712, CBV760 and CBV780 respectively. Observed BAS reduction was probably due to ion exchange between the Pt and the BAS [28]. BAS reduction may be also triggered by degradation of the zeolite structure during platinum impregnation, which agrees with the total surface area data reported in Table 2-1.

The BAS content measured by i-PA chemisorption was nearly double compared to the BAS measured by pyridine chemisorption, a phenomenon perhaps related to the size of the chemisorbed molecule. Table 2-2 also shows that BAS decreased after platinum impregnation by both techniques. The amount of LAS also decreased along with the decrease in aluminum content.

CBV720 zeolite incorporated the highest content of SBAS. On the other side Pt/USY(CBV780) catalyst incorporated the lowest density of acid sites, which is a result of the most severe dealumination condition. The density of acid sites has been pointed out as a key factor for high catalytic activity in the hydrocracking reaction [9] [10]. Along with the acid site density, catalytic activity largely depends on the access of hydrocarbons to these acid sites [42].

2.3.2 Non-isothermal hydrocracking test in HP-STA

Figure 2-3 shows the DSC curves of fluorene hydrocracking reactions on Pt/USY(CBV720) and two non-acid supports, Aerosil and MCM-41. The DSC curves show three major peak signals for non-acid catalysts and four major peak signals for acid catalysts respectively.

The first signal was consistently recorded for all three catalysts tested. Its peak temperature (Tm) between 116.6 °C and 117.5 °C corresponds to the melting of fluorene. Fluorene melting temperature as reported in the literature is 114.8 ºC [43]. The variation between measured melting temperature and the one given in the literature can be associated to the high reaction pressure and to the effect of fluorene adsorption on the support surface.

The second peak corresponds to the exothermic hydrogenation of two aromatic rings in fluorene [26] [44]. It was suggested that the hydrogenation of PAHs can be accelerated by the presence of acid sites [22] [45]. Figure 2-3 shows that the hydrogenation temperature interval depends on the catalyst. Pt/USY(CBV720) catalysts complete hydrogenation reaction at temperature 217 ºC, while the non-acidic Aerosil and MCM-41 materials complete hydrogenation at 297 ºC and 301 ºC respectively. Fluorene hydrogenation using non-acidic materials-based catalysts seems to occur in two steps. This can be deduced from two hydrogenation peaks, which correspond to the consecutive hydrogenation of each aromatic ring [44]. During the hydrogenation step, fluorene is hydrogenated into cyclic saturated perhydrofluorene [26].

The third signal occurs above 300 °C and depends strictly on the nature of the support. For instance, the signal is exothermic for the zeolitic support, while it is endothermic for the non-acidic analogues. At this point fluorene has been hydrogenated, probably into perhydrofluorene. The cyclic paraffin requires the presence of acid sites to be isomerized or cracked. Hydrocracking would occur by the subsequent saturation with hydrogen of newly scissed C-C moieties, which gives rise to the relatively sharp exothermic signal evinced in figure 2-3. Since hydrocracking requires the presence of acid sites, it cannot take place on the non-acidic supports. As a result, endothermic signals were observed instead, which may be attributed to the thermal cracking of the perhydrofluorene and subsequent evaporation of reaction products.

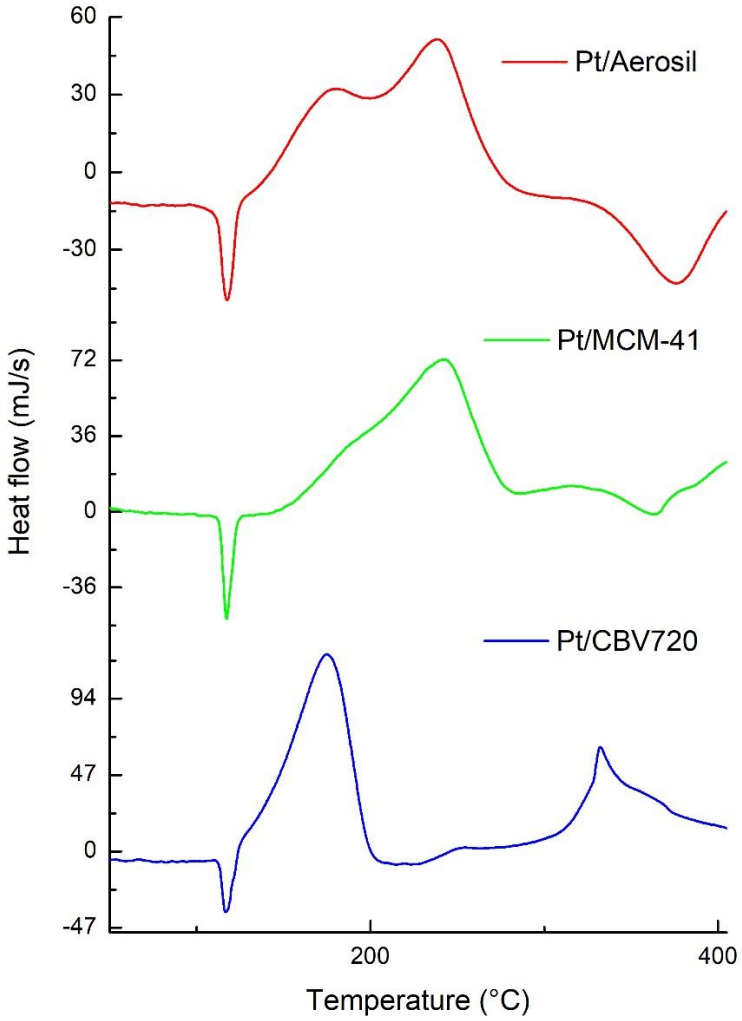

Figure 2-3 DSC curves of the fluorene hydrocracking on Pt supported on USY zeolite, Aerosil, and MCM-41.

The third signal initiates above 300 °C and depends solely on the support properties. The third signal is exothermic for the zeolitic support, while it is endothermic for the non-acidic analogues. Perhydrofluorene requires the presence of acid sites to undergo isomerization or endothermic cracking reaction. Consecutive to the endothermic cracking reaction, newly scissored C-C moieties are hydrogenated whose hydrogenation is an exothermic process. Since hydrogenation enthalpy is higher than endothermic C-C cracking enthalpy, the resultant hydrocracking process is exothermic. Consequently, hydrocracking requires the presence of acid sites. Hydrogenation of unsaturated C-C bonds does not take place on the non-acidic catalysts. Therefore, endothermic cracking reaction may be attributed to the

thermal cracking of the perhydrofluorene and subsequent evaporation of reaction products. This result insinuates that acid sites in zeolites can hydrogenate unbalanced carbon that results from cracking.

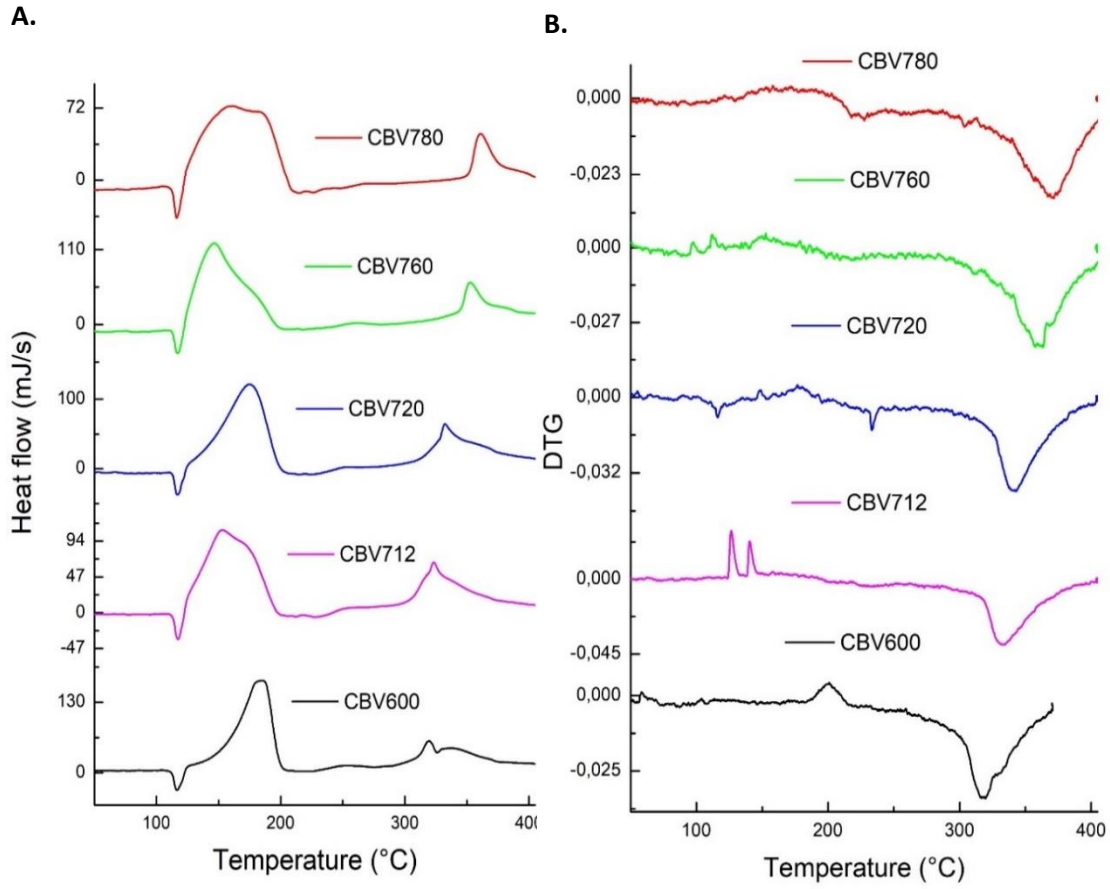

Figure 2-4 DSC and DTG curves of the fluorene fusion, hydrogenation and hydrocracking on Pt supported on USY zeolites. A. DSC profiles; B. DTG profiles.

Figure 2-4-A shows the DSC curves of fluorene hydrocracking on the series of five Pt catalysts supported on USY zeolite. DSC peak signals demonstrate three consecutive reactions: melting, hydrogenation, and hydrocracking. Additional weak exothermic signal at 250 ºC is attributed to perhydrofluorene isomerization. Peak signals corresponding to melting and hydrogenation of the fluorene overlap at 127 ºC for all USY zeolite supports under consideration. Although all Pt/USY catalysts demonstrated consistent temperature intervals, there are observable differences in the shape of the hydrogenation peaks. Notable differences among Pt/USY catalysts are also shown in the hydrocracking region (i.e., the third major peak signal). As the aluminum contents of the support decreased, Tm

shifted to a higher temperature. Moreover, the peak areas are increasing along with decreasing of aluminum in zeolites as is shown in table 2-3. This result shows that the support acidity plays a role in the hydrocracking activity of the catalysts.

Figure 2-4-B presents the DTG curves of fluorene hydrocracking Pt/USY catalysts. The DTG curves are typically flat throughout the temperature ramp, except for the hydrocracking region above 300 ºC. A negative peak indicating mass loss caused by the evaporation of hydrocracking products. The DTG curve shows signal disturbance at temperatures below 300 ºC probably due to the balance instability caused by the high pressure of the measurement system. The correlative analysis of figures 2-4-A. and 2-4-B. demonstrates that the two processes which take place at temperatures below 300 ºC, (i.e., melting and hydrogenation), did not lead to significant mass changes. At least not within the resolution of the HP-STA.

Table 2-3 Resume of DSC curves of the hydrocracking of fluorene over USY zeolites and nonacid supports.

Catalysts	Melting	Hydrogenation		Hydrocracking	
	Enthalpy (kJ/mole)	Signal position (°C)	Enthalpy (kJ/mole of fluorene)	Maximum of the Signal Position (°C)	ΔH_m[1] ($J/g_{reactant}$)
0.85%Pt/CBV600	19.41	134-207	-350	319	1530
0.85%Pt/CBV712	15.89	123-227	-351	323	1893
0.85%Pt/CBV720	13.00	124-210	-350	332	2101
0.85%Pt/CBV760	16.94	123-207	-349	355	1263
0.85%Pt/CBV780	12.38	123-217	-346	362	1020
0.85%Pt/Aerosil®	13.65	127-297	-351	306	-357
0.85%Pt/MCM-41	19.65	148-287	-341	294	-784

[1] Mass enthalpy was calculated dividing the released energy by the mass present in the crucible (pan), during PHF hydrocracking.

Nonetheless, hydrocracking leads to the formation of volatile fragments which evaporate from the reactor. The negative DTG signals associated with hydrocracking shifted towards higher temperatures with decreasing aluminum contents in the zeolite. This goes in line

with the bifunctional properties of the hydrocracking catalyst and the need for acid sites for cracking activity.

The results depicted in Figures 2-3, 2-4-A. and 2-4-B. are further explored by the data given in Table 2-3. Table 2-3. lists the reaction enthalpies calculated from the areas of the respective DSC peaks. According to Acree [43] the enthalpy of fluorene fusion is 19.5 kJ/mol. Table 2-3 shows that most of the measured values are lower than that. This dissimilarity arises from the ongoing exothermic adsorption of melted fluorene onto the catalyst support, which results in a decrease of the endothermic heat (i.e., enthalpy of fusion). The values of the hydrogenation enthalpy were consistently similar throughout tested catalyst. Measured hydrogenation enthalpies were very close to those reported by Ali (-351 kJ/mol) [44].

Moreover, Pt/USY catalyst requires lesser hydrogenation temperature than non-acidic catalysts. Although fluorene reaches similar degrees of hydrogenation on all catalysts, the process took longer and required higher temperatures on the non-acidic catalysts. The values of hydrocracking enthalpy are listed in the last two columns of Table 2-3. The shift toward high temperatures of the DSC peak decrease of hydrocracking enthalpy coincided with a decrease of aluminum content in Pt/USY catalysts. This reveals an intimate link between the catalytic activity and the amount of acid sites. Hydrocracking enthalpy was calculated by dividing the area of the DSC peaks of Figure 2-4-A. by the respective mass losses of Figure 2-4-B. in the lapse of the reaction. This quantity, denoted as ΔH_m, measures the number of hydrocracking events and the evaporation of the resulting fragments. Therefore, a higher value of ΔH_m means that the molecule is broken into more pieces, i.e., it measures how deep the fluorene is hydrocracked.

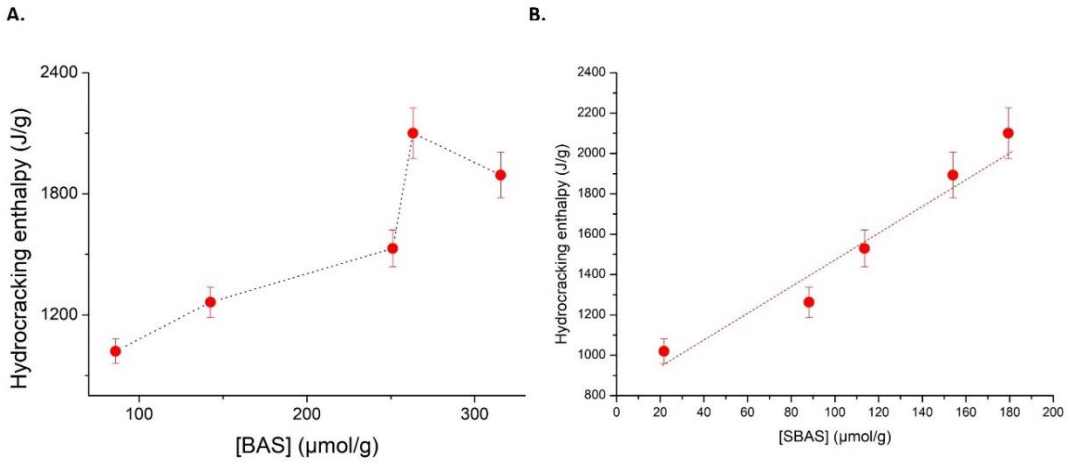

Figure 2-5 Effect of different acid sites measured by FTIR of pyridine on the perhydrofluorene hydrocracking enthalpy. A. dependence on BAS concentration, and B. SBAS concentration.

Mutual collaboration between metallic and acid sites is necessary to carry out the hydrocracking reaction. In a system where the platinum does not limit the reaction, the HC reaction would be proportional to the BAS density [3] [19]. High dispersion of platinum over the zeolites (Table 2-2), and the consistent value of hydrogenation enthalpy (Table 2-3), proved that the hydrogenation is not the limiting step of the reaction. This suggests that the catalytic activity of Pt/USY catalysts was predominantly affected by BAS content within each support.

Mass hydrocracking enthalpy (ΔH_m) as a function of the BAS density was explored in Figure 2-5. Nearly linear relationship is shown between ΔH_m and the BAS density. Linear relationship is also shown in figure 2-5-B between ΔH_m and SBAS, (i.e., of the strong acid sites). Zeolites do not have a discrete distribution of acid strengths [35], which can be affected by local chemical, structural, and topological features [45] [46]. A single technique is not sufficient to fully characterize acidity in zeolites. However, the comparison of BAS and SBAS (Figures 2-5-A and 2-5-B) indicates that not all acid sites equally participate in the fluorene hydrocracking. Moreover, the linear relationship depicted in Figure 2-5-B suggests that the low density of SBAS was limiting hydrocracking reaction and would imply a strict dependence of hydrocracking rate on this type of acid sites.

In summary, fluorene hydrocracking follows a complex reaction mechanism [26] including a set of irreversible reactions and complementary activities between platinum and acid

sites. The results showed that the specific hydrocracking reactions predominantly take place on the acid sites. Thus, the higher the density of acid sites, the lower the temperature required to start the hydrocracking reaction and the more the events of hydrocracking. Besides, a direct correlation between the ΔH_m and the SBAS concentration was found indicating that SBAS are responsible for high cracking activity in zeolites.

2.4 Conclusions

In this study fluorene hydrocracking reaction over platinum loaded acidic USY zeolites and non-acidic supports was studied. Experimental tests were carried out by Simultaneous thermogravimetric and differential scanning calorimetry. The non-isothermal experimental test showed that hydrogenation of aromatic rings, their respective isomerization and the final hydrocracking occurs at different temperatures. Complete hydrogenation of fluorene occurs at temperature interval 130 ºC to 300 ºC and the hydrocracking reaction at temperature interval 320 ºC to 400 ºC. Platinum supported on non-acidic supports performed lower catalytic activity to fluorene hydrogenation and null activity to hydrocracking. Linear relationship between the density of acid sites and the temperature of fluorene hydrocracking was evidenced. The on-set temperature of hydrocracking is lower as the population of acid sites increases. The correlative analysis suggests that acid sites promote hydrogenation of fluorene. The mass hydrocracking enthalpy (ΔH_m) was suggested as an indicator of the catalytic activity. This quantity exhibited a linear relationship with the BAS and SBAS concentration. This implies that the zeolite-based catalyst with higher amount of acid sites catalyze hydrocracking reactions more efficiently.

2.5 References

[1] N. Choudhary y D. N. Saraf, «Hydrocracking: A Review,» Ind. Eng. Chem. Prod. Res., vol. 14, nº 2, 1975.

[2] A. Martínez, M. A. Arribas y S. B. C. Pergher, «Bifunctional noble metal/zeolite catalysts for upgrading low quality diesel fractions via selective opening of naphthenic rings,» Catalysis Science & Technology, 2016.

[3] J. Weitkamp, «Catalytic Hydrocracking—Mechanisms and Versatility of the Process,» ChemCatChem, vol. 4, p. 292 – 306, 2012.

[4] D. Verboekend, N. Nuttens, R. Locus, V. J. Aelst, P. Verolme, J. C. Groen, J. Perez-Ramirez y B. F. Sels, «Synthesis, Characterization, and catalytic evaluation of hierarchical faujasite zeolites: milestones, challenges and future directions.,» Chem. Soc. Rev. , vol. 45, pp. 3331-3352, 2016.

[5] D. Verboekend y J. Perez-Ramirez, «Towards a Sustainable Manufacture of Hierarchical Zeolites.,» CHEMSUSCHEM, nº 7, pp. 753-764, 2014.

[6] M. S. Maier, A. Jentys y A. J. Lercher, «Steaming of zeolite BEA and its Effect on Acidity: A comparative NMR and IR Spectroscopic Study.,» J. Phys. Chem, nº 115, pp. 8005-8013, 2011.

[7] A. M. A. M.-S. V. Corma, «Hydrogenation of Aromatics in Diesel Fuels on Pt/MCM-41 Catalysts,» Journal of Catalysis, nº 169, pp. 480-489, 1997.

[8] J. L. Agudelo, B. Mezari, E. Hensen, S. A. Giraldo y L. J. Hoyos, «On the effect of EDTA treatment on the acidic properties of USY zeolite and its performance in vaccum gas oil hydrocracking,» Applied Catalysis A: General, nº 488, pp. 219-230, 2014.

[9] Y. L. A. J. Zhang, «Promotion of protolytic pentane conversion on H-MFI zeolite by proximity of extra-framework aluminum oxide and BrØnsted acid sites,» J. Catal., vol. 370, p. 424–433, 2019.

[10] W. O. Haag, R. M. Lago y P. B. Weisz, «The Active Site of Acidic Aluminosilicate Catalysts,» Nature, nº 309, pp. 589-591, 1984.

[11] J. L. Agudelo, E. J. M. Hensen, S. A. Giraldo y L. J. Hoyos, «Influence of Steam-Calcination and Acid Leaching treatment on the VGO Hydrocracking Performance of Faujasite Zeolite,» Fuel Processing Technology, nº 133, pp. 89-96, 2015.

[12] R. A. Beyerlein, C. Choi-Feng, J. B. Hall, B. J. Huggins y G. J. Ray, «Effect of Steaming on the Defect Structure and Acid Catalysis of Protonated Zeolites.,» Topics in Catalysis, vol. 1, nº 4, pp. 227-42, 1997.

[13] C. S. Triantafillidis, A. G. Vlessidis y N. P. Evmiridis, «Dealuminated H-Y Zeolites: Influence of the Degree and the Type of Dealumination Method on the Structural and Acidic Characteristics of H-Y Zeolites,» Ind. Eng. Chem. Res, vol. 20, pp. 307-319, 2000.

[14] M. Bricker, V. Thakkar y J. Petri, Hydrocracking in Petroleum Processing, Springer International Publishing Switzerland., 2015.

[15] M. Camblor, A. Corma, A. Martinez, V. Martinez-Soria y S. Valencia, «Mild Hydrocracking of Vacuum Gasoil over NiMo-Beta Zeolite Catalysts: The Role of the Location of the NiMo Phases and the Crystallite Size of the Zeolite,» Journal of Catalysis, vol. 179, pp. 537-547, 1998.

[16] T. Isoda, S. Maemoto, K. Kusakabe y S. Morooka, «Hydrocracking of pyrenes over a nickel-supported Y-zeolite catalyst and an assessment of the reaction mechanism based on MD calculations,» Energy and Fuels, vol. 13, nº 3, p. 617–623, 1999.

[17] H. W. Haynes, J. F. Parcher y N. E. Heimer, «Hydrocracking Polycyclic Hydrocarbons over a Dual-Functional Zeolite (Faujasite)-Based Catalyst,» Ind. Eng. Chem. Process Des. Dev, vol. 22, nº 3, p. 401–409, 1983.

[18] S. Korre, M. T. Klein y R. J. Quann, «Hydrocracking of Polynuclear Aromatic Hydrocarbons. Development of Rate Laws through Inhibition Studie,» Ind. Eng. Chem. Res., vol. 36, pp. 2041-2050, 1997.

[19] M. Guisnet, «Ideal ' bifunctional catalysis over Pt-acid zeolites,» vol. 218–219, pp. 123-134, 2013.

[20] U. Roland, T. Braunschweig y F. Roessner, « On the Nature of Split-over Hydrogen,» J. Mol.Catal., vol. 127, pp. 61-84, 1997.

[21] Kissin y Y. V., «Chemical mechanisms of catalytic cracking over solid acidic catalysts, alkanes and alkenes.,» Catalysis Reviews: Science and Engineering, 2001.

[22] R. Prins, «Hydrogen spillover. Facts and fiction,» Chem. Rev., vol. 112, nº 5, p. 2714–2738, 2012.

[23] R. Ueda, T. Kusakari, K. Tomishige y K. Fujimoto, «Nature of Spilt over Hydrogen on Acid Sites in Zeolites: Observation of the Behavior of Adsorbed Pyridine on Zeolite Catalysts by Means of FTIR,» Journal of Catalysis, vol. 194, p. 14–22, 2000.

[24] H. Du, C. Fairbridge, H. Yang y Z. Ring, «The chemistry of selective ring-opening Catalysts.,» Applied Catalysis A: General, nº 294, pp. 1-21, 2005.

[25] T. A. Lapinas, B. C. Gates, A. Macris y E. J. Lyons, «Catalytic Hydrogenation and Hydrocracking of Fluorene: Reaction Pathways, Kinetics, and Mechanisms.,» Ind. Eng. Chem. Res, nº 30, pp. 42-50, 1991.

[26] L. Wang, Y. Chen, S. Jin, X. Chen y C. Liang, «Selective Ring-Shift Isomerization in Hydroconversion of Fluorene over Supported Platinum Catalysts,» Energy and Fuels, nº 30, pp. 3403-3412, 2016.

[27] J. Beck, J. Vartulli, W. Roth, M. Leonowicz, C. Kresge, K. Schmitt, C. Chu, D. Olson, E. Sheppard, S. McCullen, J. Higgins y J. Schlenker, «A new family of mesoporous molecular sieves prepared with liquid crystal templates,» J. Am. Chem.Soc., vol. 1, 1992.

[28] J. Zecevic, G. Vanbutsele, K. P. De Jong y J. A. Martens, «Nanoscale intimacy in bifunctional catalysts for selective conversion of hydrocarbons,» Nature, vol. 528, nº 7581, p. 245–254, 2015.

[29] P. J. K. B. T. J. V. B. y. D. C. K. M. K. Oudenhuijzen, «Understanding the Influence of the Pretreatment Procedure on Platinum Particle Size and Particle-Size Distribution for SiO2 Impregnated with [Pt2+C(NH3)4](NO3-)2: A combination of HRTEM, Mass Spectroscopy, and Quick EXAFS,» Journal of Catalysis, vol. 205, pp. 135-146, 2002.

[30] O. Kresnawahjuesa, R. J. Gorte, D. de Oliveira y L. L., « A simple, inexpensive, and reliable method for measuring Bronsted acid site densities in solid acids,» Catalysis Letters, vol. 82, pp. 155-160, 2002.

[31] O. Y. Perez, P. L. A. Forero y C. D. V. T. C. A. Torres, «Bronsted acid site number evaluation using isopropylamine decomposition on Y- zeolite contaminated with vanadium in a simultaneous DSC-TGA analyzer.,» Thermochimica Acta, vol. 10, nº 1-2, pp. 36-39, 2008.

[32] M. Niwa, N. Katada y K. Okumura, Characterization and Design of Zeolite Catalysts, Tottori. Japan: Springer Series in Material Science, 2010.

[33] W. Lutz, «Zeolite Y: Synthesis, Modification, and Properties—A Case Revisited,» Advances in Materials Science and Engineering, p. 20, 2014.

[34] M. Thommes, K. Kaneko, A. V. Neimark, P. J. Olivier, F. Reinoso-Rodriguez, J. Rouquerol y K. S. W. Sing, «Physisorption of gases, with special reference to the evaluation of surface area and pore size distribution (IUPAC Technical Report).,» 2015.

[35] M. J. Remy, D. Stanica, G. Poncelet, E. J. P. Feijen, P. J. Grobet, J. A. Martens y A. Jacobs P., « Dealuminated H-Y Zeolites: Relation Between Physicochemical Properties and Catalytic Activity in Heptane and Decane Isomerization.,» J. Phys. Chem, vol. 100, pp. 12440-12447, 1996.

[36] G. Busca, «Catalytic materials based on silica and alumina: Structural features and generation of surface acidity.,» Progress in Materials Science, vol. 104, p. 215–249, 2019.

[37] A. Jentys y A. J. Lercher, «Techniques of Zeolite Characterization,» Introduction to Zeolite Science and Practice, ScienceDirect, 2001, pp. 345-386..

[38] O. Cairon, «Impacts of Composition and Post-Treatment on the Bronsted Acidity of Steam-Treated Faujasite: Insights from FTIR Spectroscopy,» ChemPhysChem, vol. 14, nº 1, pp. 244-251, 2013.

[39] S. Shallmoser, T. Ikuno, M. F. Wagenhofer, R. Kolvenbach, G. Haller, M. Sanchez-Sanchez y J. Lercher, «Impact of the local environment of Bronsted acid sites in ZSM-5 on the catalytic activity in n-pentane cracking.,» J. Catal., vol. 316, pp. 93-102, 2014.

[40] N. Xue, A. Vjunov, S. Schallmoser, J. Fulton, M. Sanchez-Sanchez, J. Hu, D. Mei y J. Lercher, «Hydrolysis of zeolite framework aluminum and its impact on acid catalyzed alkane reactions.,» J. Catal., vol. 365, pp. 359-366., 2018.

[41] R. Lago, W. Haag, R. Mikovsky, D. Olson, S. Hellring, K. Schmitt y G. Kerr, «The nature of the catalytic sites in HZSM-5-activity enhancement,» Stud. Surf. Sci. Catal., vol. 28, pp. 677-684, 1986.

[42] F. Thibault-Starzyk, I. Stan, S. Abelló, A. Bonilla, K. Thomas, C. Fernandez, J.-P. Gilson y J. Pérez-Ramírez, «Quantification of enhanced acid site accessibility in hierarchical zeolites - The accessibility index.,» Journal of Catalysis, vol. 264, nº 1, pp. 11-14, 2009.

[43] J. W. E. Acree, «Thermodynamic properties of organic compounds: enthalpy of fusion and melting point temperature compilation.,» Thermochimica Acta, vol. 189, pp. 37-56., 1991.

[44] S. A. Ali, «Thermodynamic Aspects of Aromatic Hydrogenation.,» Petroleum Science and Technology, vol. 10, nº 25, pp. 1293-1304, 2007.

[45] F. Alvarez, F. R. Ribeiro, G. Perot, C. Thomazeau y M. Guisnet, «Hydroisomerization and Hydrocracking of Alkanes 7. Influence of the Balance between Acid and Hydrogenating Functions on the Transformation of n-Decane on Pt/HY Catalysts,» Journal of Catalysis, vol. 162, pp. 179-189, 1996.

[46] W. Karim, «Catalyst support effects on hydrogen spillover,» Nature, vol. 541, nº 7635, p. 68–71, 2017.

3. Design, construction, and validation of a trickle-bed reactor to the study phenanthrene hydrocracking over USY zeolite-based catalyst

Abstract

A laboratory-scale trickle bed reactor (TBR) was designed and constructed to study hydrocracking catalysts based on USY zeolites. Fitting and tubing materials were selected to sustain resistance to the high-pressure hydrogen attack as well as elevated temperature in the hydrocracking reaction. Design variables such as pressure drop, liquid holdup, wet efficiency, interphase mass transfer coefficients, and axial dispersion allow for the prediction of the reactor hydrodynamic behavior in a given range of gas and liquid flow rate. The reactor design presents arrangement details of the parts required to construct a TBR, including safety measures and construction heuristics. Constructed TBR was evaluated for the phenanthrene hydrocracking efficiency using platinum catalysts on USY zeolite and alumina as support. Reactor performance was tested at the liquid and gas flow rates determined in the design stage. Determining gas and liquid flow rates facilitated complete wetting of the catalysts during the operation. Liquid flow rates above 0.7 mL/min provided the operation under plug-flow regime operation. Thereby, the observed hydrocracking reaction rate depends on the reaction on the catalyst surface rather than on external diffusion limitations. Differences in activity reported for two different catalysts confirm the above. These results validated the proposed design of the trickle-bed reactor with the objective to study heterogeneous catalysis.

3.1 Introduction

Trickle-Bed Reactors (TBR) are an important driving motor of the process industries. A large field of TBR applications includes petrochemical, chemical industries, waste treatment, biochemical, and electrochemical processing [1] [2] [3]. TBR integrates several fixed beds made of solid catalysts through which liquid and gas flow. The material may flow in a co-current and countercurrent direction. Depending on the process, the catalytic bed is designed in different configurations, shapes, and sizes [4].

Existing literature studies different aspects related to the TBR, ranging from an understanding of hydrodynamics [5] [6] to the catalytic activity of materials [7]. Obtaining experimental data requires the use of a laboratory-scale reactor. Laboratory-scale reactor offers the following advantages: (i) design and construction is cheaper, (ii) lower consumption of reactants, and (iii) operation is safer than in industrial-scale reactor [8] [9].

The design of a laboratory-scale TBR should consider the involved physicochemical phenomena (i.e., physicochemical properties of feedstock, hydrodynamics, operating conditions, catalyst properties, and geometry), the reactor dimensions (i.e., diameter and bed volume), and mechanical aspects (i.e., mechanical and thermal resistance of tubing, fittings, and equipment) [10] [11] [12] [13] [14] [15] [16].

The Good design of a TBR system should guarantee a high process performance through a hydrodynamic study and the mechanical and thermal resistance of construction materials. The design should also take into account the chemical and thermodynamic nature of the process [2] [17].

The hydrodynamic analysis allows defining the interaction regime between the liquid and gas phase in the TBR at given flow conditions. Charpentier and Favier [18] modeled approximate flow patterns in a downward TBR. They proposed two types of flow regimes: high and low interaction. High interaction regime (pulsing flow, in bubble and mist) is recommended to study chemical kinetics because it ensures that the whole packed bed is in contact with the liquid phase. A low interaction regime (trickle flow) is more common when the intention is to simulate the behavior of an industrial-scale reactor [3]. Modeling of

TBR hydrodynamics involves the following aspects: physical properties of the fluids, reactor dimensions, pellet size, and bed arrangement (empty fraction and catalyst/pellet shape).

Various models for flow regime prediction have been proposed for three-phase TBR, considering the fluid properties, the operation conditions, and the packed bed characteristics [19] [20]. For high-pressure systems, computational fluid dynamics models (CFD) have been used, like the one described by Atta et. al. [21] [22] to study hydrodynamic regimes.

Perego proposed the packed-bed dimensions where external particle diffusion did not limit the reaction rate [12]. For solid-gas systems, (i) the packed bed diameter should be ten times the catalyst particle diameter (DPB/dP>10), and (ii) the bed length should be 50 times the particle diameter. For TBR, the last heuristic must be greater than 100 (LB/dP>100). However, to obtain reliable kinetic experimental data, the researcher must ensure no mass transport limitation by external particle diffusion. Two reaction tests are employed for verification of mass transport limitation in laboratory-scale TBR. Both tests are based on the assumption that conversion is independent of linear velocity through the bed. The construction materials must be mechanically resistant to corrosion, sustain the operating conditions (i.e., temperature and pressure), and be economically affordable. ASME BPV code section D1 describes how to predict material resistance to the pressure according to the working temperature [23].

The objective of the present work is to shows the design and construction of a TBR and its validation for phenanthrene hydrocracking. The reactor dimensions, bed configuration, liquid, and gas flow rates were set by empirical models proposed in the literature so that TBR operates in a high interaction flow regime. Thus, it was assumed that the mass transport by external particle diffusion is not a limiting factor in reactor performance. The above allows the design of a reaction test to study the effect of catalysts support properties on the phenanthrene hydrocracking reaction.

3.2 Brief description of reaction and previous considerations

Phenanthrene hydrocracking over Pt/USY catalysts involves a large number of endothermic and exothermic reactions. Hydrogenation/dehydrogenation, catalytic cracking

of C-C bonds, alkylation, and isomerization are dominant reactions during hydrocracking. These reactions occur simultaneously making the hydrocracking reaction an overall exothermic process [24]. Hydrogenation/dehydrogenation reaction is attributed to the metal phase. While isomerization, alkylation, and cracking of C-C bonds are associated with the acid phase [25]. Alternative mechanisms propose that hydrogenation also occurs on acid sites by hydrogen spillover [26].

Phenanthrene is fed to TBR as a 2.0 %wt solution in cyclohexane. Since cyclohexane's critical point is at 281 °C and 40.7 bar, TBR is maintained at 70 bar and below 300 °C in order to keep cyclohexane in a liquid phase. The phase diagram of the cyclohexane-hydrogen system at the given conditions is shown in Appendix B (Figure B-1). The phase diagram indicates that the molar liquid fraction of cyclohexane is 1. For reactions at temperatures above the critical temperature of cyclohexane, the density of the solvent will decrease from 0.775 g/mL to 0.273 g/mL [27] [28]. At critical conditions, liquid and gas phases coexist, and the densities of the two phases are identical. However, phenanthrene requires liquid cyclohexane to flow through the catalytic bed. Therefore, it is recommended to keep the temperature under 300 °C and pressure over 70 bar.

3.3 Tubing and fitting material

The material must be mechanically resistant to corrosion at the operating conditions (i.e., temperature and pressure) [29]. For high hydrogen pressure, the risk of a High-Pressure Hydrogen Attack (HPHA) over steels with high carbon content must be considered [30] [31] [32] [33] [34]. Figure B-2 in Appendix B shows that stainless steel with 0.25 %Wt of carbon is susceptible to HPHA when the temperature exceeds 210 °C, while for steels with Cr and Mo, the HPHA occurs above 400 °C. For that reason, SS316 (0.08 %Wt carbon content) with an HPHA risk above 600 °C was selected for this work.

The ASME BPV code section D1 shows how to determine the material resistance to the pressure with respect to the working temperature for cylindrical reactors [29]. Cylindric or tubing thickness is calculated by Equation 3.1. That allows relating the wall thickness of tubing with the operating conditions of the process.

$$t = \frac{P_i D_i}{2S - P_i} \qquad Eq.3.1 \quad [23]$$

Where P_i is the working pressure in ksi (1ksi = 1000 psi), Di is the internal diameter in inches, t the wall thickness in inches, and S is the maximum pressure stress allowed for the material in ksi. The S value for different materials and temperatures is shown in Table B-1 (Appendix B). Thus, the reactor's internal diameter was settled at 7.62 mm (3/10 inch internal and 1/2 inch external diameter), which is the tubing offered by Swagelok with higher temperature and pressure stress resistance. Table 3-1 showed that tubing with an external diameter of 1/2 inches requires wall thickness larger than 0.065 inches to sustain 180 bar of pressure at 450°C.

Table 3-1 Pressure and temperature resistances of stainless steel (SS316) for different tubing diameters

		Maximum pressure resistance (bar)		
External diameter of tubing (in)	**Thickness (in)**	**38°C**	**260°C**	**482°C**
0,125	0,01	204,3	135,9	117,5
	0,016	313	208,1	179,9
	0,035	603,3	401,2	346,9
0,25	0,01	106,1	70,5	61
	0,016	338,7	225,2	194,7
	0,035	569,1	378,4	327,2
0,5	0,01	54,1	36	31,1
	0,016	317,3	211	182,4
	0,035	292,6	261,1	225,8

3.4 Engineering design of a trickle bed reactor

Laboratory scale TBR is designed according to the different transport processes occurring at various time and length reactor scales in a reaction [4]. The microscale process considers the events on the active sites of the catalysts. Mesoscopic processes take into account the molecular transport through the mesoporous channels of catalysts. While macroscale regards the bed scale mass transport processes [1]. The main focus of this research is the understanding of properties on the active sites of the catalysts. The mesoscale and microscale mass transport limit the rate of reaction. Thus, it is required to operate the system under a pulsing flow hydrodynamic regime. Larachi et. al [35] correlated the fluid

properties, flow operational conditions, and the dimension of the reactor with the flow regime for high-pressure processes, based on the Charpentier and Favier diagram [18], shown in Figure 3-1. Table 3-2 shows the bed and reactor dimensions based on an extended Charpentier and Favier diagram.

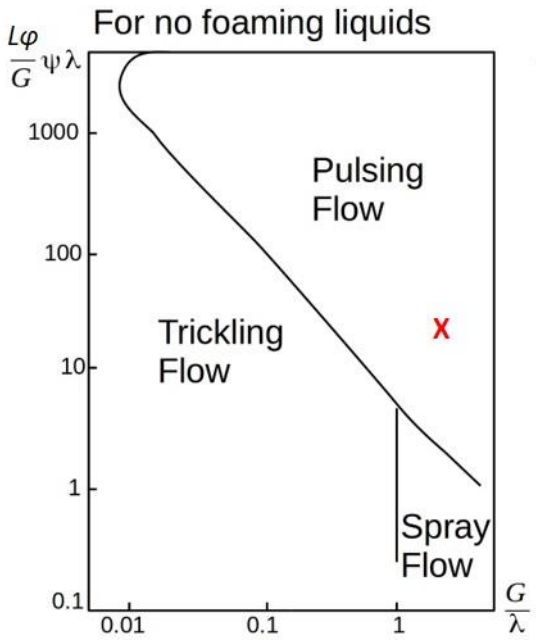

Figure 3-1 Extended Charpentier and Favier diagram adapted from [1]. Red “X” in the plot indicates the flow regime at the operational conditions given in Table 3-2.

Pellet diameter was determined considering the heuristic proposed by C. Perego et. al. to operate TBR in a pulsing flow regime, shown in Table B-2 (Appendix B) [12]. Charpentier and Favier's equation was applied varying liquid flow rates from 0.1 mL/min to 4 mL/min and gas flow rates from 10 mL/min to 100 mL/min. The final calculation indicated that at the gas flow of 45 mL/min, the liquid flow must be higher than 1 mL/min to operate the TBR under a plug flow regime (high interaction regime). Symbol “X” in Figure 3-1 shows with a red, the position in the extended Charpentier and Favier diagram at the given operating conditions.

Table 3-2 Reactor dimensions and bed configuration.

Reactor dimension	**Value**
Bed Diameter-D_B (mm)[1]	5.308
Bed length-L_B (mm)	10
Bed volume-V_B (mm^3)	142

Transversal area-A_T (mm^2)	37.7
Pellet diameter-d_p (mm)[2]	0.044
L_B/d_p	222
D_B/d_p (a)	118
Bed porosity[3]	0.362

[1] Bed diameter is defined as the internal diameter of a tubing 1/2 inch minus the external diameter of thermowell (1/8 inch) located along the axial center of the reactor.
[2] Sieve size 200x325, corresponding to a pellet diameter between 0.044 mm to 0.074 mm.
[3] Bed porosity calculated according to [4], explained in Appendix B.

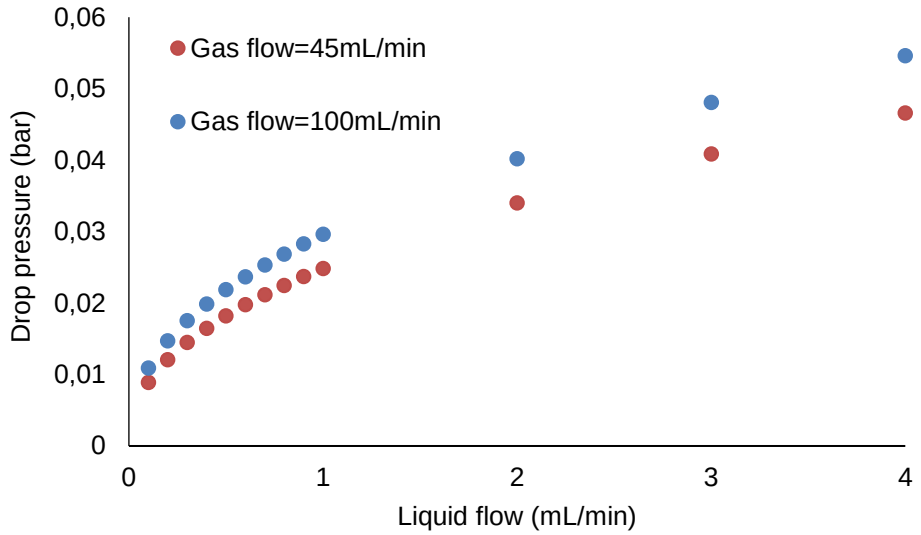

Figure 3-2 Drop pressure of the gas as a function of liquid and gas flow rate. (brown) associate to the gas flow rate 45mL/min, (blue) associate to the gas flow rate 100 mL/min. Drop pressure was calculated according to Kan and Greenfield expression [1]

Figure 3-2 shows the drop pressure in a TBR at a different liquid and gas flow rate. Figure 3-2 shows that at elevated liquid flow (> 2 mL/min), drop pressure ranges from 0.04 to 0.05 bar. That drop pressure could be negligible at 70 bar of pressure. Another parameter describing the distribution of phases in the bed is the liquid holdup. The liquid holdup is the liquid fraction in the bed during operation [1] [29]. The liquid holdup is divided into a dynamic and static holdup. They are defined by flowing liquid and the liquid retained by the capillarity forces of particle pores and wall effects, respectively [1] [36] [37]. Design parameters such as wetting efficiency, heat, and mass transfer coefficients depend on liquid holdup. Estimation of the liquid holdup is based on the expressions proposed by Wammes et.al [38] and Larachi et.al [35]. The estimated liquid holdup was then compared to the reactor

dimensions given in Table 3-2 and the same liquid and gas flow ranges. Figures 3-3 shown that the liquid fraction occupied for our TBR achieves 0.45 at 1 ml/min of liquid flow rate where approximately 0.05 corresponds to static holdup. Such high liquid holdup is typical of TBR operating under high interaction regime.

The wetting of the catalyst particles depends on a liquid and gas flow. Bedwetting efficiency is determined using the expressions proposed by Dudukovic and Mills (Figure 3-4-I) [39] [40]. Figure 3-4-II shows that at a gas flow rate of 100 mL/min the wetting efficiency remains below 30%. Operation of TBR with the gas flow rate of 45 mL/min or lower guarantees wet efficiency above 45 %. Besides, the proposed TBR hardware has a thermowell crossing in the middle of the bed. That positively contributes to bedwetting efficiency by increasing capillary forces and directing liquid flow toward the catalytic bed.

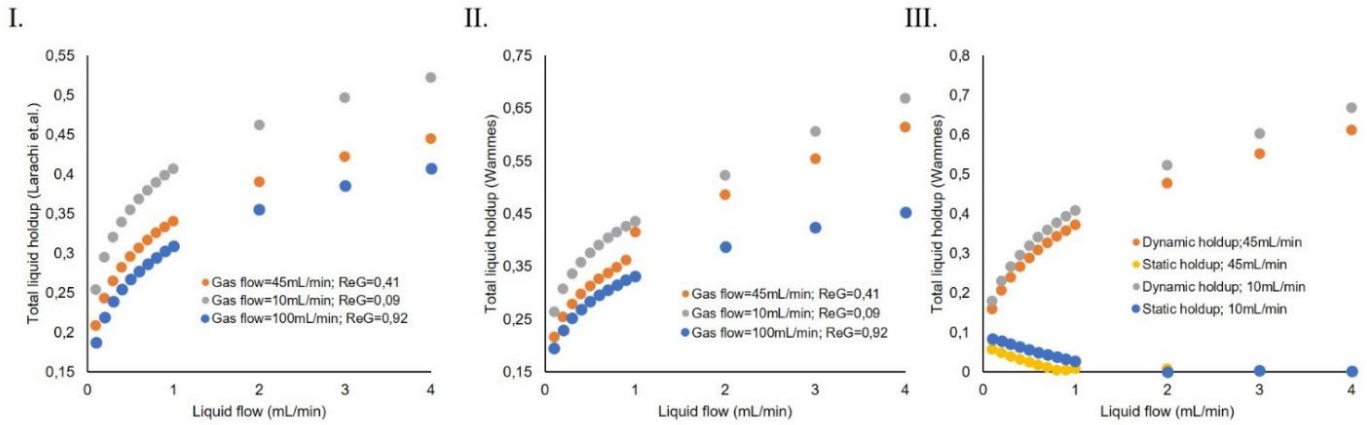

Figure 3-3 Total liquid holdup of the TBR at different gas and liquid flow rates. I) Total liquid holdup according to Larachi et. al. (1991), II) Total liquid holdup according to Wammes and Westerterpery, 1991. III) Dynamic and static liquid holdup according to Wammes and Westerterpery, 1991.

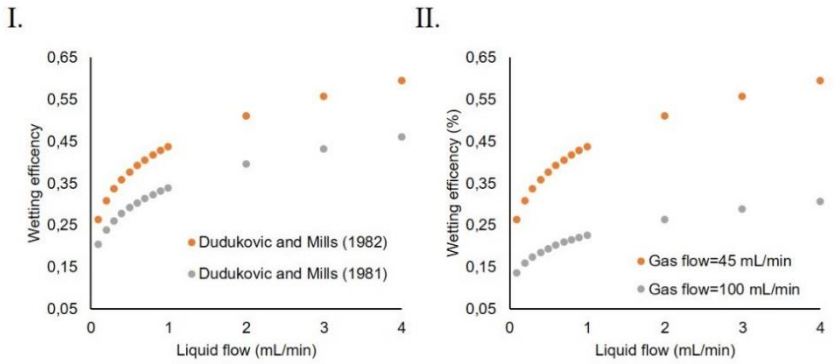

Figure 3-4 Bedwetting efficiency at different gas and liquid flow rates. I. Wetting efficiency according to Dudukovic and Mills, 1981;1982 and II. Wetting efficiency at different gas flow rates.

Mass transfer between phases (gas-liquid, liquid-solid, and gas-solid) in a TBR is usually lower than in other reactor configurations due to an absence of a rigorous mixing mechanism [1] [29]. Therefore, mass transfer rates often become the rate-limiting step in the performance of the process. Illiuta et.al. [41] correlate mass transport coefficients between liquid and gas phases (K_{GL}) with dynamic liquid holdup, drop pressure, and bed length as it is shown in Appendix B.

K_{GL} multiplied by the liquid-gas interfacial area (a_{GL}) with values over 0.035 1/s indicates that the TBR operates at a pulsing flow regime (i.e., high interaction regime), as shown in Figure B-10 (Appendix B) [41]. Table B-3 shows the $K_{GL}a_{GL}$ values calculated under the proposed hardware reactor configuration at different liquid flow rates. The table shows that even at the lower liquid flow rates, $K_{GL}a_{GL}$(=0.22 1/s) is higher than 0.035 1/s suggesting that the gas-liquid mass transfer is not the limiting factor in the reaction. Liquid-solid mass transfer coefficient (K_{LS}) expressed in terms of Schmidt number and Reynolds number with wetting factor was estimated following the Eq. 3.3:

$$\eta_W Sh = a{Re_L}^b Sc^{1/3} \quad ; Sh = \frac{K_{LS} d_p}{D_B} \quad Eq.3.3 \quad [42]$$

Constants a and b proposed by various studies are given in Table B-4 [1] [43] [44]. K_{LS} coefficients calculated for all the approaches ranged from 0.01 m/s to 0.05 m/s at 0.1 mL/min of liquid flow rate and 45 mL/min of gas flow rate, which are higher than the experimentally values reported in Figure B-11. Thus, the liquid-solid mass transfer could not limit the reaction product yield.

$$K_{LS}a_s\varepsilon_s = 0.75D_{H_2,L}\left(\frac{dR}{dp}\right)^{0.82}\left(\frac{\delta_L u_L}{\mu_L}\right)^{0.9} {Sc_{H_2,L}}^{0.5} \quad Eq.3.4$$

However, according to the expression proposed by Nelson and Galloway [44] (see Eq. 3.4), K_{LS} tends to zero. The expression proposed by Nelson and Galloway [44] expresses K_{LS} in terms of the porosity and surface area of catalysts. In the case of USY zeolites, these values are high (see table 2-1 in chapter 2). Therefore, the incomplete wetting of zeolite pores could be the limiting factor in the reaction.

$$K_{GS} = 0.18\left(\frac{D_{H_2,]G}}{dp}\right){\varepsilon_s}^{0.33}({\varepsilon_s}^{-0.33} - 1)(Re_G){Sc_{H_2,G}}^{2/3} \quad Eq.3.5$$

The gas-solid mass transfer coefficient (K_{GS}) was calculated using the Nelson and Galloway expression (Eq. 5) which depends on the gas Reynolds number, self-hydrogen diffusivity, and solid porosity [45]. K_{GS} coefficient calculated with that expression is 0.18 m/s, which is considered a high value compared with the other coefficients. The calculation of mass transport coefficients for TBR has been extensively studied in the literature [1] [43], there are few works related to high-pressure systems [29].

Finally, the criterion proposed by Mears et.al [45] was applied to define the minimal bed length, so the reaction does not present limitations for axial dispersion (See E.q. 3.2). According to Mears et.al. [46], the bed length must be longer than the function at the right side of Equation 3.2 to ensure no axial dispersion in the stream of reaction.

$$\frac{L_B}{d_p} > \frac{20n}{Pe_L}\ln\left(\frac{C_{in}}{C_{out}}\right) \qquad eq.3.2$$

Where n is the order of reaction, and Pe_L is the liquid Peclet number. Axial dispersion refers to the degree of back mixing and molecular diffusion of fluid elements in the axial direction [46][21]. Figure B-12 shows that the ratio L_B/d_p is higher than the expression of the Pe_L number in the entire range of d_p, for the given reactor conditions and assuming 50% of conversion efficiency. It means that at such short bed lengths the back mixing by axial dispersion is negligible.

For the purpose of this work, TBR dimensions, bed configuration, gas and liquid flow rates were chosen considering the available materials, key hydrodynamics parameters, and to facilitate a pulsing flow operation. The TBR tubing with a wall thickness of 0.083 was chosen

because of its high thermal and pressure resistance (max temperature 450°C; max pressure 225 bar). 0.2 bar of pressure drop for a bed length and particle diameter set in 1 cm and pellet diameter 0.45 μm are negligible for a TBR operating at 70 bar. The Peclet number criteria corroborate that under selected operating conditions, TBR does not suffer axial dispersion. Theoretical estimation of the liquid holdup, bed wetting efficiency, and mass transport coefficients allowed for the prediction of liquid and gas flow rates at which TBR operates in a high interaction regime. Results suggest operating the TBR at high liquid flow rates and low gas flow rates to guarantee a high interaction regime.

3.5 Description of reactor layouts considered

This section describes details about the TBR arrangements considered during the design. Figure 3-5 shows the process stages for hydrocracking without considering recycling systems [47]. The location, piping arrangements, and security of each process stage are briefly discussed below.

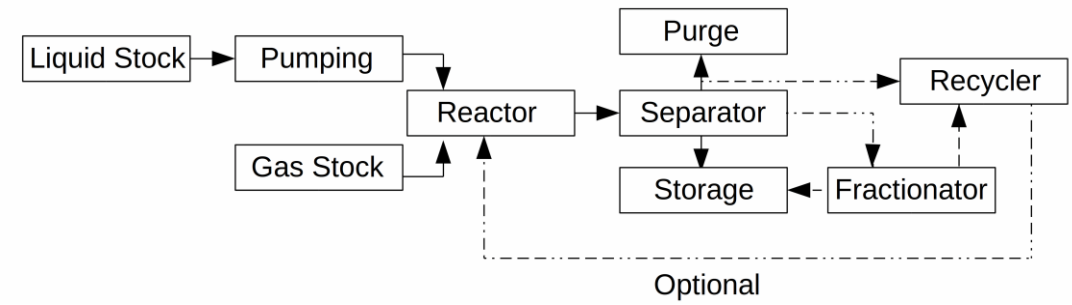

Figure 3-5 Process stages for hydrocracking in a TBR.

3.5.1 Liquid storage system

The capacity of the feedstock storage tank should sustain a continuous operation. In the case of highly volatile or very viscous feedstock, a jacketed vessel to control the temperature can be installed. When the tubing that connects the storage tank with the pumping system has small internal diameters, the gravity force is not enough to propel the liquid to the pump; then, a push gas is required. The push gas should be an inert and insoluble gas with respect to the liquid feedstock. Also, it should have a relief valve and a pressure indicator as a security instrument.

The inlet of the push gas to the storage tank should be located at the top of the tank to avoid foam formation. The push gas line should be always equipped with an escape valve, for the cases of evacuation or feeding the liquid feedstock. The feeding of the liquid feedstock may take place on the top or the bottom of the storage tank, as shown in Figure 3-6.

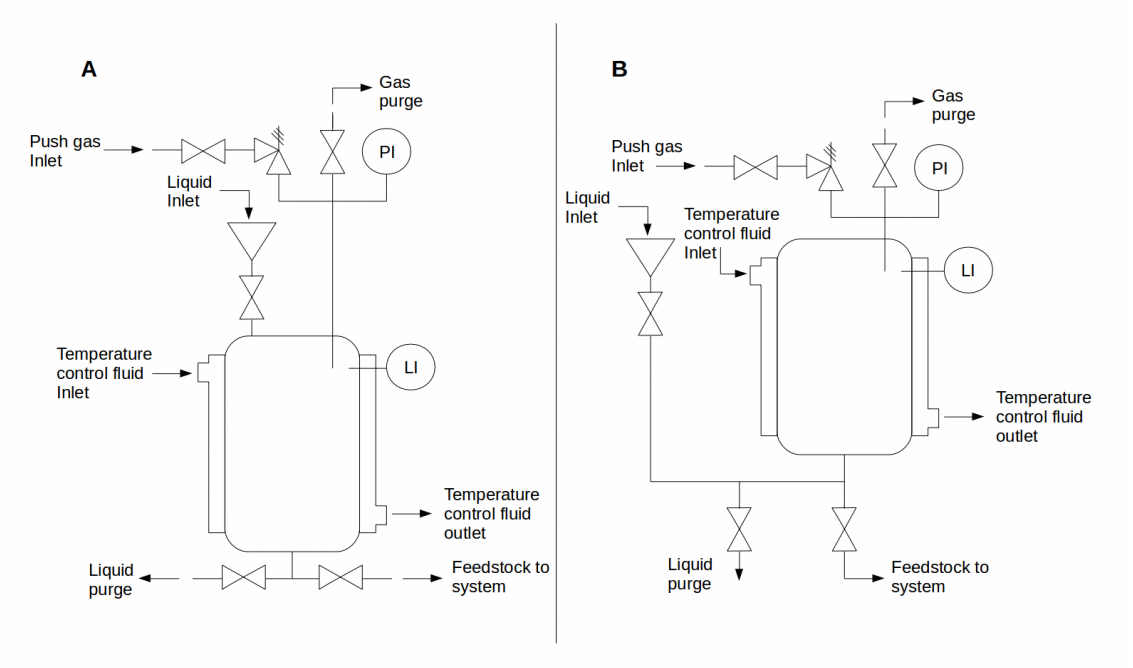

Figure 3-6 Arrangements for a liquid storage system.

3.5.2 Pumping system

The pump choice should be based on lifetime, endurance, safety, maintenance, and reliability [29]. If required flows are lower than 1 mL/min, micro-metering pumps are the best option. Piston, diaphragm, gear, and spinning pumps are the types of micro metering pumps available. These kinds of pumps can operate with one or two pulsation-free metering flows (e.g., 10 to 103 mL/h), allowing for pressures up to several thousand bar. Pumps with systems in parallel controlled by sensors can also be operated without essential interruption. By superposing two displacement pistons, or by controlling the angular velocity with a special cam drive, small metering flows with low pulsation are achieved up to a pressure of 700 bar [29].

To preserve the integrity of the pump it is recommended to place a filter at the inlet of the pump to prevent particulate material from entering. Additionally, in a multiphase system, as is the TBR, it is recommended to place a check valve after the pump, to avoid gas-fluids black flow into the pump.

3.5.3 Gas feeding system

The feeding of gas to the process may be done either through a compressor or just with the pressure force of the gas cylinder. The inlet flow can be controlled employing (i) a millimetric needle valve or (ii) a gas flow controller. In both cases, a valve has to be installed before the flow controller, which allows closing the gas flow in case of emergency. In the latter case, a filter must be installed to protect the gas flow controller of any liquid or solid impurities. To avoid the backflow of the liquid feedstock into the gas flow controller, a check valve must also be placed after the controllers.

3.5.4 Reaction system

The reaction system is divided into two sections: (i) external and (ii) internal. The external section includes the arrangement for sampling, the heating system, the feeding of fluid phases, and the setup for temperature monitoring. The internal section includes the holder of the packed bed and the thermocouple arrangement inside the reactor.

3.5.4.1. External section

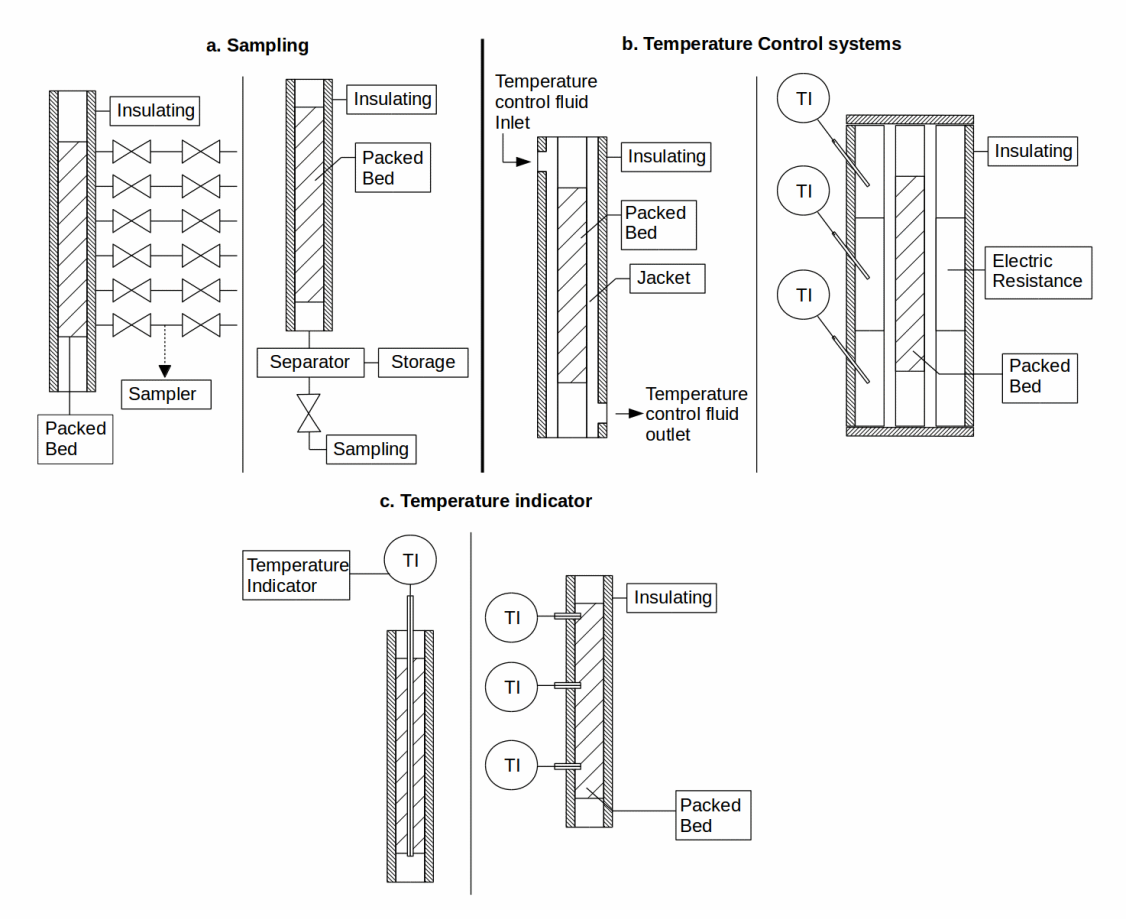

Figure 3-7 Reactor arrangements for a) sampling, b) temperature control systems, and c) Temperature indicator

Sampling can be carried out as: (i) in situ or (ii) after the reaction. In situ sampling is possible by locating the valves along the packed bed. In situ sampling is schematically demonstrated in Figure 3-7a. The advantage of in situ samplings is monitoring chemical reactions for axial location of the packed bed. However, the next operating considerations should be considered:

- In situ sampling requires at least two valves placed in series for each sampling point. The first valve serves to open/close the reactivation system. The second valve sets the outlet sampling flow.
- The section between the valves must provide the volume that corresponds to the amount required for the sample.

- During sampling, there is a high risk of leaks due to high temperature and pressure.
- Heating the reactive packed bed is not easy when using an oven, since it requires putting the sampling valves through complex arrangements of piping.

The temperature can be adjusted by using a thermal fluid or an electrical oven (Figure 3-7b). The electrical oven offers shorter response times, a simple control setup, and enables higher operation temperatures. Generally, the reactor ovens have at least two electrical resistances, each one of them with its independent power control. Independent power control enables a longer isothermal region in the reactor tube. If the test reaction requires temperatures below ambient temperature, the jacket with cooling fluid can be installed around the reactor. The temperature monitoring can be made by means of thermocouples in various configurations. The two common configurations are shown in Figure 3-7c. A thermowell inside the packed bed (Figure 3-7-c) is less accurate and its operation is harder, but it allows for temperature monitoring at several axial points in the reactor. The internal diameter of the thermowell should be only slightly larger than the external diameter of a thermocouple to avoid heat losses in the intermediate empty spaces.

Liquid feedstock can be fed into the reactor through the same line as gases or through a different line. When the purpose of the TBR study is the liquid phase distribution, the feeding is made in separated lines. A liquid distributor is recommended in the internal section to ensure the complete wetting of catalysts [48]. The feeding through the reactor bottom also ensures the full contact between the catalyst with the liquid feedstock [12]. The reactor should have a pressure gauge and a relief valve for over-pressure situations or explosions while using flammable substances. These safety systems can be found at the reactor inlet or its outlet.

3.5.4.2. Internal section

The bed packaging is placed over a holder, which can be a mesh, a porous tablet holder, or a tubing. The holder material should be chemically inert and resistant to operating conditions. For the packed bed made of small pellets, the porous tablet holder may be the best choice. The tubing holder is practical, but it must fulfill the following conditions: i) it does not work for pellets with a very small size, and ii) the external diameter should tightly fit the internal diameter of the reactor, to prevent pellets from falling in between. The mesh can be used when the internal diameter of the reactor allows it. A disadvantage of the mesh is that it alters the bed geometry and contributes to the pressure drop. Figure 3-8 shows several arrangements of bed packaging.

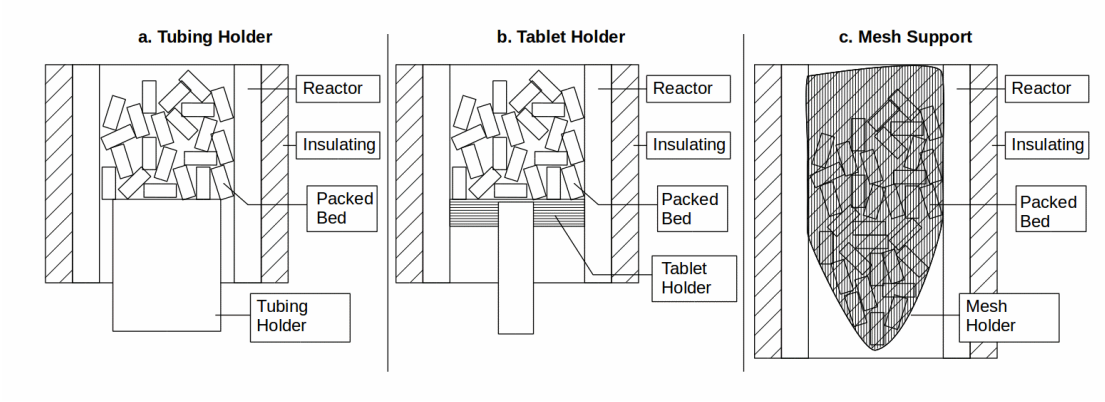

Figure 3-8 Packed bed holders. a) Tubing holder, b) tablet holder, c) Mesh support.

3.5.5 Phase separation systems

Due to the triphasic nature of TBR and the fact that the sampling can only be carried out in one phase (liquid or gas), it is essential to implement a phase separation system. The separation depends on the chemical and physical properties of the present substances. Therefore, the design should be specific for each process. If the liquid and gas phases have a significantly different boiling point (i.e., hydrocracking), the separation systems shown in Figure 3-9 can be used [42]. Figure 3-9a shows flash separators that take advantage of the

expansion and gravity force. The gas leaves the tank through the top and the liquid through the bottom.

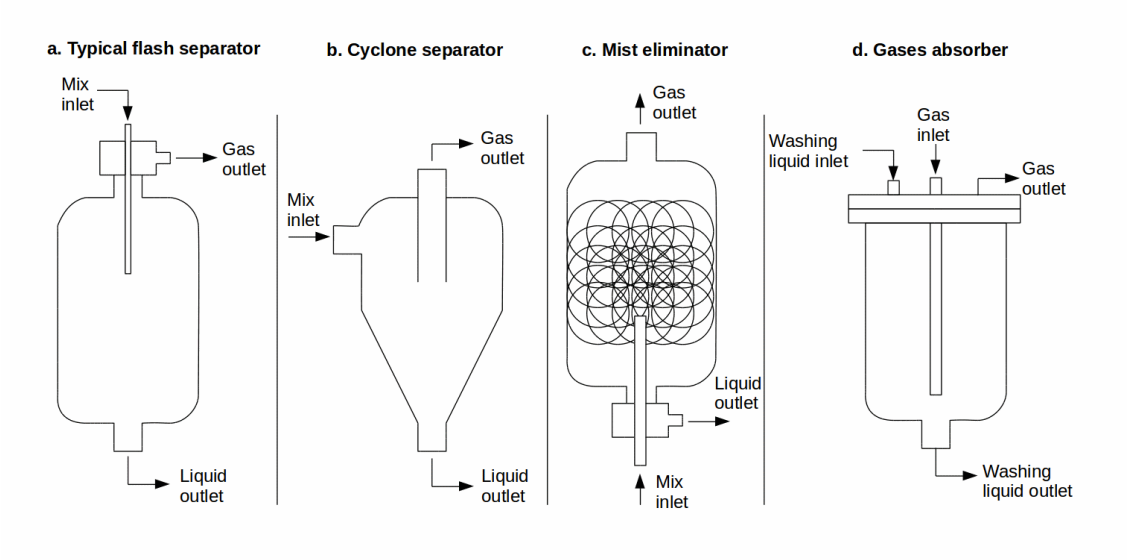

Figure 3-9 Arrangements of the gas-liquid separator. a) Flash separator, b) Cyclone separator, c) Mist eliminator, d) gas absorber.

3.5.6 Pressure control and gas washing systems

The pressure control system must sustain pressures above 100 bar. The pressure control system is placed at the gas outlet and can consist of an automatic pressure controller or a manual millimetric valve. A phase separation system (i.e., mist eliminator) must be placed before the pressure controller to prevent the entry of any liquid. A mist eliminator arrangement is illustrated in Figure 3-9c.

A gas washing unit is required when the outlet gas contains pollutants, such as hydrogen sulfide (H_2S) frequently found in hydrotreatment processes. To wash off sulfides, washing units use strong hydroxides such as NaOH or KOH [47]☐. Figure 3-9d proposes an arrangement of a gas washing system.

3.5.7 Gas Mass Flow Control (GMFC)

Automatic control is recommended for continuous and laboratory systems. However, the control can be conducted manually by means of a millimetric valve. The choice of the GMFC should consider gas flow ranges, chemical reactivity of the gas, response time, pressure and temperature resistance, and the required accuracy. All GMFCs exert control action

through a solenoid valve, bellows valves (for low-pressure systems) or a variant pressure valve (for oscillating pressure systems) [49] [50].

3.6 Detailed design: Piping and fitting dimensions, schematic design of process instrumentation.

The detailed schematic design follows the block diagram proposed in Figure 3-5. Note, that recycling options are not presented here. The piping of the liquid storage system (Figure 3-6b) has 1/4 inch of external diameter and used fittings sealed with splints (OD type connector). The main storage tank has female NPT connections. Hence it is required to use an adapter at the inlet and outlet of the tank that allows changing NPT connection to OD type connector. A double piston micro-metering pump was selected to move, liquid phase, with flow rate 0.001-5.000 mL/min and pressure between 20-1200 bar. The piston micro-metering pump connectors of 1/16 inch required an adapter to connect to the ¼ inch tubing.

The maximal TBR pressure is limited by the pressure in the hydrogen cylinder (maximum 140 bar). A thermal Gas Mass Flow Controller (GMFC) from Bronkhorst® with a solenoid valve and 1/4 inch OD connectors controlled the gas flow rate. The GMFC was chosen considering the high pressure of the hydrocracking reaction. Before the reactor, the gas and liquid are mixed in the tee connection. This allows feeding into the reactor by one single line.

The temperature control utilizes an electric oven with three electric resistances to independently maintain a large isothermal region in the reactor tube. A PID controller regulates the oven voltage to keep the reaction at the desired temperature. K-type thermocouple with 1/16 inch of external diameter was employed to measure the temperature inside the catalytic bed. Thermocouple contact with the catalytic bed was indirect because the thermocouple was enclosed in a thermowell of 1/8 inch inner diameter. Thermowell is an SS316 tubing. At one end it was sealed by silver solder and enough length to an extent throughout the oven. This way, the solder end did not reach high temperatures during operation.

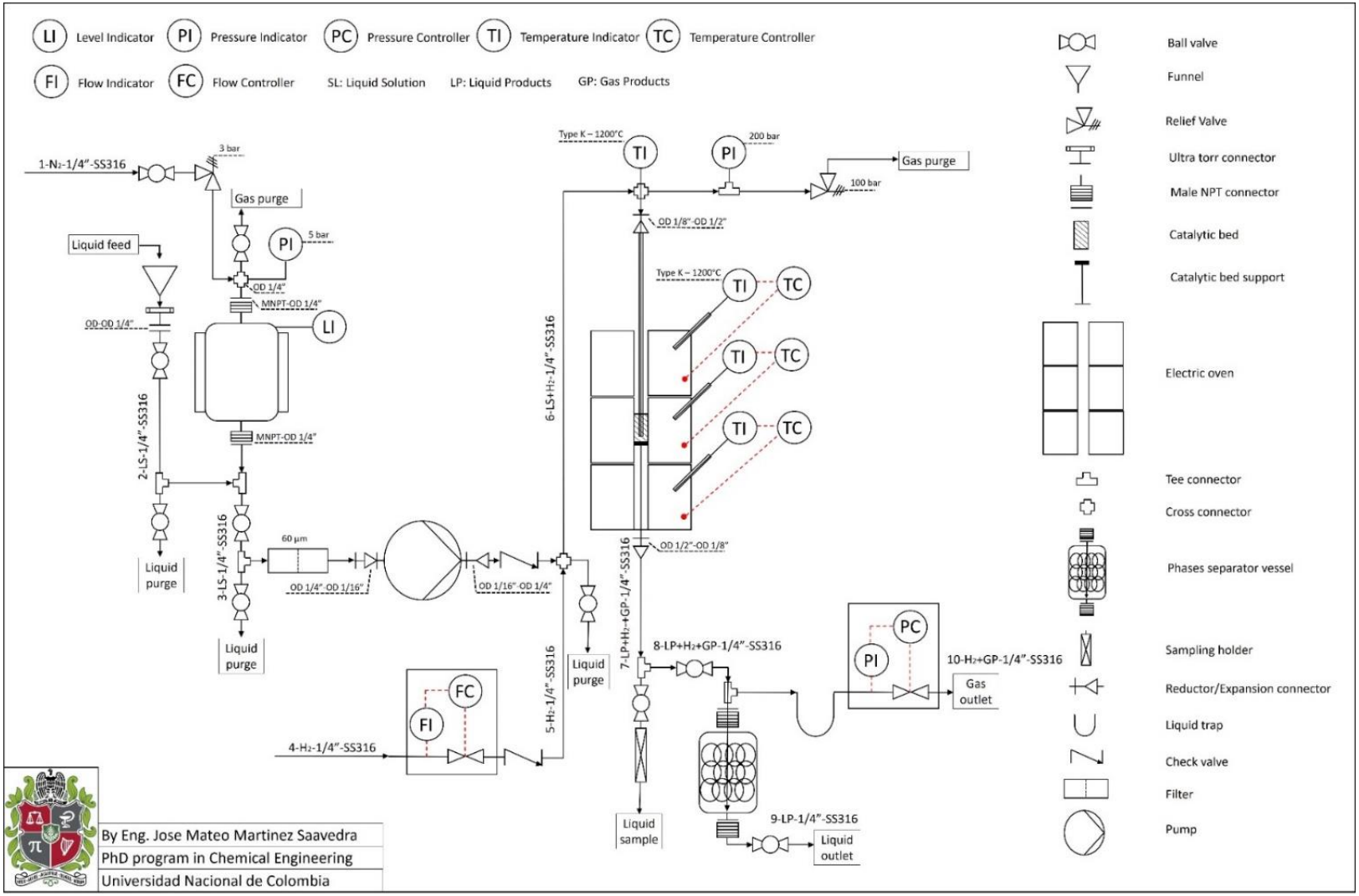

Figure 3-10 P&ID diagram of a TBR for hydrocracking process.

The reactor is a 1/2 inch tube 60 cm in length, taking into account that the electric oven is 45 cm high. A 1/4 inch tube supported the catalytic bed located in the isothermal zone of the reactor tube. The mist eliminator shown in Figure 3-9c was chosen as a phase separation system preventing the liquid from entering the Back Pressure Control (BPC) placed in the gas outlet. A gas washing system after BPC was installed for the possible study of the hydrodesulfurization process. The entire system Piping's and Instrumentations diagram (P&ID) is shown in Figure 3-10.

3.7 Experimental evaluation of the constructed TBR

3.7.1 Catalyst preparation

A composite of 40%Wt of γ-Al_2O_3 was prepared from CBV600 commercial USY zeolite and aluminum hydroxide (Pural TH100, Sasol®). Aluminum hydroxide was soaked in an aqueous solution of acid nitric at 1 %v/v. Then, CBV600 USY zeolite was mixed with aluminum hydroxide at the desired ratio. The blend was extruded through a syringe to form pellets. Pellets dried at room temperature for 8 hours and then heated up at 3 °C/min until 550 °C for 8 h. At 550 °C impurities and internal water are removed from the catalyst surface. At this stage, the γ-Al_2O_3 phase is formed. Finally, pellets were crushed and sieved to a particle size between 45 µm and 150 µm.

The precursor salt of platinum ($Pt(NH_3)_4Cl_2$) was added over the pellet surface by wet impregnation. Wet impregnation adds up 0.85%Wt of platinum to the total mass of the catalyst. Wet impregnation was performed by rotary evaporator in a vacuum atmosphere at 90 °C and 90 rpm, while keeping the pH of the solution at 5.2. Under these conditions, platinum is impregned preferably over zeolite than over γ-Al_2O_3 [51]. J. Zecevic et. al. impregnated a blend of HY zeolite-alumina with platinum using ($Pt(NH_3)_4Cl_2$) and hexachloroplatinic acid (H_2PtCl_6). They found that platinum is deposited better over zeolite when using $Pt(NH_3)_4Cl_2$ whereas deposition over alumina was better with H_2PtCl_6. Water was removed in a rotary evaporator and the solid product was oven-dried at 100 ºC before being loaded into the reactor. Platinum activation was carried out in the reactor under a vacuum atmosphere at a heating ramp of 2 °C/min until 350 °C. Then, TBR was kept at 350 °C for 30 minutes at 50 bar of hydrogen.

3.7.2 Characterization

CBV600 USY zeolite was characterized by XRD, N_2 physisorption, FTIR pyridine desorption, and i-Pam decomposition, as described in Chapter 2. Additionally, the final catalyst was characterized by H_2 chemisorption as described in Chapter 2. Scanning transmission electron microscopy (STEM) imaging was taken in a Titan G2-300 from FEI, in collaboration with the Technical University of Munich (TÜM) Germany.

3.7.3 Reaction test

Two reaction tests were carried out to validate the TBR designed to study the effect of catalyst properties on a phenanthrene hydrocracking reaction. Reactions were performed at the following operational conditions: 70 bar, 300 °C, 0.15 g of 1%Wt Pt/[CBV600-USY (40%Wt)/γ-Al_2O_3] catalyst. Additionally, catalysts were diluted in 1.5 g of SiC and supported over the compacted spun glass. The first test verifies the work of Perego examining mass transport limitations in a TBR [12]. The mass transport limitation test consisted of two reactions using 0.15 g and 0.3 g of catalyst while keeping almost the same contact time for both reactions. In the first trial the liquid flows were: 0.2; 0.4; 0.6; 0.8, and 1mL/min. In the second trial the liquid flows were: 0.4; 0.8; 1.4; 1.8 mL/min. Therefore, both test trials were carried out at almost the same contact times: 1.20; 0.60; 0.34 and 0.24 minutes for the first trial, and 1.20; 0.60; 0.34 and 0.26 minutes for the second trial. Samples were taken at 30 minutes intervals. When the liquid flow changed, the interval between sampling was 1h to guarantee that the system achieved stable liquid flow.

The temperature effect on the reaction was studied using 0.15 g of 1 %Wt Pt/[γ-Al_2O_3] at 70 bar and 1mL/min of liquid flow rate. The reaction was carried out at temperatures 270 °C, 285 °C, and 300 °C. Samples were taken every 30 minutes. With temperature change, the interval between sampling was 1h to guarantee that the system achieved thermal stability. Finally, to study the effect of γ-Al_2O_3 in the reaction, the same reaction was carried out using a 1wt%Pt/γ-Al_2O_3 catalyst.

Liquid samples were analyzed using an HP GC 5890 series with an FID detector and a DB-5 column of 50 m. The temperature program initiated at 70 °C was maintained for 4 minutes to separate lighter products. The temperature was further ramped at 30 °C/min until 250 °C and kept for 16 minutes. At this time temperature section, phenanthrene, and heavy

products were eluted and detected by FID. 1,3,5-Tri-isopropyl benzene (TiPB) was used as an internal standard after sampling.

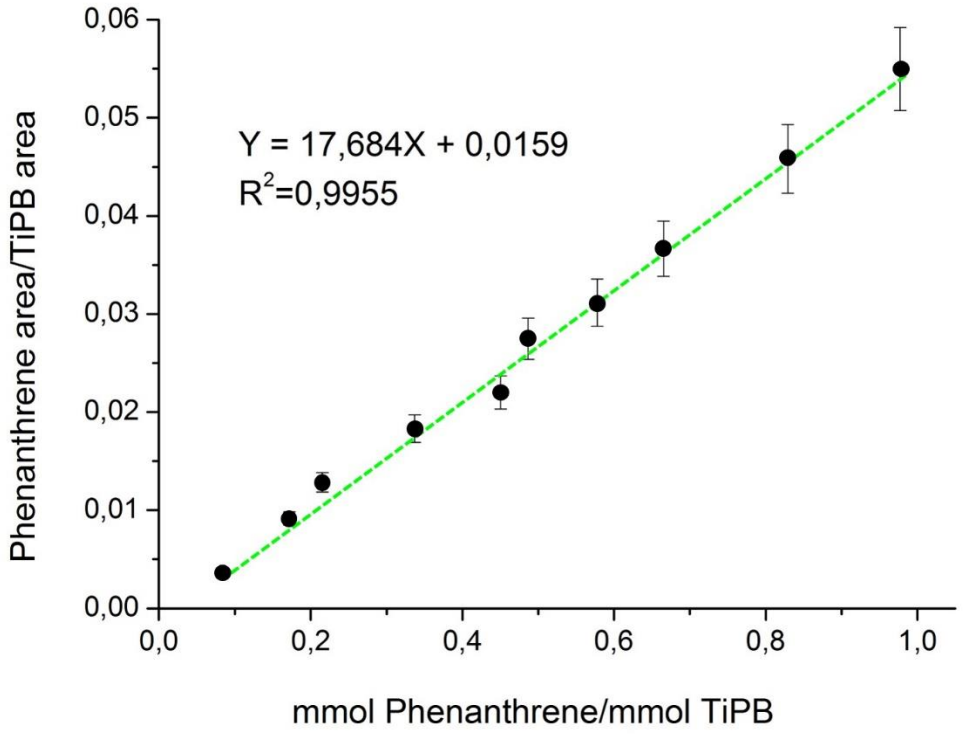

Figure 3-11 Calibration curve FID response as a function of Phenanthrene/TiPB concentration.

Phenanthrene concentration was calculated following the calibration curve which correlates the integration area of the FID signal to the concentration of the phenanthrene. The response factor of the phenanthrene was corrected according to the effective carbon number (ECN) reported in the reference [52]. The linear equation and the resulting calibration lot of the calibration curve are shown in Figure 3-11.

Phenanthrene conversion efficiency was calculated according to the following equation:

$$\%Phenanthrene\ Conversión\ = \frac{\frac{A_{Phen_0}}{A_{TiPB_0}} - \frac{A_{Phen_i}}{A_{TiPB_i}}}{\frac{A_{Phen_0}}{A_{TiPB_0}}} \times 100\,; \quad Eq.3.3$$

Where $APhen_0$ corresponds to the integration area of the initial phenanthrene feedstock at time 0. A_{Pheni} is the integration area of the phenanthrene signal at the time i. A_{Tipb0} corresponds to the integration area of TiPB at time 0, while A_{TiPBi} is the integration area of the $TiPB_i$ signal at the time i. The reaction rate was calculated using the general mass balance for FBR/TBR showed in Eq. 3.4 [53]:

$$-r_i = C_0 \frac{dX}{dW} \; ; \quad Eq. 3.4$$

3.7.4 Results and discussions

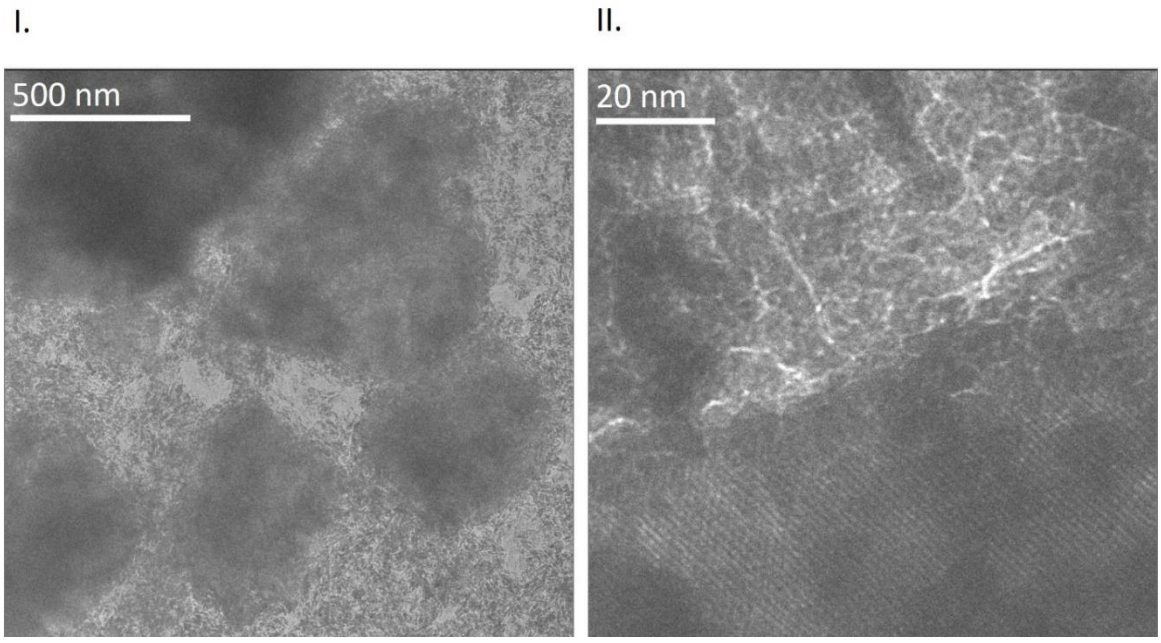

Figure 3-12 TEM image of CBV600 USY zeolite with 40 %wt of γ-Al_2O_3. I.) Zeolite crystals distribution in γ-Al_2O_3, with scale 500 nm; II.) Zeolite-γ-Al_2O_3 interphase, with a scale of 20 nm.

The main structural and acid properties of the CBV600 are presented and discussed in Table 2-1 in Chapter 2. Figure 3-12 shows the TEM pictures of the zeolite-γ-Al_2O_3 composite at a different order of magnification. The darkest zone in the picture corresponds to a zeolite particle incorporated into the amorphous γ-Al_2O_3. The estimated zeolite particle size is between 350 nm and 500 nm. Figure 3-12-II shows the crystalline structure of the zeolite along with the interphase between the crystalline phase and amorphous phase. Additionally, Figure 3-12-II reveals white, bright, non-uniform lines in the amorphous phase.

These lines may act as channels to transport bulk liquid phenanthrene to the zeolite crystals [54].

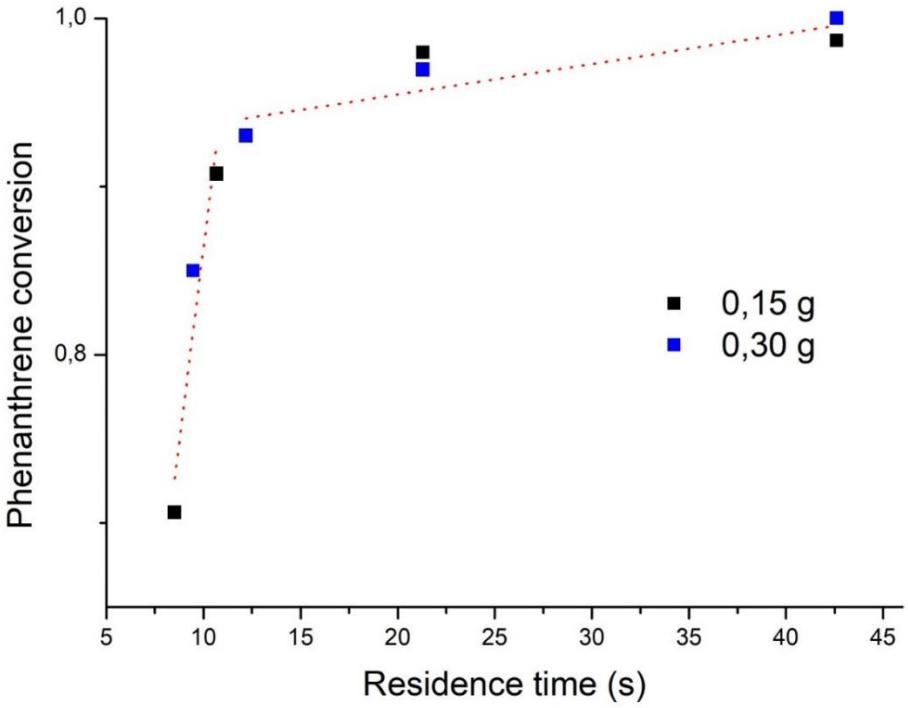

Figure 3-13 Phenanthrene conversion efficiency as a function of residence time and the amount of catalyst, at 300°C and 70 bar.

Figure 3-13 shows that conversion efficiency depends on the residence time. At long residence times of liquid feedstock (low liquid flow), the conversion efficiency is near to 100%. At 12.5 s the conversion efficiency suddenly drops (0.7 mL/min in the bed of 0.15 g or 1.4 mL/min for the bed of 0.30 g). Increasing the liquid flow rate decreases the residence time, reducing the probabilities of catalytic reaction to occur. At these conditions, Reynolds number is high enough to liquid form swirls over pellet surface. These swirls over the pellet surface contribute to reducing extra-particle diffusion limitations. This finding agrees with the hydrodynamic analysis, where high liquid flows (low residence time) help to operate the reactor in a high interaction regime. Additionally, Figure 3-13 shows that the conversion efficiency is not affected by the mass of catalysts at the same residence time, suggesting an absence of limitations due to interphase mass transfer in porous catalysts.

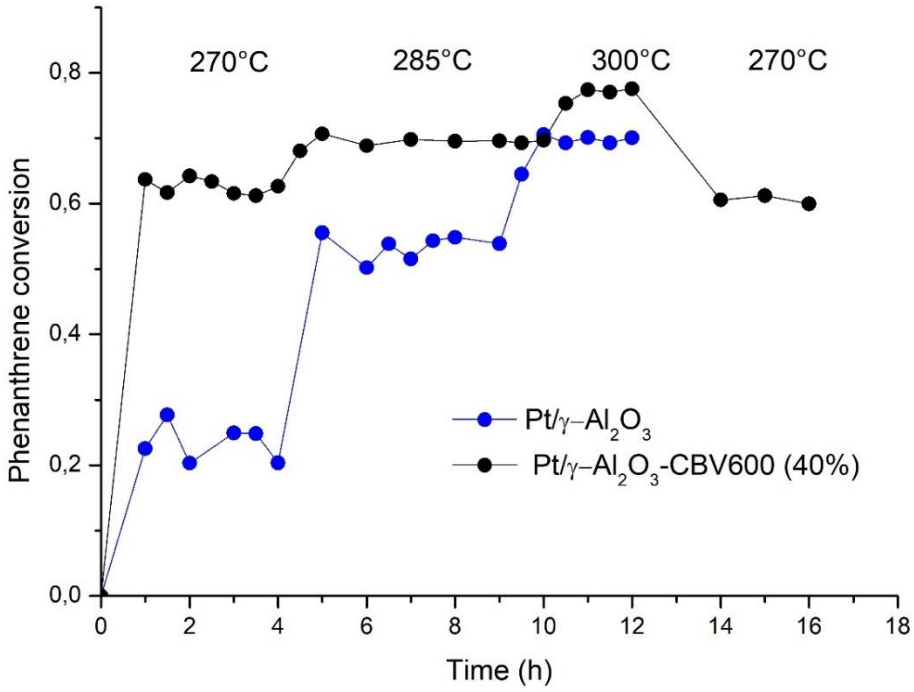

Figure 3-14 Phenanthrene conversion efficiency in a hydrocracking reaction as a function of temperature and the type of catalyst.

Figure 3-14 shows the phenanthrene conversion efficiency at different hydrocracking temperatures over Pt/γ-Al_2O_3 and Pt/γ-Al_2O_3-CBV600(40%) catalysts. Figure 3-14 shows, the positive effect of elevated temperature on phenanthrene conversion is evidenced for both catalysts. Phenanthrene conversion depends on the rate of hydrogenation of aromatic rings. Aromatic ring hydrogenation reactions are reversible and exothermic reactions unfavored at high temperatures [55] [56]. However, the presence of acid along with the increased temperature promotes hydrogenation conversion. Acid sites in USY zeolite and γ-Al_2O_3 shift chemical equilibrium by reforming hydrogenated products into cracked products. Reforming the saturated products into cracked products promotes saturated products desorption from platinum clusters. Hence, platinum clusters available for phenanthrene molecules increases, facilitating phenanthrene hydrogenation reaction [55].

Considering that the hydrogenation reaction does not depend on extra-particle diffusion, the differences in catalytic activity are attributed to the intrinsic properties of catalysts. The Lewis acid sites are mainly responsible for the hydrocracking reactions in the Pt/γ-Al_2O_3 catalyst. While in the Pt/γ-Al_2O_3-CBV600(40%) catalyst, the Brønsted acid sites play a major role in hydrocracking. Figure 3-14 shows that at the same reaction conditions, Brønsted acid sites of zeolite are more active than the Lewis acid sites of the Alumina. However, Pt/γ-Al_2O_3 catalyst strongly depends on temperature increase. Hydrocracking activity in Pt/γ-Al_2O_3 catalysts depends on the Lewis acid sites concentration, while in the Pt/γ-Al_2O_3-CBV600(40%) catalyst depends on the BAS. Lewis's acid sites in Pt/γ-Al_2O_3 catalysts are more accessible and abundant than the Brønsted acid sites in the Pt/γ-Al_2O_3-CBV600(40%) catalyst. Also, with the increase of temperature, phenanthrene molecules earn kinetic energy diffusing faster through catalytic particles. Therefore, at elevated temperatures, phenanthrene molecules will have more chances to find a catalytic site in the Pt/γ-Al_2O_3 catalysts than in the Pt/γ-Al_2O_3-CBV600(40%) catalyst.

3.8 Conclusions

This work presents the design, construction, and evaluation of a laboratory-scale Trickle Bed Reactor (TBR) with the objective to study heterogeneous catalysts for the phenanthrene hydrocracking reaction. Hydrodynamic properties were considered account for the design of catalytic bed dimension, catalysts particle size, and gas-liquid flow rates. Fitting and tubing characteristics, including materials and dimensions, match the requirements of operating conditions. Hydrodynamical analysis shows that the operation at high liquid flow rates and low gas flow rates ensures a high interaction regime. Also, determination of the particle size and the length of the bed reduced negative effects due to the drop pressure and axial dispersion. The catalytic test carried out at different residence times indicated the minimal liquid flow rate (0.7 mL/min) where external-particle diffusion does not limit the performance of the reactor. Experimental results validated the hydrodynamic prediction model for the liquid flow rate of 1 mL/min. Once optimal hydrodynamic parameters were determined, two catalysts with different chemical nature were tested for their phenanthrene hydrocracking performance. Catalysts were tested at three temperatures. Results suggest that elevated temperature favors the phenanthrene conversion. This is associated with the catalytic activity of the acid sites. These results

validate the functionality of the TBR and that the TBR can be utilized to study the effect of catalytic properties on the phenanthrene hydrocracking reaction.

3.9 References

[1] R. V. Vivek, V. Raghunath, G. Chaudhari y R. Prashant, Trickle Bed Reactors Reactor Engineering & Applications, Elsevier, 2011.

[2] A. Gianetto y V. Specchia, «Trickle-Bed reactors: State of art and perspectives,» *Chemical Engineering Science,* vol. 47, nº 13114, pp. 3197-3213, 1992.

[3] C. N. Satterfield, «Trickle-Bed Reactors,» *AIChe Journal,* vol. 21, nº 2, p. 209–228, 1975.

[4] M. J. Taulamet, *Fenómenos de transporte y reacción química en lechos fijos. Influencia de la forma del relleno catalítico,* La Plata - Argentina: Universidad Nacional de La Plata, 2015.

[5] G. S. Honda, P. Gase, D. A. Hickman y A. Varma, «Hydrodynamics of Trickle Bed Reactors with Catalyst Support Particle Size Distributions,» *Ind. Eng. Chem. Res,* vol. 53, pp. 9027-9034, 2014.

[6] I. Iliuta, A. Ortiz-arroyo, B. P. A. Grandjean y G. Wild, «Hydrodynamics and mass transfer in trickle-bed reactors: an overview,» *Chemical Engineering Science,* vol. 54, pp. 5329-5337, 1999.

[7] J. Guo y A.-D. Muthanna, «Modeling Catalytic Trickle-Bed and Upflow Packed-Bed Reactors for Wet Air Oxidation of Phenol with Phase Change,» *Ind. Eng. Chem. Res,* vol. 44, nº 17, p. 6634–6642, 2005.

[8] H. Gierman, «Design of laboratory hydrotreating reactors scaling down of trickle-flow reactors,» *Appl. Catal.,* vol. 43, nº 2, p. 277–286, 1988.

[9] A. d. Klerk, «Adiabatic Laboratory Reactor Design and Verification,» *Ind. Eng. Chem. Res.,* vol. 4, nº 25, p. 9440–9445, 2005.

[10] D. Mears, «Diagnostic criteria for heat transport limitations in fixed bed reactors,» *J. Catal.,* vol. 20, nº 2, pp. 127-131, 1971.

[11] D. A. Hickman, M. T. Holbrook, S. Mistretta y S. J. Rozeveld, «Successful Scale-up of an Industrial Trickle Bed Hydrogenation Using Laboratory Reactor Data,» *Ind. Eng. Chem. Res.,* vol. 52, nº 44, p. 15287–15292, 2013.

[12] C. Perego, «Experimental methods in catalytic kinetics,» *Catal. Today,* vol. 52, nº 2-3, p. 133–145, 1999.

[13] W. L. M. Weerts, M. H. J. M. de Croon y G. B. Marin, «A laboratory reactor for kinetic studies of gas-solid reactions at low pressures: Design and modelling in the presence of irreducible transport phenomena,» *Chem. Eng. Sci,* vol. 51, nº 11, pp. 2583-258, 1996.

[14] J. D. Carruthers y J. Dicamillo, «Pilot Plant Testing of Hydrotreating Catalysts Influence of Catalyst Condition , Bed Loading and Dilution,» *Applied Catalysis,* vol. 43, p. 253–276, 1988.

[15] C. Boyer, V. Volpi y G. Ferschneider, «Hydrodynamics of trickle bed reactors at high pressure: Two-phase flow model for pressure drop and liquid holdup, formulation and experimental validation,» *Chemical Engineering Science,* vol. 62, p. 7026–7032, 2007.

[16] M. H. M. Lim, A. J. Sederman, L. F. Gladden y E. H. Stitt, «New insights to trickle and pulse flow hydrodynamics in trickle-bed reactors using MRI,» *Chemical Engineering Science,* vol. 59, p. 5403–5410, 2004.

[17] A. Gianetto y V. Specchia, «Trickle-Bed reactors: State of art and perspectives,» *Chemical Engineering Science,* vol. 47, pp. 3197-3213, 1992.

[18] J. C. Charpentier y M. Favier, «Some Liquid Holdup Experimental Data in Trickle-Bed Reactors for Foaming and Nonfoaming Hydrocarbons,» *AIChe J.,* vol. 21, nº 6, p. 1213–1218, 1975.

[19] M. F. Pinto Moreira y M. d. C. Ferreira, «Evaluation of pseudohomogeneous models for heat transfer in packed beds with gas flow and gas–liquid cocurrent downflow and upflow,» *Chem. Eng. Sci.,* vol. 61, p. 2056–2068, 2005.

[20] M. E. Trivizadakis y A. J. Karabelas, «A study of local liquid/solid mass transfer in packed beds under trickling and induced pulsing flow,» *Chem. Eng. Sci,* vol. 61, p. 7684–7696, 2006.

[21] A. Atta, S. Roy y K. D. P. Nigam, «Investigation of liquid maldistribution in trickle-bed reactors using porous media concept in CFD,» *Chemical Engineering Science,* vol. 62, pp. 7033-7044, 2007.

[22] R. G. Carbonell, «MULTIPHASE FLOW MODELS IN PACKED BEDS,» *Oil & Gas Science and Technology,* vol. 55, nº 4, pp. 417-425, 2000.

[23] G. Towler y R. Sinnott, Chemical Engineering Design: Principles, Practice and Economics of Plant and Process Design, Buterworth, 2008.

[24] J. Sánchez Castañeda, *Catalizadores bifuncionales ultradispersos para la hidroconversión de fenantreno-decalina,* Medellin: Universidad de Antioquia, 2018.

[25] J. Weitkamp, «Catalytic Hydrocracking—Mechanisms and Versatility of the Process,» *ChemCatChem,* vol. 4, p. 292 – 306, 2012.

[26] F. Roessner y U. Roland, «Hydrogen spillover in bifunctional catalysis,» *J. Mol. Catal. A Chem,* vol. 112, nº 3, p. 401–412, 1996.

[27] T. E. Daubert, «Vapor−Liquid Critical Properties of Elements and Compounds. 5. Branched Alkanes and Cycloalkanes,» *Journal of Chemical & Engineering Data,* vol. 41, nº 3, p. 365–372, 1996.

[28] A. A. Clifford y J. R. Williams, «Introduction to Supercritical Fluids and Their Applications,» *Supercritical Fluid Methods and Protocols ,* vol. 13, pp. 1-16, 2000.

[29] A. Bertuco y G. Vetter, «High pressure process technology: Fundamentals and applications,» *Industrial Chemistry Library,* vol. 9, 2001.

[30] J. R. Thygeson y M. C. Molstad, «High Pressure Hydrogen Attack of Steel,» *Journal of Chemical & Engineering Data,* vol. 9, nº 2, p. 309–315, 1964.

[31] P. G. Shewmon, «Hydrogen attack of carbon steel,» *Metallurgical Transactions A,* vol. 7, nº 2, p. 279–286, 1976.

[32] D. Eliezer, «High-temperature hydrogen attack of carbon steel.,» *Journal of Materials Science,* vol. 16, nº 11, pp. 2962-2966, 1981.

[33] D. J. Benac y P. McAndrew, «Reducing the Risk of High Temperature Hydrogen Attack (HTHA) Failures,» *Journal of Failure Analysis and Prevention,* vol. 12, nº 6, p. 624–627, 2012.

[34] G. N. Howard, «Hydrogen Embrittlement. Materials and Test engineering Branch,» *TREATISE ON MATERIALS SCIENCE AND TECHNOLOGY,* vol. 25, 1983.

[35] F. Larachi, A. Laurent, N. Midoux y G. Wild, «Experimental study of a trickle-bed reactor operating at high pressure: two-phase pressure drop and liquid saturation,» *Chemical Engineering Science,* vol. 46, pp. 1233-1246, 1991.

[36] P. R. Gunjal, M. N. Kashid, V. V. Ranade y R. V. Chaudhari, «Hydrodynamics of Trickle-Bed Reactors: Experiments and CFD Modeling,» *Industrial & Engineering Chemistry Research,* vol. 44, nº 16, p. 6278–6294, 2005.

[37] K.-M. Kan y P. F. Greenfield, «Pressure Drop and Holdup in Two-Phase Cocurrent Trickle Flows through Beds of Small Packings,» *Industrial & Engineering Chemistry Process Design and Development,* vol. 18, nº 4, p. 740–745, 1979.

[38] W. J. A. Wammes y K. R. Westerterp, «Hydrodynamics in a pressurized cocurrent gas-liquid trickle-bed reactor,» *Chemical Engineering Technology,* vol. 14, nº 406, 1991.

[39] P. L. Mills y M. P. Dudukovic, «Evaluation of liquidesolid contacting in trickle-bed reactors by tracer methods,» *AIChE Journal,* vol. 27, pp. 893-904, 1981.

[40] A. A. El-Hisnawi, M. P. Dudukovic y P. L. Mills, «Trickle-bed reactors: dynamic tracer tests, reaction studies and modelling of reactor performance,» *ACS Symposium Series,* vol. 196, pp. 421-440, 1982.

[41] I. Iliuta y F. C. Thyrion, «Gase-liquid mass transfer in fixed beds with two-phase cocurrent downflow: gas Newtonian and non-Newtonian liquid systems,» *Chemical Engineering and Technology,* vol. 20, pp. 538-549, 1997.

[42] R. E. Treybal, Operaciones de Transferencia de Masa, Mc Graw Hill, 1980.

[43] Y. Kawase y J. J. Ulbrecht, «NEWTONIAN FLUID SPHERE WITH RIGID OR MOBILE INTERFACE IN A SHEAR-THINNING LIQUID: DRAG AND MASS TRANSFER,» *Chemical Engineering Communications,* vol. 8, nº 4-6, p. 213–231, 1981.

[44] P. A. Nelson y T. R. Galloway, «Particle-to-fluid heat and mass transfer in dense systems of fine particles,» *Chemical Engineering Science,* vol. 30, pp. 11-16, 1975.

[45] D. E. Mears, «The role of axial dispersion in trickle flow laboratory reactions,» *Chemical Engineering Science,* vol. 26, p. 1361, 1971.

[46] A. Bahadori, «Prediction of Axial Dispersion in Plug-Flow Reactors Using a Simple Method,» *Journal of Dispersion Science and Technology,* vol. 33, nº 2, pp. 200-205, 2012.

[47] J. G. A. Scherzer, Hydrocracking Science and Technology, Marce Decker Inc, 1996.

[48] A. Atta, S. Roy y K. D. P. Nigam, «Investigation of liquid maldistribution in trickle-bed reactors using porous media concept in CFD,» *Chemical Engineering Science,* vol. 62, pp. 7033-7044, 2007.

[49] R. Bolger y P. Valves, *Pressure Regulators vs. Backpressure Regulators.*

[50] T. Wyatt, *Coriolis Flow meters for Gas Measurement,* Flow Control Mag..

[51] J. Zecevic, G. Vanbutsele, K. P. De Jong y J. A. Martens, «Nanoscale intimacy in bifunctional catalysts for selective conversion of hydrocarbons,» *Nature,* vol. 528, nº 7581, p. 245–254, 2015.

[52] J. T. Scanlon y D. E. Willis, «Calculation of Flame Ionization Detector Relative Response Factors Using the Effective Carbon Number Concept,» *Journal of Chromatographic Science,* vol. 23, nº 8, p. 333–340, 1985.

[53] H. S. y Fogler, Elements of chemical reaction engineering, Mexico : Pearson Education, 2006.

[54] S. Mitchel, A. B. Pinar, J. Kenvin, K. J. Crivelli Paolo y J. Pérez Ramírez, «Structural analysis of hierarchically organized,» *Nature Communications,* nº 8633, 2014.

[55] L. Lorraine, B. Eric y M.-G. Nathali, «Hydrocracking of phenanthrene over bifunctional Pt catalysts,» *Catalysis Today,* pp. 241-247, 2001.

[56] A. Stanislaus y H. B. Cooper, «Aromatic Hydrogenation Catalysis: A Review,» *CATAL. REV.-SCI. ENG,* pp. 75-123, 1994.

4. The effect of the USY zeolite properties on the phenanthrene hydrocracking performance

Summary

The effect of structural and acid properties of USY zeolites blended in alumina are studied concerning their catalytic activity for phenanthrene hydrocracking. Hydrocracking is studied in a continuous Trickle-Bed Reactor (TBR). Test reactions were performed at 70 bar and 270 °C, 285 °C, and 300 °C. Tested USY zeolites varied in Si/Al ratio and mesoporous volume. The properties of the zeolites and associated catalysts were characterized by X-ray diffraction (XRD), N_2 physisorption, Transmission Electron Microscopy (TEM), i-PA decomposition, pyridine, and H_2 chemisorption. Tested catalysts were composites of USY zeolite at 40% in γ-Al_2O_3 impregnated with 0.85 %wt of platinum. The platinum dispersion was similar across all catalysts with an average cluster size of 1.5 nm. The catalytic activity for phenanthrene hydrocracking was evaluated by calculating the Turn-Over Frequency (TOF) of both active sites: platinum (Pt) and Brønsted Acid Sites (BAS). Catalysts with low BAS concentration display low TOF_{Pt} value and low yield of middle distillates. That indicates BAS favored phenanthrene hydrogenation by reforming hydrogenated species in cracked products. The decreasing of hydrogenated species favored phenanthrene hydrogenation according to the Le Chatelier principle. The value TOF_{BAS} indicates the participation of BAS in a phenanthrene hydrocracking reaction. Catalyst with low BAS concentration requires a higher temperature to reach maxima BAS catalytic activity despite its favorable high mesopore volume. This catalyst also presented high gas formation. This is explained by two BAS activities: BAS in cooperation with platinum enables hydrocracking reactions via hydrogen spillover mechanism, while BAS alone performs catalytic cracking via the so-called classic mechanism. This work contributes to the understanding of the effect of the properties of Pt/USY-based catalysts on the phenanthrene hydrocracking reaction.

4.1 Introduction

Petroleum crude oil provides most of the world's demand for transportation fuels through its transformation into middle boiling distillates such as gasoline, diesel, kerosene, and jet fuel [1]. The crude oil refining process has to comply with strict environmental regulations demanding constant improvements in the technology [2]. The oil refining industry successfully addresses environmental challenges due to the fast technological development of catalysts and processes [2]. Catalytic hydrocracking technologies offer flexible and versatile processes able to refine oil cuts into clean fuels [1]. Hydrocracking reaction cracks C-C bonds in hydrocarbons followed by hydrogenation of unsaturated carbon bonds [3].

Hydrocracking has been studied extensively [4] [5] [6] [7] [8] [9] [10]. Several studies have focused on the hydrocracking of polyaromatic hydrocarbons (PAHs) using model compounds [11] [12] [13]. These studies investigate the hydrogenation of aromatic rings as well as selective ring-opening reactions. Stanislaus et. al [11] studied catalytic hydrogenation of benzene, naphthalene, anthracene and phenanthrene. They found that hydrogenation of the first aromatic ring is more feasible in compounds with a greater number of aromatic rings. In other terms, hydrogenation of the first aromatic ring occurs faster in anthracene than in benzene. Phenanthrene is an exception since its resonance energy is higher than in the other PAHs. This slows down the hydrogenation reaction rate [14].

Lapinas et. al. [15] carried out the hydrocracking of fluorene using NiMo-S/USY catalysts. They found that catalysts with the metal-sulfide phase performed the ring-opening reaction of cyclopentane in fluorene molecule before the hydrogenation of aromatic rings is completed. Wang et. al. [5] investigated fluorene hydrocracking over Pt/USY catalysts. The reaction over Pt/USY catalysts completed hydrogenation of the aromatic rings before termination of the opening ring reaction. Similar findings were reported by Leite et. al. [7] who carried out the phenanthrene hydrocracking over Pt/γ-Al_2O_3 catalyst. They have also observed limited diffusion of perhydrophenanthrene through zeolites with a pore size smaller than the kinetic ratio of the molecule. The dimensions of perhydrophenanthrene are: x = 0.114 nm, y = 0.69 nm, and z = 0.51 nm; zeolites pore sizes are defined as: H-ZSM-5 = 0.53 nm, H-β = 0.64 nm, and H-Y = 0.74 nm [7].

To overcome diffusion limitations, USY zeolites have been modified by steaming treatment to obtain materials with an extensive range of mesoporous volume able to process the diverse compounds in oil [16] [17] [18]. USY zeolites with mild acidity and large mesopores produce high yields of middle distillates during hydrocracking. Adequate distribution of acidity and mesoporous volume in USY zeolites also avoid coke formation [19] [20].

Cracking, isomerization, and alkylation reactions have been attributed to the Brønsted acid sites (BAS) in USY zeolites. BAS are the charge-balancing tetrahedrally-coordinated aluminum atoms (Al^{3+}) [21] [22]. The removal of this aluminum atom by steaming treatment gives chemical and thermal stability to the zeolite. Steaming treatment results in extra-framework aluminum (EFAl) species being released into the crystal structure of zeolites [20] [21] [23]. EFAl species could be favorable to hydrocracking although its effect depends on the concentration, size, and dispersion of the hydroxyl clusters [24] [25]. Excess of EFAl species promotes coke formation blocking the access of hydrocarbons to catalysts micropores and mesopores [24]. In contrast, well-dispersed EFAl clusters could favor the hydrocracking reaction through a synergistic effect between EFAl and BAS [24] [25]. However, the true nature of the catalytic activity of the different acid sites families in USY zeolites is still a controversial topic in the scientific community [26] [27] [28] [29] [30] [31]. The contribution of this work is to investigate the role of the USY properties concerning catalytic phenanthrene hydrocracking.

4.2 Experimental

4.2.1 Catalyst preparation

Composites of 60%wt-γ-Al_2O_3/40%wt-USY-zeolite were prepared using commercial USY zeolites and aluminum hydroxide (Pural TH100 from Sasol®). USY zeolites CBV600, CBV720, and CBV780 were acquired from Zeolyst International ®. First, a sticky blend is formed from the Pural TH100 by wetting 1g with 1 mL of acid nitric at 1%v/v. Then, USY zeolite was added to the sticky blend and mixed until achieving a homogeneous mixture. Pellets were formed by forcing out the mixture throughout a syringe. Two-stage drying was applied to the pellet. First, 8 hours at the ambient temperature followed by a heating rate of 3°C/min until 550°C for the next 8 h of calcination process. During calcination, impurities and physically bound water were removed from the catalyst surface, and the γ-Al_2O_3 phase

was formed. Finally, pellets were crushed and sieved to a particle size between 45 µm and 150 µm.

The resulting composites were impregnated with platinum at 0.85 %wt and activated according to the procedure described in chapter 3.

4.2.2 Catalyst's characterization

Catalytic properties of the zeolites employed in this work were characterized by XRD, N_2 physisorption, TEM pictures, i-PAM decomposition, pyridine, and hydrogen chemisorption, following the procedures described in Chapter 2.

4.2.3 Reaction test

Phenanthrene hydrocracking reaction was carried out in (0.85 %wt)Pt/[(40 %wt)USY-γ-Al_2O_3] catalysts, using three different USY zeolites supports (CBV600, CBV720, and CBV780). The reactions were carried out in a tubular continuous Trickle bed reactor. TBR employed 0.15 g of catalyst diluted in 1.5 g of silicon carbide (SiC) through which flowed 1 mL/min of liquid phenanthrene solution and 10 mL/min of H_2 gas flowed. Test reactions were performed at three temperatures: 270 °C, 285 °C, and 300 °C, and 70 bar of pressure. At those operational conditions, phenanthrene solution is kept in the liquid phase. Liquid samples were taken each 30 minutes, and when the temperature was changed, the interval between sampling was 1 h to guarantee that the system achieves stability. Finally, to study the effect of γ-Al_2O_3 in the reaction, the same reaction was carried out using a (0.85 wt%)Pt/γ-Al_2O_3 catalyst.

All liquid samples were analyzed using a GC Hewlett Packard 5890 series II coupled with an FID detector. For compound separation, a nonpolar DB-5 capillary column (50 m) has been installed. FID detector was calibrated by a curve that correlates the response area of the FID with the concentration of the phenanthrene. Liquid products were also analyzed by gas chromatography coupled to mass spectroscopy (GC-MS) carried out by a collaborator at the Corporación Autonoma Regional de Cundinamarca (CAR). The method of chromatographic separations was identical for both detectors, FID and MS.

The Turn Over-Frequency (TOF) of platinum was calculated according to equation [4.1]. As the amount and dispersion of platinum are almost the same in all catalysts, the role of the acid sites will be more evident.

$$TOF_{as} = \frac{r}{[as]} \quad [4.1]$$

Where r is the rate of phenanthrene conversion calculated by equation [3.2], and [as] is the concentration of the active site.

4.3 Results and discussions

4.3.1 Catalyst Characterization

Figure 2-1-I shows XRD patterns of various USY zeolites, exhibiting characteristic peaks associated with the Faujasite crystalline structure. The crystallinity of CBV600, CBV720, and CBV780 zeolites were 92%, 102%, and 87%, respectively. The decreasing of crystallinity is attributed to a fraction of aluminum removed from the crystal network. Since the Al-O (0.172 nm) bonds are longer than Si-O bonds (0.165 nm), the (111) reflection shifts towards lower 2θ values with an increasing amount of aluminum in the framework [32].

Table 4-1 summarizes chemical properties of the USY zeolites used in this study. In chapter 2 characterization results are discussed in detail. The most dealuminated CBV780 USY zeolite also presents the highest mesoporous volume. This zeolite is prepared by consecutive steaming and washing treatments that remove both crystalline and extra framework aluminum [33]. Platinum dispersion in catalysts varies from 70% to 84%. High platinum dispersion value guarantees high hydrogenation activity of catalysts during the hydrocracking reaction [29].

Pt/CBV720 catalyst contains the highest concentration of Strong Brønsted Acid Sites (SBAS) (141 µmol/g) measured by pyridine chemisorption. SBASs are claimed as responsible for the increased hydrocracking activity in certain USY based catalysts. The catalytic activity of SBAS is associated with a synergistic effect between the BAS in the crystalline network and the isolated Lewis Acid Sites (LAS) in the extra framework aluminum (EFAl) [24]. However, the Pt/CBV600 catalysts present a high LAS concentration (376 µmol/g) but a low amount of SBAS (96 µmol/g), probably, due to a poor dispersion of

the EFAl. Excess of EFAl species clogs up the BAS, limiting phenanthrene access to BAS during hydrocracking.

Table 4-1 Acidity and metal characterization of zeolite supports and associated Pt catalysts.

Catalysts	Si/Al	Acidity[1] i-Pa (µmol/g)	Acidity[2] Py BAS (µmol/g)	Acidity[2] Py LAS (µmol/g)	Acidity[2] Py SBAS (µmol/g)	Pt[3] Dispersion (%)	Cluster Size (nm)
CBV 600	9.8	783	795	911	723	-	-
CBV 720	15.3	556	592	112	459	-	-
CBV 780	54.3	130	200	321	38	-	-
Pt 0,85%wt/CBV 600(40%)	-	365	361	376	96	71	1.4
Pt 0,85%wt/CBV 720(40%)	-	201	248	220	141	84	1.2
Pt 0,85%wt/CBV 780(40%)	-	136	160	244	30	80	1.3

[1] Amount of isopropylamine decomposed on the material surface, measured by a DSC-TG.

[2] Amount of pyridine adsorbed on the material surface, measured by FTIR.

[3] Platinum dispersion over material surface determined by hydrogen chemisorption.

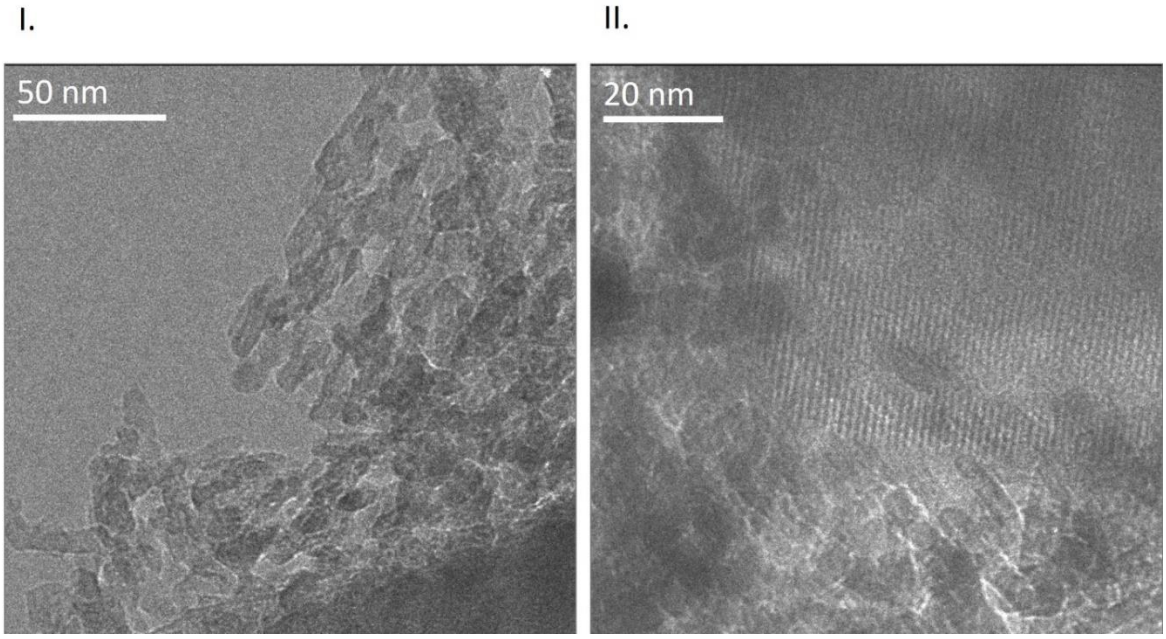

Figure 4-1 TEM imaging of CBV600-USY(40%)/γ-Al_2O_3 composite.

Figure 4-1 shows TEM imaging of the CBV600(40 %wt)/ γ-Al_2O_3 composite at 20 nm and 50 nm. In Figure 4-1-II two solid phases can be distinguished clearly. The ordered crystalline phase corresponds to the USY zeolite structure, while the amorphous phase to the γ-Al_2O_3. The amorphous phase consists of large mesoporous channels, where phenanthrene molecules can enter without restriction [34] [35].

4.3.2 Reaction test

GC-MS analysis allowed for the identification of 19 compounds eluted between the TiPB signal and the phenanthrene signals (Appendix C.). Identified compounds are classified into four principal groups: (i) phenanthrene hydrogenation products (C14hydro), (ii) ring-opening reaction products (C12), (iii) isomerized products (i-C14), and (iv) light products with less than 12 carbons (<C12). Some of the hydrogenated products identified were Tetrahydro phenanthrene (THP), Octahydrophenanthrene (OHP), Perhydro Phenanthrene (PHP), and its respective isomers. In the C12 group bicyclohexyl, bicyclohexyl phenyl, and biphenyl were identified.

Figure 4-2 shows the reaction pathways of the phenanthrene hydrocracking according to the detected intermediate products and the pathways proposed in the literature [7] [36] [37] [38]. Hydrogenation of phenanthrene to perhydrophenanthrene takes place over platinum clusters on the external surface of catalysts. After hydrogenation, hydrogenated products diffuse to the acid sites in USY support, where these are cracked and isomerized [7]. Hydrocracking occurs via two known mechanisms: (i) classic mechanism and (ii) hydrogen spillover mechanism. The classic mechanism proposes that cracked species diffuse back to platinum metal sites where they are hydrogenated. In the hydrogen spillover mechanism, the hydrogen molecule first splits over the platinum surface, and then monoatomic hydrogen diffuses through surface to the acid sites. Acid sites use this monoatomic hydrogen for the hydrogenation of cracked species. Simultaneous cracking and hydrogenation over acid sites is a hydrocracking reaction by the hydrogen spillover mechanism. However, the monoatomic hydrogen has a limited surface cover ratio [39]. That implies not all acid sites can perform hydrocracking by a spillover mechanism.

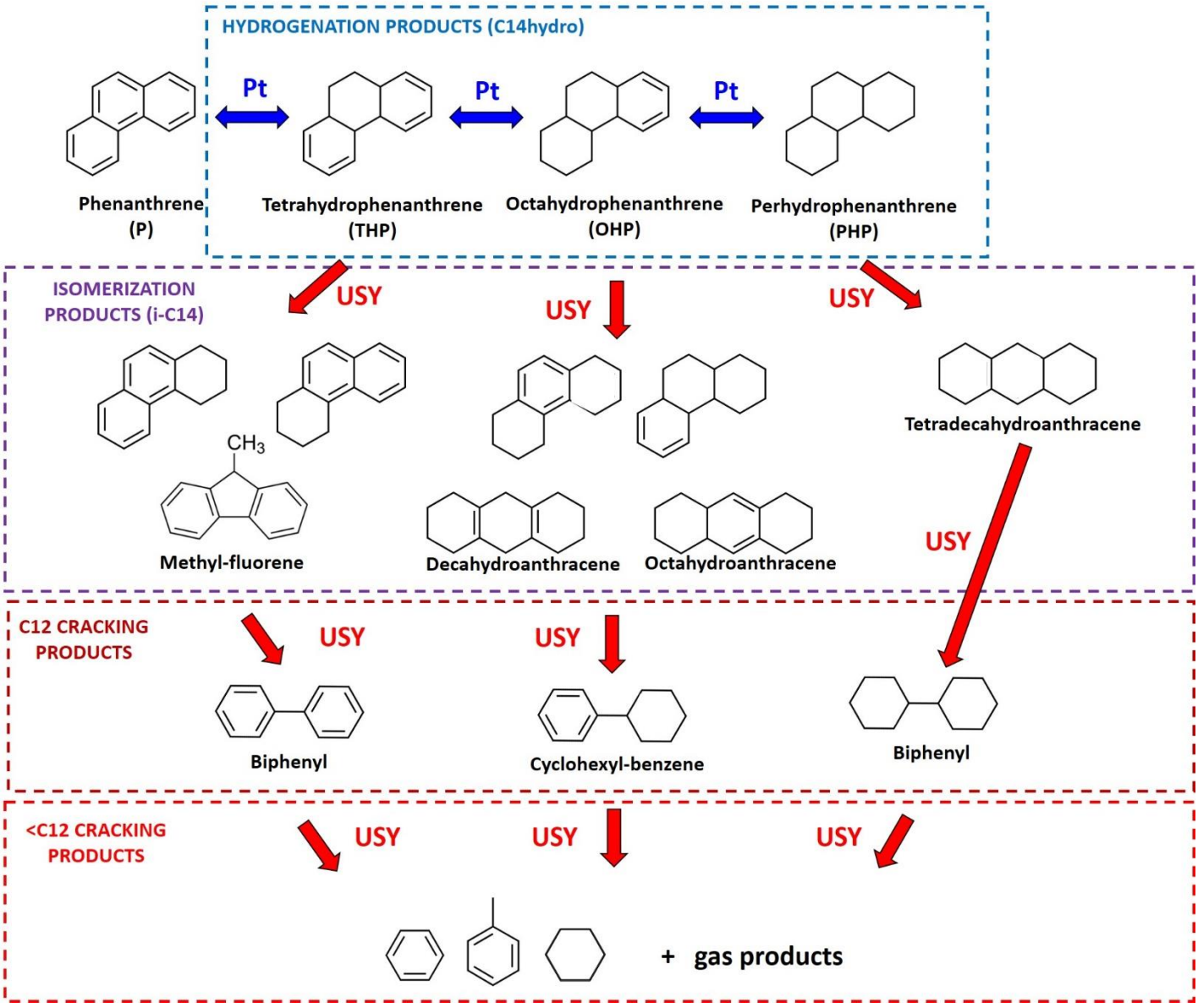

Figure 4-2 Phenanthrene hydrocracking network over bifunctional Pt/USY catalysts.

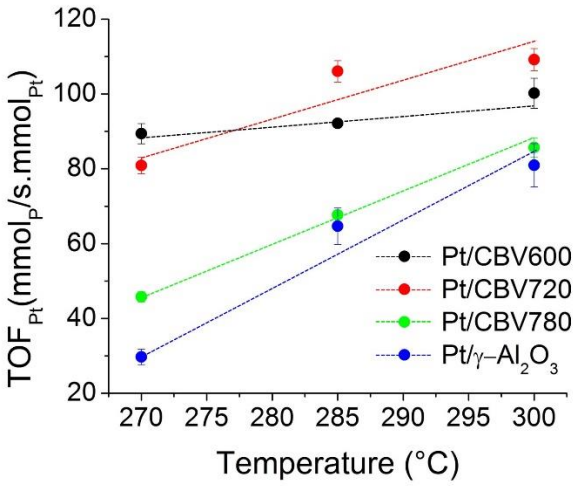

Figure 4-3 Turn-Over Frequency of platinum with respect to the type of catalysts and the temperature of phenanthrene hydrocracking.

Figure 4-3 shows the catalytic activity of platinum sites referred to as Turn-Over Frequency of platinum (TOF_{Pt}) calculated according to equation 4.1 [36] [37]. TOF_{Pt} values are given as an average of 6 measurements together with its standard deviation in Appendix C. The TOF_{Pt} values vary, although catalysts have the same amount of platinum and similar platinum dispersion. TOF_{Pt} values vary due to distinct BAS concentration that also affects hydrocracking reaction. BAS shifts the chemical equilibrium of hydrogenation/dehydrogenation reactions, reforming hydrogenated species into small compounds [7] [38]. Figure 4-3 indicates that a higher BAS concentration (Pt/CBV600 and Pt/CBV720) results in a higher TOF_{Pt} value. At low temperature, Pt/CBV600 catalyst demonstrate higher TOF_{Pt} value (TOF_{Pt} = 89.39 $mmol_P/s.mmol_{Pt}$) than CBV720 (TOF_{Pt} = 80.89 $mmol_P/s.mmol_{Pt}$). TOF_{Pt} values agree with corresponding BAS concentration ($BAS_{Pt/CBV600}$ = 365 $\mu mol_{i\text{-}Pa}/g$ > $BAS_{Pt/CBV720}$ = 201 $\mu mol_{i\text{-}Pa}/g$). At low temperatures, phenanthrene hydrocracking reactions may take place principally over the external surface of catalysts. The small size of microporous concerning the phenanthrene kinetic ratio limits the intra-crystalline diffusion of phenanthrene. Also, a higher concentration of BAS means more BAS concentration on the external particle surface. Therefore, Pt/CBV600 catalyst requires a lower temperature to initiate a hydrocracking reaction compared to the other catalysts tested in this study.

At high temperature, TOF_{Pt} in the Pt/CBV720 (TOF_{Pt} = 109.18 $mmol_P/s.mmol_{Pt}$) is higher compared to Pt/CBV600 (TOF_{Pt} = 100.22 $mmol_P/s.mmol_{Pt}$). That is associated with the

structural properties of the USY zeolites. CBV600 presents the lowest micropore volume (0.22 cm^3/g) despite presenting a well-conserved crystalline structure (crystallinity at 92%). CBV600 zeolite has an excess of EFAl species that clogs up the crystal structure and avoids molecules to access. It indicates that only a fraction of BAS in the CBV600 crystals are available for reaction, even with the increased temperature. Also, higher temperatures increase the kinetic energy of molecules, increasing the rate of diffusion [34]. The Pt/CBV720 catalysts present a favorable distribution of micropores and mesopores. These well-distributed channels enable access to the most occluded BAS. However, to reach those occluded BAS, phenanthrene requires an increment of the temperature. SBAS concentration also contributes to the TOF_{Pt} value in the Pt/CBV720 catalysts at incremented temperatures [7] [21]. The Pt/CBV780 catalyst exhibits the lowest TOF_{Pt} value due to the low BAS concentration. As stated earlier, a low concentration of BAS disfavors phenanthrene hydrogenation [38]. A high concentration of BAS increases the conversion of hydrogenated species into small compounds, which changes the chemical equilibrium of hydrogenation/dehydrogenation reactions.

The apparent activation energy of the process was calculated as is described in Appendix C. Apparent activation energy (E_{aa}) is the activation energy of the limiting step of the reaction. For the Pt/CBV600 and Pt/CBV780 catalysts, the E_{aa} is -36.2 kJ/mol and -54.3 kJ/mol, respectively. The absolute value of the E_{aa} for Pt/CBV600 catalysts is lower than 40kJ/mol, indicating that the limiting reaction step is related with mass transport [40]; this is in agreement with the stated earlier. E_{aa} for the Pt/CBV780 catalysts is low enough to consider that this catalyst is also limited by mass transport processes, although Pt/CBV780 catalysts present abundant mesoporous channels. The mesoporous channels in Pt/CBV780 should avoid phenanthrene diffusion limitation. Hence, the apparent energy of activation observed is attributed to the monoatomic hydrogen diffusion through the external surface of the zeolite. That is based on two facts. First, the platinum clusters placed mainly on the outer surface of catalysts are responsible for hydrogen adsorption. Second, Pt/CBV780 catalysts present a low concentration of BAS. Thus, the lack of BAS could limit the reaction because hydrogen has to diffuse relatively large distances to find a BAS, which requires hydrogen to perform hydrocracking reactions by the spillover mechanism. Pt/CBV720 and Pt/γ-Al_2O_3 catalysts presented E_{aa} of -132.7 kJ/mol and -124.3 kJ/mol, respectively. An absolute value of E_{aa} higher than 40 kJ/mol indicates a reaction limited by

a chemical reaction [40]. Pt/γ-Al_2O_3 catalysts lack of BAS required to perform selective ring opening reactions and hydrocracking reactions. This lack of BAS limits the rate of reaction explaining the E_{aa} value for the Pt/γ-Al_2O_3 catalyst. E_{aa} estimated for Pt/CBV720 catalysts agrees with its structural and acidic properties; the value indicates that the hydrocracking reaction is not limited by mass transport processes.

Figure 4-4 shows the yield of hydrocracking products formed over different Pt catalysts. Figure 4-4 indicates that alumina-based catalysts (i.e., Pt/ γ-Al_2O_3) deliver the highest hydrogenation yield at 285 °C. That is attributed to Lewis's acid sites in the γ-Al_2O_3 no perform selective ring-opening reactions due to its chemical nature [41]. Therefore, the hydrogenated species remain the dominant species among final liquid products. However, at 300 °C hydrogenation yields drop for alumina-based catalysts because at such high temperatures exothermic hydrogenation reactions are unfavorable.

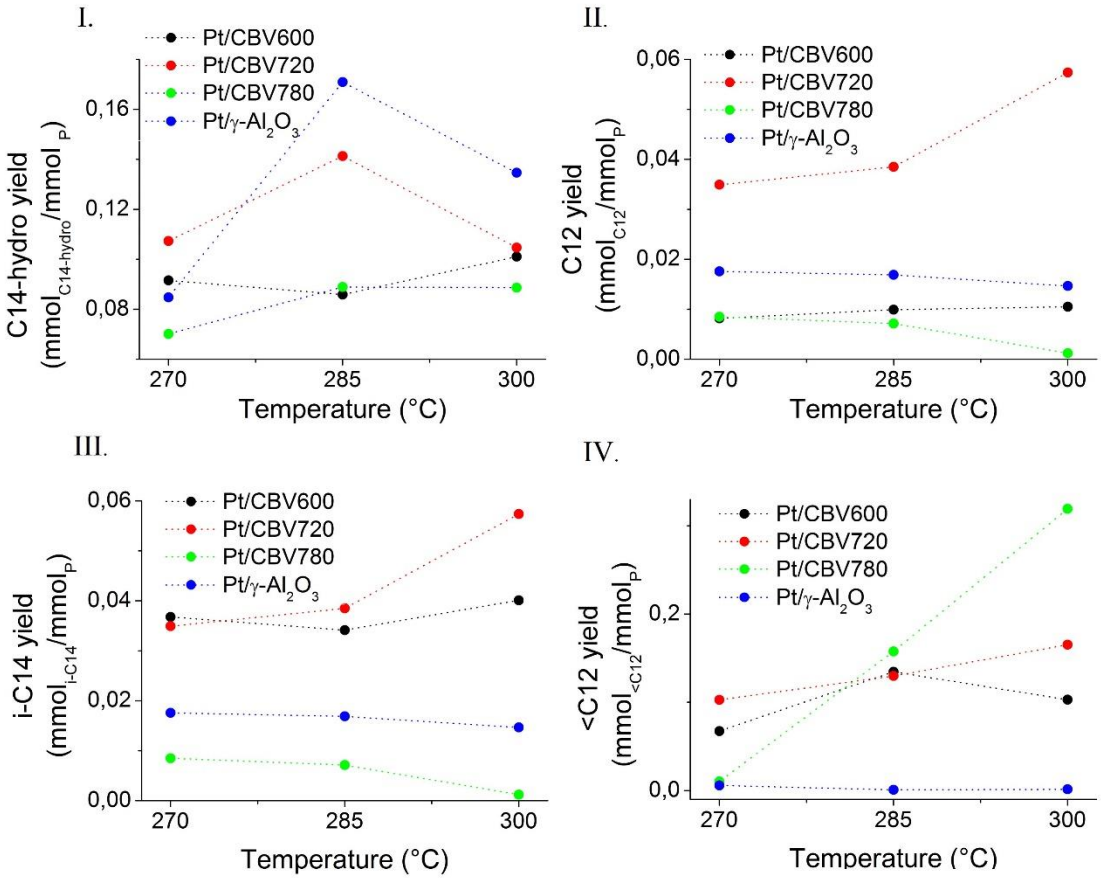

Figure 4-4 Product yields of phenanthrene hydrocracking over of Pt/USY based catalysts. I. saturated C14, II. C12 products, III. Isomerization products, and IV. <C12 products.

Zeolite-based catalysts (i.e., Pt/CBV600/CBV720/CBV780) demonstrate lower hydrogenation yield than alumina-based catalysts at the temperature range investigated in this work. In the zeolite-based catalysts hydrogenation yield decreases because BAS transform hydrogenated products into C12 products. Figure 4-4 shows that the catalyst based on CBV720 presents the highest yield to hydrogenation reactions among zeolite-based catalysts. At 300 °C, hydrogenation yield decreases because the rate of opening ring reaction is faster than the rate of phenanthrene hydrogenation. That is because increased temperature favors endothermic opening ring reactions while disfavors exothermic hydrogenation reactions.

Pt/CBV720 catalyst yields the highest C12 and isomerized products but yields low <C12 among the evaluated catalysts [7] [38]. After hydrogenation products are cracked on BAS, these desorb as C12 species and diffuse outside catalyst through the network of mesoporous channels in the Pt/CBV720 catalyst.

Pt/CBV780 catalyst presented a low C12 yield and a high <C12 yield. To explain this result considering that the Pt/CBV780 catalysts contain the lowest BAS concentration and large mesoporous surface area. Also consider that during platinum impregnation, platinum is preferably placed on the BAS of the zeolite [28]. That implies a larger space between the BAS and the platinum clusters. Thus, if a split monoatomic hydrogen cannot reach the BAS, the BAS cannot perform a hydrocracking reaction via a hydrogen spillover mechanism. Therefore, most of the BAS in Pt/CBV780 catalyst carried out hydrocracking reactions via classical mechanism where cracked products must diffuse towards platinum clusters to be hydrogenated. The classical mechanism contemplates that the cracking reaction occurs by typical catalytic cracking, in which the limitation step is the desorption of olefins [3]. When split hydrogen does not reach the BAS, perhydrophenanthrene molecules remain adsorbed longer, until its conversion into unsaturated gas products.

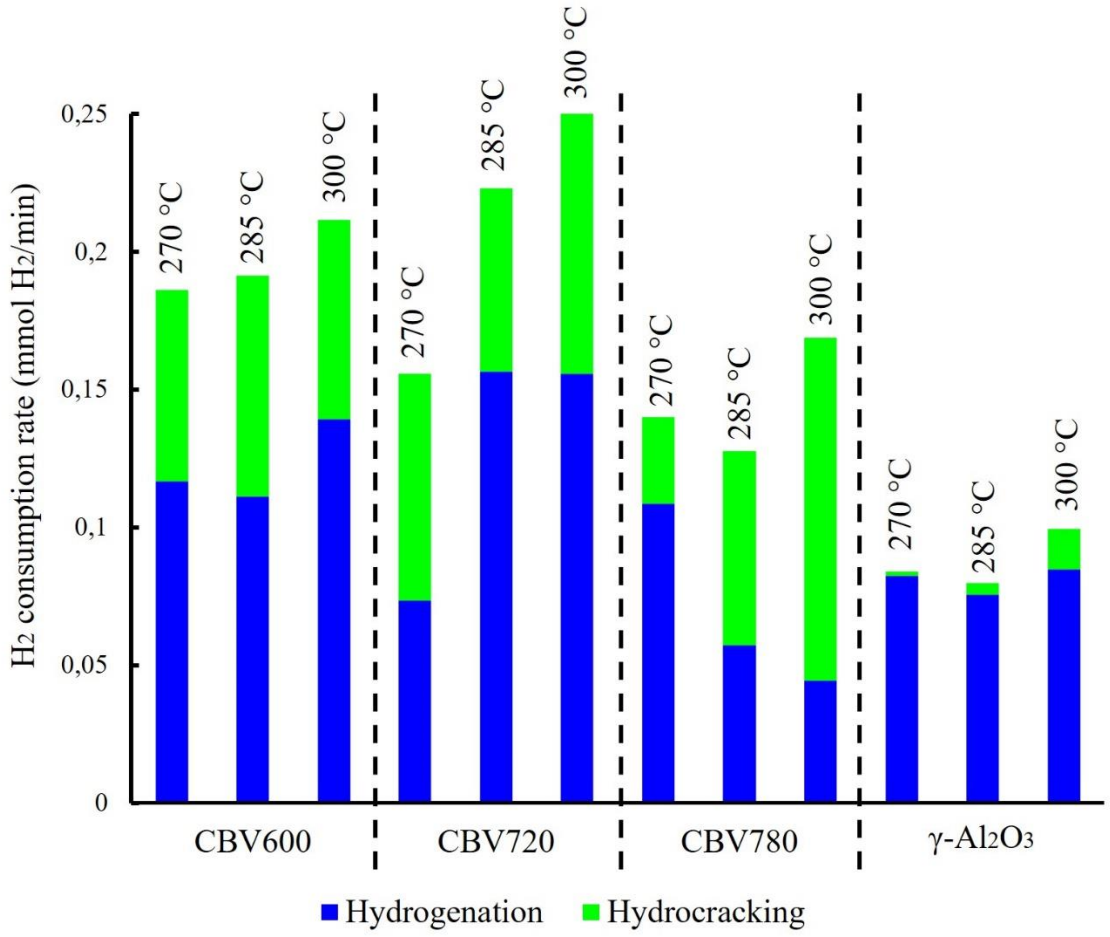

Figure 4-5 Hydrogen consumption as a function of catalyst type, temperatures, and type of reaction.

The product yield of Pt/CBV600 catalyst is not notably affected by the temperature because most of the BAS in the crystalline network are not accessible for phenanthrene. As was stated earlier, CBV600 zeolite has the micropores plugged with amorphous material product of the steaming. Then, phenanthrene molecules cannot access micropores of zeolite, even with the increase in temperature.

Hydrogen used to generate the liquid products was calculated considering the reactions scheme shown in Figure 4-2. Figure 4-5 shows the H_2 consumed to produce the C14hydro, C12, and <C12 products, assuming no olefins are formed aside. Hydrogen consumption associated with hydrogenation reactions is found in a linear relationship with TOF_{Pt} values of respective catalysts. Except for the Pt/CBV780 catalyst where the C14hydro exhibits a negative shift with the increase of temperature, although the phenanthrene conversion

increases. Biphenyl is the main hydrocracking product of compounds hydrogenated over Pt/CBV780 catalysts. The highest <C12 yield also indicates that Pt/CBV780 catalysts efficiently reform biphenyl further into lighter products.

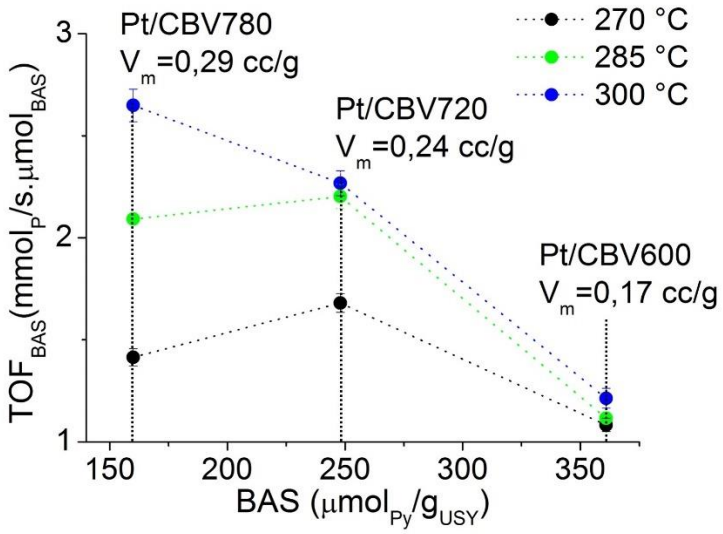

Figure 4-6 The effect of temperature on the ratio between Turn-Over Frequency of Brønsted Acid Sites (TOF_{BAS}) of phenanthrene hydrocracking.

Figure 4-6 shows TOF_{BAS} for three zeolite-based catalysts calculated according to Equation 4.1. TOF_{BAS} is an inverse function of BAS participating in phenanthrene hydrocracking. The results depicted in Figure 4-6 show that the effect of temperature in the TOF_{BAS} correlates with the mesoporous volume of USY zeolites (Table 2-1.). TOF_{BAS} in Pt/CBV600 catalyst changes only moderately with the increase of temperature. This suggests that maximal BAS activity is achieved at 270°C, and a further increase in temperature does not enhance catalytic activity. In Pt/CBV600 catalyst a part of BAS is blocked by EFAl species. Blocked BASs are therefore inaccessible for phenanthrene molecules.

The increased temperature rises TOF_{BAS} in Pt/CBV780 catalysts. Pt/CBV780 has a low BAS concentration, indicating possible far distances between platinum clusters and BAS in the catalysts. Therefore, the diffusion of the monoatomic atom through the catalytic surface could limit the reaction, as indicates the E_{aa} for Pt/CBV780 catalysts. However, the increase of temperature extends the monoatomic cover ratio over the catalyst surface, allowing hydrogen to achieve far BAS that are not reachable at low temperatures.

TOF_{BAS} in Pt/CBV720 catalyst increases with temperature from 270°C to 285°C, while further temperature increase seems not to have a notable effect on TOF_{BAS} values. This suggests that at 270°C, part of BAS in the Pt/CBV720 catalysts remains inaccessible. At 285°C improved diffusion of phenanthrene reaches deeply occluded BAS enabling complete BAS activity in the hydrocracking reaction.

4.4 Conclusions

The structural and acidic properties of USY zeolites affect the phenanthrene hydrocracking reaction. The structural and chemical characterization of USY zeolites enables a better understanding of catalytic activity associated with the platinum and acid sites content. The respective Turn-Over Frequency (TOF) was calculated for measuring the rate of conversion of phenanthrene divided by the number of active sites. Catalysts with a high BAS concentration led to high $TOF_{Pt.}$ Since BAS reforms hydrogenated products into lighter hydrocarbons, this shifts the chemical equilibrium of hydrogenation/dehydrogenation reactions toward higher conversion of phenanthrene by hydrogenation.

TOF_{BAS} changes with respect to temperature are associated with the structural properties of zeolites in catalysts. Pt/CBV600 catalysts show no changes in TOF_{BAS} value with the increase of temperature because EFAl material clogs up the crystalline network of CBV600 zeolite, avoiding phenanthrene from reaching internal BAS. The apparent activation energy (E_{aa}) of hydrocracking calculated for this catalyst confirmed the aforementioned. The absolute value of E_{aa} for Pt/CBV600 catalysts (E_{aa}=36.2 kJ/mol) is lesser than 40kJ/mol, indicating a process limited by a diffusional process.

Pt/CBV720 catalysts give the highest yield of middle-size C12 products due to the optimal ratio between BAS concentration and mesoporous volume. On the other hand, Pt/CBV780 catalysts with large mesoporous volume and low BAS concentration deliver short size <C12 product yield. The main difference in selectivity between these two zeolites catalysts is attributed to the space between BAS and platinum clusters. In Pt/CBV720, BASs are closer to a platinum cluster because of their higher BAS concentration. BAS near a platinum cluster can perform cracking and hydrogenation reactions simultaneously via hydrogen spillover coming from platinum. BAS located far from platinum clusters cannot perform hydrogenation of cracked species due to the absence of split hydrogen. Such dislocated BAS crack excessively hydrogenated products into light products.

4.5 References

[1] M. Bricker, V. Thakkar y J. Petri, Hydrocracking in Petroleum Processing, Switzerland: Springer International Publishing, 2015.

[2] J. H. Gary, G. E. Handerwerk y M. J. Kaiser, Petroleum Refining Technology and Economics, CRC Pree, 2007.

[3] J. Weitkamp y H. Schulz, «Olefinic Intermediates in Catalytic Hydrocracking of Paraffins» J. Catal., vol. 29, p. 361–366, 1973.

[4] K. De Jong, J. Zecevic, H. Friedrich, P. E. De Jongh, M. Bulut, S. v. Donk, K. Régine, A. Finiels, V. Hulea y F. Fajula, «Zeolite Y crystals with trimodal porosity as ideal hydrocracking catalyst» Angew. Chem. Int, nº 49, pp. 10074-10078, 2010.

[5] L. Wang, Y. Chen, S. Jin, X. Chen y C. Liang, «Selective Ring-Shift Isomerization in Hydroconversion of Fluorene over Supported Platinum Catalysts» Energy and Fuels, nº 30, pp. 3403-3412, 2016.

[6] A. Martínez, M. A. Arribas y S. B. C. Pergher, «Bifunctional noble metal/zeolite catalysts for upgrading low quality diesel fractions via selective opening of naphthenic rings» Catalysis Science & Technology, 2016.

[7] L. Leite, E. Benazzi, N. Marchal-George y H. Toulhoat, «Hydrocracking of Phenanthrene over Pt/SiO2-Al2O3, Pt/H-Y, Pt/H-B and Pt/H-ZSM5 Catalysts: Reaction Pathway and Products Distribution» Studies in Surface Science and Catalysis, nº 130, 2495-2500.

[8] N. Choudhary y D. N. Saraf, «Hydrocracking: A Review» Ind. Eng. Chem. Prod. Res., vol. 14, nº 2, 1975.

[9] S. Korre, M. T. Klein y R. J. Quann, «Hydrocracking of Polynuclear Aromatic Hydrocarbons. Development of Rate Laws through Inhibition Studie,» Ind. Eng. Chem. Res., vol. 36, pp. 2041-2050, 1997.

[10] E. Schachtl, L. Zhong, E. Kondratieva, J. Hein, Y. O. Gutierrez, A. Jentys y A. J. Lercher, «Understanding Ni Promotion of MoS2/γ-Al2O3 and its Implications for the Hydrogenation of Phenanthrene» CHEMCATCHEM, nº 7, pp. 4118-4130, 2015.

[11] A. Stanislaus y H. B. Cooper, «Aromatic Hydrogenation Catalysis: A Review» CATAL. REV.-SCI. ENG, pp. 75-123, 1994.

[12] S. A. Ali, «Thermodynamic Aspects of Aromatic Hydrogenation» Petroleoum Science and Technology, vol. 10, nº 25, pp. 1293-1304, 2007.

[13] H. Du, C. Fairbridge, H. Yang y Z. Ring, «The chemistry of selective ring-opening Catalysts» Applied Catalysis A: General, nº 294, pp. 1-21, 2005.

[14] C. Moreau y P. Geneste, «Factors Affecting the Reactivity of Organic Model Compounds in Hydrotreating Reactions» Theoretical Aspects of Heterogeneous Catalysis, pp. 256-310, 1990.

[15] T. A. Lapinas, B. C. Gates, A. Macris y E. J. Lyons, «Catalytic Hydrogenation and Hydrocracking of Fluorene: Reaction Pathways, Kinetics, and Mechanisms» Ind. Eng. Chem. Res, nº 30, pp. 42-50, 1991.

[16] D. Verboekend, N. Nuttens, R. Locus, V. J. Aelst, P. Verolme, J. C. Groen, J. Perez-Ramirez y B. F. Sels, «Synthesis, Characterization, and catalytic evaluation of hierarchical faujasite zeolites: milestones, challenges and future directions» Chem. Soc. Rev., vol. 45, pp. 3331-3352, 2016.

[17] D. Verboekend y J. Perez-Ramirez, «Towards a Sustainable Manufacture of Hierarchical Zeolites» CHEMSUSCHEM, nº 7, pp. 753-764, 2014.

[18] M. S. Maier, A. Jentys y A. J. Lercher, «Steaming of zeolite BEA and its Effect on Acidity: A comparative NMR and IR Spectroscopic Study.,» J. Phys. Chem, nº 115, pp. 8005-8013, 2011.

[19] A. Corma, A. Martinez y V. M. Soria, «Hydrogenation of Aromatics in Diesel Fuels on Pt/MCM-41 Catalysts» Journal of Catalysis, vol. 169, nº 2, pp. 480-489, 1997.

[20] J. L. Agudelo, B. Mezari, E. Hensen, S. A. Giraldo y L. J. Hoyos, «On the effect of EDTA treatment on the acidic properties of USY zeolite and its performance in vaccum gas oil hydrocracking» Applied Catalysis A: General, nº 488, pp. 219-230, 2014.

[21] Y. L. A. J. Zhang, «Promotion of protolytic pentane conversion on H-MFI zeolite by proximity of extra-framework aluminum oxide and BrØnsted acid sites» J. Catal., vol. 370, p. 424–433, 2019.

[22] W. O. Haag, R. M. Lago y P. B. Weisz, «The Active Site of Acidic Aluminosilicate Catalysts» Nature, nº 309, pp. 589-591, 1984.

[23] J. L. Agudelo, E. J. M. Hensen, S. A. Giraldo y L. J. Hoyos, «Influence of Steam-Calcination and Acid Leaching treatment on the VGO Hydrocracking Performance of Faujasite Zeolite» Fuel Processing Technology, nº 133, pp. 89-96, 2015.

[24] R. A. Beyerlein, C. Choi-Feng, J. B. Hall, B. J. Huggins y G. J. Ray, «Effect of Steaming on the Defect Structure and Acid Catalysis of Protonated Zeolites» Topics in Catalysis, vol. 1, nº 4, pp. 227-42, 1997.

[25] C. S. Triantafillidis, A. G. Vlessidis y N. P. Evmiridis, «Dealuminated H-Y Zeolites: Influence of the Degree and the Type of Dealumination Method on the Structural and Acidic Characteristics of H-Y Zeolites» Ind. Eng. Chem. Res, vol. 20, nº 20, pp. 307-319, 2000.

[26] P. B. Weisz, E. W. Swegler «Stepwise Reaction on Separate Catalytic Centers: Isomerization of Saturated Hydrocarbons» Science, vol. 126, p. 31, 1957.

[27] J. Francis, E. Guillon, N. Bats, C. Pichon, A. Corma y L. J. Simon, «Design of Improved Hydrocracking Catalysts by Increasing the Proximity Between Acid and Metallic Sites» Applied Catalysis A: General, vol. 1, nº 2409-410, pp. 140-147, 2011.

[28] J. Zecevic, G. Vanbutsele, K. P. De Jong y J. A. Martens, «Nanoscale intimacy in bifunctional catalysts for selective conversion of hydrocarbons» Nature, vol. 528, nº 7581, p. 245–254, 2015.

[29] F. Alvarez, F. R. Ribeiro, G. Perot, C. Thomazeau y M. Guisnet, «Hydroisomerization and Hydrocracking of Alkanes 7. Influence of the Balance between Acid and Hydrogenating Functions on the Transformation of n-Decane on Pt/HY Catalysts» Journal of Catalysis, vol. 162, pp. 179-189, 1996.

[30] P. S. F. Mendes, G. Lapisardi, C. Bouchy, M. Rivallan, J. M. Silvaa y M. F. Ribeiroa, «Hydrogenating activity of Pt/zeolite catalysts focusing acid support and metal dispersion influence» Applied Catalysis A General, 2015.

[31] P. S. Mendes, J. M. Silva, M. F. Ribeiro, A. Daudin y C. Bouchy, «Synergies, cooperation and other effects: a review for hydroconversion catalysts» Catalysis Today, 2019.

[32] W. Lutz, «Zeolite Y: Synthesis, Modification, and Properties—A Case Revisited» Advances in Materials Science and Engineering, p. 20, 2014.

[33] M. J. Remy, D. Stanica, G. Poncelet, E. J. P. Feijen, P. J. Grobet, J. A. Martens y A. Jacobs P., « Dealuminated H-Y Zeolites: Relation Between Physicochemical Properties and Catalytic Activity in Heptane and Decane Isomerization.,» J. Phys. Chem, vol. 100, pp. 12440-12447, 1996.

[34] S. Mitchel, A. B. Pinar, J. Kenvin, K. J. Crivelli Paolo y J. Pérez Ramírez, «Structural analysis of hierarchically organized» Nature Communications, nº 8633, 2014.

[35] P. Kortunov, S. Vasenkov, J. Karger, R. Valiullin, P. Gottschalk, M. F. Elia, M. Perez, M. Stocker, B. Drescher, G. McElhiney, C. Berger, R. Glaser y J. Weitkamp, «The role of mesopores in intracrystalline transport in USY zeolite: PFG NMR diffusion study on various lenght scales» J.AM.CHEM.SOC, vol. 127, pp. 13055-13059, 2005.

[36] U. Roland, T. Braunschweig y F. Roessner, «On the Nature of Split-over Hydrogen» J. Mol.Catal., vol. 127, pp. 61-84, 1997.

[37] W. Karim, «Catalyst support effects on hydrogen spillover» Nature, vol. 541, nº 7635, p. 68–71, 2017.

[38] E. Benazzi, L. Leite, N. Marchal-George, H. Toulhoat y P. Raybaud, «New insights into parameters controlling the selectivity in hydrocracking reactions» Journal of catalysis, vol. 217, pp. 376-387, 2003.

[39] R. Prins, «Hydrogen spillover. Facts and fiction,» *Chem. Rev.,* vol. 112, nº 5, p. 2714–2738, 2012.

[40] Gilberth F. Froment, Kenneth B. Bischoff, Juray De Wilde, «Chemical Reactor Analysis and Design», Jhon Wiley & Sons Inc, 3rd edition, 2011

[41] J. Abbot, «Role of Brønsted and Lewis acid sites during cracking reactions of alkanes,» *Applied Catalysis,* vol. 47, nº 1, p. 33–44, 1989.

5. Effect of phenanthrene accessibility in USY zeolites during the hydrocracking reaction

The effect of the phenanthrene accesses to the Brønsted Acid Sites (BAS) in USY zeolites during the hydrocracking reaction was studied. USY zeolite was treated to remove the excess amorphous material. The first, previously studied treatment consisted of washing steamed USY zeolite with Na_2H_2EDTA solution. The second novel treatment involved washing steamed USY zeolite with a choline chloride solution. Novel treatment was introduced to remove only amorphous material composed of silicon oxides. SEM-EDX analysis of removed amorphous material with choline chloride disproved that choline chloride treatment removes silicon oxides selectively. Treated and untreated USY zeolites were characterized by: X-Ray Diffraction (XRD), N_2 physisorption, i-PA decomposition, pyridine, and H_2 chemisorption. The XRD and SEM-EDX analysis demonstrated that the choline chloride treatment effectively removed the amorphous material. Na_2H_2EDTA treatment was found more detrimental to the crystalline structure of the zeolite compared to choline chloride treatment. Treated and untreated USY zeolites diluted in 40%wt γ-Al_2O_3 and impregnated by 0.85%wt platinum were tested for catalytic phenanthrene hydrocracking at different temperatures. Turn Over-Frequency values of platinum and Brønsted acid sites indicated that both Na_2H_2EDTA and choline chloride treatments improved the platinum and Brønsted acid sites catalytic activity due to facilitated phenanthrene accessibility to the BAS.

5.1 Introduction

Fuel oils are the most employed energy in the world and dominate the gas exhausts emissions to the atmosphere [1]. In 2019, 12.36 billion CO_2 tons were emitted to the atmosphere by oil fuel utilization [2]. Fuel oils can be upgraded to decrease CO_2 emissions in the final exhausts gas by removing contaminants such as Polycyclic aromatic hydrocarbons (PAHs). PAHs increase the formation of undesirable CO_2 in the exhaust gas

emissions contributing to the contamination of the air [3] [4] [5]. Bifunctional catalysts with metal and acid phases have been found as a plausible solution for the conversion of PHAs into clean fuels [6]. The role of the metal phase is to hydrogenate aromatic compounds, while the acid phase promotes selective ring-opening of the naphthenic compounds (a.k.a. naphthenes) to alkanes (a.k.a. paraffin) [6] [7] [8] [9] [10].

Refineries utilize Y zeolite as catalyst support for the hydrocracking of PAHs [3][5]. The design of novel Y zeolites with controlled structural and acidic properties gaining momentum in the research and development (R&D) field [11] [12]. The introduction of mesoporous channels to the crystalline structure of the Y zeolite improves the accessibility of larger molecules to the acid sites inside the zeolite [3][5] [13]. Introduction of mesoporous channels to the crystalline structure of the Y zeolite is performed by dealumination processes. Dealumination processes have successfully fabricated hierarchical Y zeolites with both pore size distributions: micropores and mesopores. Hierarchical Y zeolites are referred to as Faujasite crystal structures with two or more pore size distribution interconnected. The type of hierarchical crystal structure is defined according to how the pore size distributions are interconnected. USY zeolites obtained by dealumination processes presented hierarchy type II, typical of pore systems where the mesopores traverse the micropores [14].

Dealumination processes of HY zeolite include steaming, washing with alkaline and acid solutions, or pseudomorphic synthesis, mesostructuring, and recrystallization. D. Verboekend et. al have conducted base and acid treatments modifying HY zeolite into hierarchical Y zeolites. Also, W. Schwieger et. al reviewed the treatments associated with the modification of NH_4Y zeolite into hierarchical USY zeolites by steaming. Disintegration techniques (dealumination, alkaline, and acid treatments) of zeolite crystals produce extra-framework aluminum (EFAl) [12] [15]. EFAl species are a big family of cations (i.e., Al^{3+}, $Al(OH)^{2+}$, $Al(OH)^{2+}$), and polymerized aluminum (i.e., $AlO(OH)$, $Al(OH)_3$, Al_2O_3) [16]. High content of EFAl in the crystalline network restricts the access of hydrocarbons to the Brønsted Acid Sites (BAS). This causes deterioration of the catalyst performance [17] [18]. Beyerlein et al. stated that an optimal concentration and dispersion of EFAl around BAS enhance the acidity in USY zeolites. It is believed that BAS and well-dispersed clusters of EFAl generate a superacid site associated with a synergic effect between the acid species [19]. However, this statement is still a matter of debate in the scientific literature [16] [20].

The removal of EFAl species in excess is necessary to unblock inaccessible BAS [16]. Washing steamed zeolites with different chemicals such as mineral acids and organic acids has been proven as a successful method [12] [16] [14] [21] [22] [23]. Acid washing treatment after steaming in Y zeolites removes EFAl species selectively while preserving crystallinity. J. L. Agudelo et. al have fabricated USY zeolites with abundant mesoporous and high Vacuum Gas Oil (VGO) hydrocracking activity. Na_2H_2EDTA was used as a washing agent under mild conditions (EDTA concentration: 0.11 mol_{EDTA}/L) [24]. At an Na_2H_2EDTA concentration above 0.18 mol/L, zeolites suffered high losses in the BAS content [24] [25].

Alkaline treatment causes desilication on dealuminated zeolites. NaOH concentration above 3M deteriorates the crystalline structure of zeolites but the formation of a new mesoporous network does not occur [12] [14]. On the other hand, alkaline treatment performed under NaOH concentration below 0.1 M decreases the framework Si/Al ratio due to the reincorporation of EFAl into the crystal structure. Reincorporated Al into the crystalline network deteriorates the catalytic performance [14]. Other approaches using base treatment following the acid washing have demonstrated the successful fabrication of hierarchical USY zeolites with improved catalytic properties [14] [26].

In this work, a commercial USY zeolite was treated with choline chloride to dissolve amorphous silicates selectively. That is based on the ability of diatoms present in sea environments to dissolve sand and transform it into complex silica structures, utilizing polyamides such as choline cations [27]. Asunción et al. utilized the solution of choline hydroxide to dissolve silicates present in the rice hull ash and measured the rate of dissolution. Silica dissolution rate at standard conditions achieved 45% over 43 days of duration of the experiment [28]. Deep eutectic solvents based on choline chloride have been used as a solvent for metal oxides [29] [30]. Abbott et. al. found that at 60 °C Al_2O_3 dissolves poorly in urea/choline chloride [29]. The aforementioned studies motivated us to explore the application of choline for selective removal of amorphous silicates from steamed zeolites and its effects on phenanthrene hydrocracking [30].

5.2 Experimental

5.2.1 Catalyst's preparation

In this study commercially available CBV600 USY zeolite purchased from Zeolyst® was treated. CBV600 USY zeolite is a steamed NH_4Y zeolite with amorphous material occluded inside its crystalline structure. This amorphous material was removed employing two different solutions. The zeolite was washed with choline chlorine and Na_2H_2EDTA. 1.0 g of CBV600 USY zeolite was added to 50 mL of 0.24 M choline chlorine solution. The suspension was kept in the steel reactor at 95°C for 3 hours and stirred by 50 rpm [30]. Additional details on the treatment method are described in [30]. After treatment, samples were filtered, washed with deionized water, and dried at 120 °C for 4 h. Final zeolite calcination was conducted at 550 °C for 9 h. Amorphous material removed from zeolites was studied by drying, weighing, and analyzing by SEM-EDX residual wastes after each treatment. CBV600 also was treated with an aqueous solution of Na_2H_2EDTA at 0.11 M, stirred at 100 °C for 6 hours. Details of the treatment with Na_2H_2EDTA are given in [14].

Treated zeolite was converted into the catalyst by platinum impregnation according to the procedure described in Chapter 3. A reference catalysts Pt/CBV600, omitting treatment, was prepared to study the effect of choline and Na_2H_2EDTA.

5.2.2 Catalysts Characterization

Catalytic properties of the zeolites were determined by XRD, N_2 physisorption, i-PAM chemisorption, FTIR pyridine desorption, and the Pt supported catalysts properties by N_2 physisorption and hydrogen chemisorption. Details on chemical analysis are described in Chapter 2.

5.2.3 Phenanthrene hydrocracking reaction

Phenanthrene hydrocracking over Pt/USY based catalysts was performed according to the procedure described in chapter 4. The catalysts were coded as Pt/CBV600, Pt/CBV600-Choline, and Pt/CBV600-EDTA referred to the catalyst based on untreated CBV600, the CBV600 treated with choline chloride, and the CBV600 treated with Na_2H_2EDTA, respectively.

5.3 Results and discussion

Untreated CBV600 USY zeolite and treated zeolites with choline chloride and Na_2H_2EDTA presented XRD patterns typical for the faujasite zeolite (Figure 5-1-I). Table 5-1 shows that the crystallinity of treated CBV600 USY zeolite deteriorates regarding the untreated CBV600 USY zeolite reference. Concerning treated zeolites, the choline chloride treatment preserves the crystallinity better than the Na_2H_2EDTA treatment under the experimental conditions. Table 5-1 also shows that BAS content in zeolites measured by i-pam and pyridine FTIR is inversely proportional to the deterioration of the crystalline structure. That is because the detriment of the crystalline structure is associated with the BAS removal. The removal of amorphous material occluded inside the zeolite by choline chloride reduces the BAS strength in a zeolite (SBAS). Such reduction in SBAS content could diminish catalytic activity [20]. Contrary, Na_2H_2EDTA treatment increases the SBAS content in the USY zeolite compared to CBV600 USY reference. This is attributed to some well-dispersed Extra-Framework Aluminum (EFAl) clusters remain inside the crystal network of the zeolite after Na_2H_2EDTA treatment. That is based on the SBAS are conformed for a cluster of Extra-Framework Aluminum (EFAl) around to a BAS [19].

Table 5-1 Metal and acidic properties of treated Pt catalysts and untreated Pt catalysts as reference material.

Catalysts	Si/Al	Cristallynity (%)	Acidity[a] i-Pa BAS (µmol/g)	Acidity[b]Py BAS (µmol/g)	Acidity[b] Py LAS (µmol/g)	Acidity[b] Py SBAS (µmol/g)	Pt[c] Dispersion (%)	Cluster Size (nm)
CBV600	9.8	100	783	361	376	96	21	4.9
CBV600-Choline	12.7	79	786	356	353	39	32	3.2
CBV600-EDTA	17.1	64	729	305	197	130	29	3.5

[a] Amount of isopropylamine decomposed on the material surface, measured by a DSC-TG.

[b] Amount of pyridine adsorbed on the material surface, measured by FTIR.

[c] Platinum dispersion over material surface determined by hydrogen chemisorption.

Figure 5-1-II shows N_2 physisorption isotherms for the treated zeolites and the CBV600 USY zeolite. The N_2 isotherm displayed high uptake at low relative pressures for the treated zeolites, indicating that treatments unblock the micropores by removing amorphous material. Table 5-2 shows that the micropore area of CBV600 USY zeolite increase after

the washes. Under the operational conditions of the washes, there is no formation of new crystals. Therefore, the increase in the microporous surface area is due to the treatments uncover blocked porous. Besides, other structural properties as the mesoporous volume and the total surface area increased after treatments (Table 5-2.). Zeolite treated with choline chlorine almost doubled the mesopore volume of the CBV600. Zeolites treated with EDTA increase the mesoporous volume by 56% approximately.

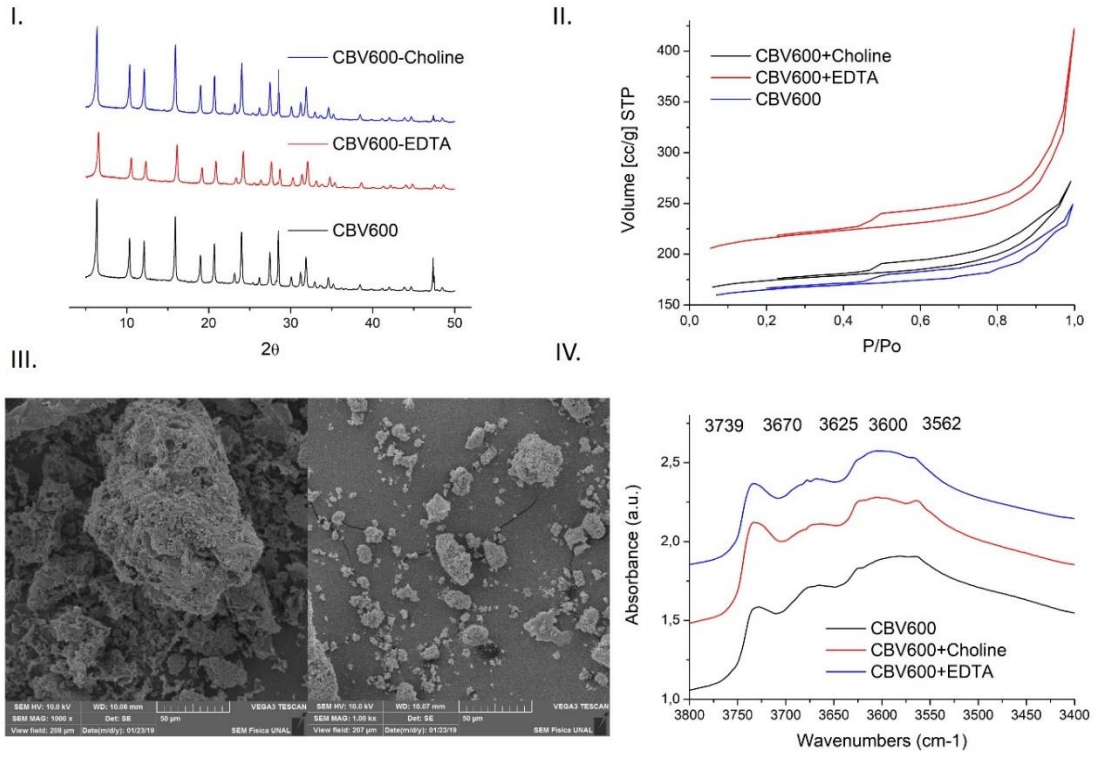

Figure 5-1 Characterization of USY zeolites after choline chloride treatment. I.) X-ray diffraction patterns of untreated and treated USY zeolites, II.) N_2 physisorption isotherms, III.) SEM images of residual solids after choline chloride treatment, IV) FTIR spectra of treated and untreated USY zeolites.

Table 5-2 N_2 physisorption analysis of treated and untreated USY zeolites.

Zeolites	**Volume$_{meso}$ (cm^3/g)**	**Volume$_{micro}$ (cm^3/g)**	**Area$_{meso}$ (m^2/g)**	**Area$_{micro}$ (m^2/g)**
CBV600	0.17	0.26	28.7	663.3
CBV600-Choline	0.30	0.28	42.6	1068.5
CBV600-EDTA	0.25	0.31	50.9	1119.3

SEM-EDX images of residual material removed from CBV600 by choline chloride treatment show that the residual is mainly amorphous material (Figure 5-1-III). Analysis EDX spectrum revealed that with each Si atom, three Al atoms are removed (Table 5-3). This suggests that despite a high removal yield of amorphous material, choline chloride is not selective to amorphous silicates. Choline chloride cannot directly interact with the alumina inside of USY zeolite to remove them [28]. But choline cations can interact with the silicate anions mixed with alumina generating complex octasilicates ($[OSiO_{1.5}]_8[Me_3NCH_2$-$CH_2OH]_8$) [28]. Thus, probably, when these amorphous silicas are formed, they trap amorphous aluminum oxides which are released from the interior of the network by mechanical agitation.

Table 5-3 Mass balance of choline chloride leaching of CBV600 USY zeolite

Initial weight of CBV600 (g)	1,7976
Final weight of CBV600 (g)	1,7638
Weight leached (g)	0,0255
Total weight recovered (g)	1,7893
% Error (g)*	0,464%
% Recovered leached (g)	1,417%

* % error referred to the missing mass with respect to the initial weight.

Figure 5-2-I shows that the Turn-Over Frequency (TOF) referred to as Pt increases with both treatment methods. TOF_{Pt} is also in agreement with the platinum dispersion values and their respected treatment methods. The platinum dispersion increases concerning untreated Pt/CBV600 catalyst. 11% increase corresponds to choline chloride treatment and 9% increase corresponds to Na_2H_2EDTA treatment, respectively. Enhanced Pt dispersion in treated catalysts is attributed to the removal of amorphous material. According to Zecevich et. al, when Pt is deposited as a precursor salt $[Pt(NH_3)_4]Cl_2$ is rather placed over the crystalline aluminum network than over the amorphous aluminum [31]. When CBV600 USY zeolite is washed, BAS clogged up by amorphous material became available adsorption sites for platinum during impregnation. This suggests that enhanced Pt dispersion is due to the higher availability of BAS in treated catalysts.

Catalysts with a high BAS content perform phenanthrene hydrogenation reactions more efficiently [32] [33]. These catalysts also promote cracking and hydrocracking reactions. The cracking and hydrocracking of hydrogenated species shift the hydrogenation/dehydrogenation reaction equilibrium towards phenanthrene hydrogenation

[34] [35]. The removal of amorphous material by two treatment methods should therefore promote phenanthrene conversion through BAS accessibility.

Figure 5-2 shows the graphical representation of phenanthrene distribution in the zeolite particles during hydrocracking regarding temperatures. At low temperatures, phenanthrene molecules barely diffuse through the zeolite crystal structure, due to accessibility limitations. Thus, phenanthrene reforming occurs mainly in the BAS located on the outer surface of the particle. At higher temperatures, phenanthrene molecules earn enough kinetic energy to pass throughout the crystals of zeolite. Then, BAS placed deep inside zeolite particles can participate in the phenanthrene reforming.

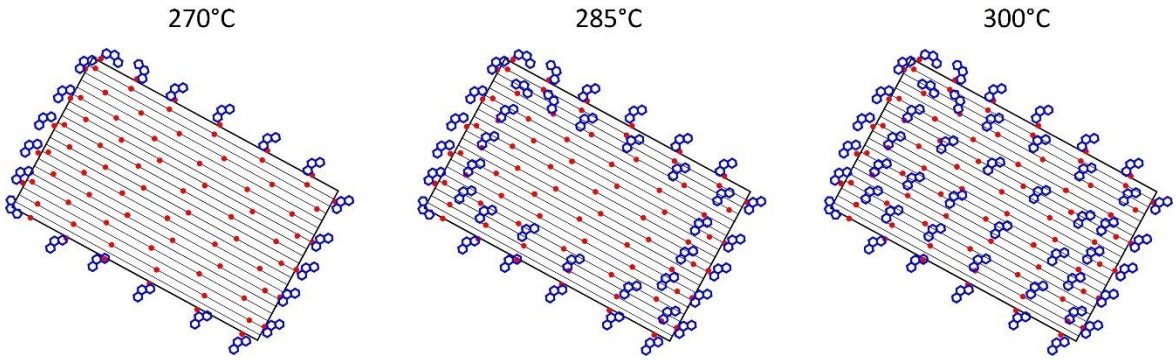

Figure 5-2 Graphical representation of phenanthrene distribution in the zeolite particles during hydrocracking with respect to temperatures.

At 270 °C, the TOF_{Pt} value for the Pt/CBV600-EDTA catalysts is similar to the TOF_{Pt} value of untreated CBV600 catalysts. This is probably because, at low temperatures, hydrogenated species molecules reform mainly in the BAS located on the outer surface of the zeolite (Figure 5-2). The TOF_{Pt} for the Pt/CBV600-EDTA catalyst exceeds the TOF_{Pt} of untreated CBV600 at 285 °C and 300 °C. At 285°C for 17% and at 300 °C 28%. With the rise of temperature, the mobility of phenanthrene molecules increases [36], improving the accessibility to the BAS deeper inside Pt/CBV600-EDTA catalysts. The temperature effect on the TOF_{Pt} value of untreated CBV600 catalyst is lower because BASs are blocked by amorphous material.

Pt/CBV600-Choline catalyst shows the highest TOF_{Pt} over the entire temperature range tested. This suggests a high amount of accessible BAS in Pt/CBV600-Choline catalysts. Therefore, the treatment with choline chloride removes more efficiently amorphous material

compared to Na_2H_2EDTA. This is also evident from the results given in Table 5-2.

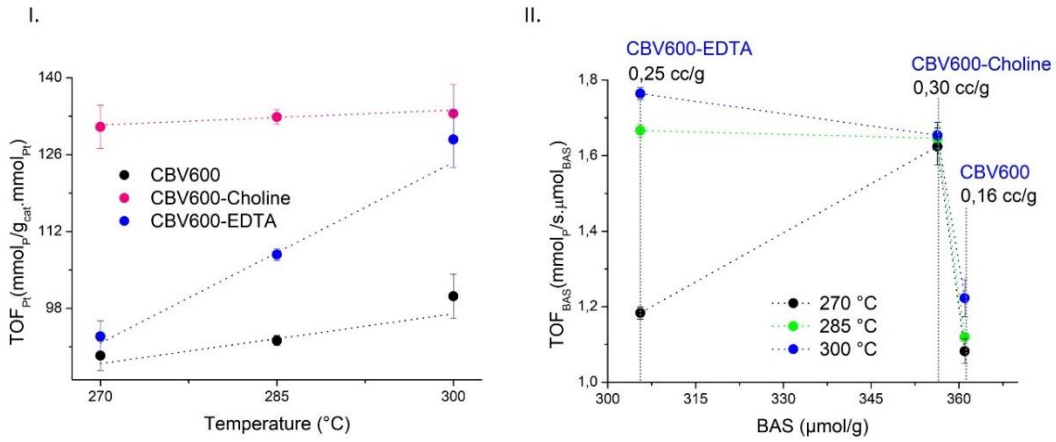

Figure 5-3 Turn Over Frequency (TOF) of different catalytic active sites. I. Platinum turn-over frequency (TOF_{Pt}), and II. BAS turn-over frequency (TOF_{BAS}), of CBV600 USY zeolite and treated zeolites.

Figure 5-3-II shows the BAS available (i.e., TOF_{BAS}) in the hydrocracking reaction as a function of BAS concentration and temperature. Untreated CBV600 catalyst has the lowest BAS participation despite the highest BAS content according to pyridine chemisorption measured by FTIR. The increase of temperature does not notably affect the amount of BAS participating in the hydrocracking reaction. This suggests that only the BAS located on the outer surface of the catalyst are participating in the hydrocracking reaction. Data in Table 5-2 and XRD patterns in figure 5-1-I confirm this hypothesis.

BAS activity of Pt/CBV600-EDTA catalyst strongly depends on temperature. It can be attributed to the incomplete removal of amorphous material by EDTA treatment. The remaining amorphous material inside the mesoporous channel limits phenanthrene transport through mesopores. However, with the increase of temperature, phenanthrene molecules can diffuse through those partially blocked mesopores. BAS activity in choline chloride treated catalyst does not seem to be affected by the temperature. Choline-treated catalysts thoroughly remove amorphous material present in the CBV600 zeolite, leaving free access to the BAS.

At 300°C TOF_{BAS} value for the Pt/CBV600-Choline catalyst does not surpass the TOF_{BAS} value for the Pt/CBV600-EDTA catalysts. A high concentration of SBAS species in the Pt/CBV600-EDTA catalysts enhances hydrocracking reaction. SBAS catalytic activity is

attributed to synergy between BAS and small clusters of amorphous aluminum [19]. Pt/CBV600-Choline catalysts have the lowest SBAS content, probably due to thorough removal of amorphous aluminum [37]. However, this is only valid at higher temperatures because Pt/CBV600-EDTA catalysts do not present enhanced activity at low temperatures. That suggests SBAS requires high temperatures for activation.

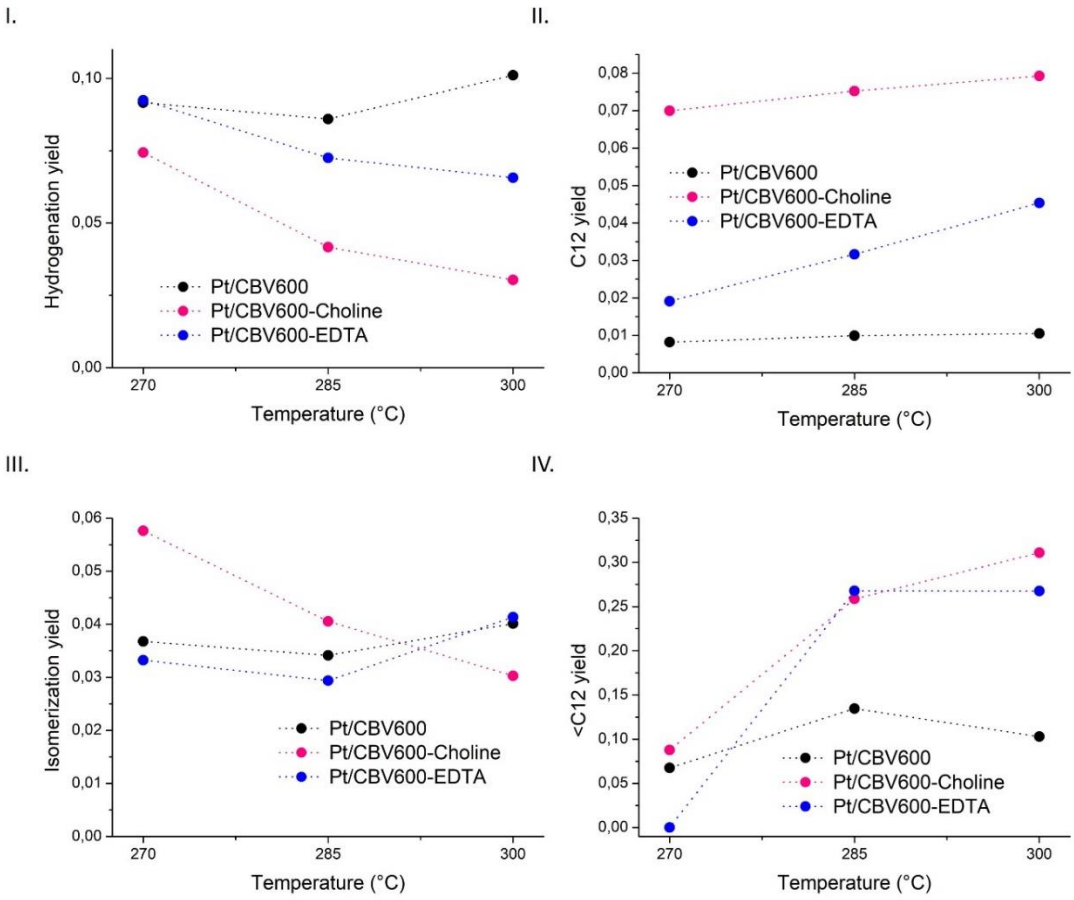

Figure 5-4 Product yields of phenanthrene hydrocracking over treated and untreated Pt/CBV600 catalysts. I.) Saturated C14, II.) C12 products, III.) isomerization products, and IV.) <C12 products.

Differences in the structural and chemical properties of tested catalysts affect the selectivity of the hydrocracking reaction. The products detected were classified into four groups: (i) phenanthrene hydrogenation products (C14hydro), (ii) ring-opening reaction products (C12), (iii) isomerized products (i-C14), and (iv) light products with less than 12 carbons (<C12). Identified phenanthrene hydrogenation products were tetrahydro phenanthrene (THP), octahydro phenanthrene (OHP), perhydro phenanthrene (PHP), and the respective isomers. In the C12 group, bicyclohexyl, bicyclohexyl phenyl, and biphenyl were identified.

Figures 5-4 -II and 5-4-IV show that both treatments result in an increase of C12 and <C12 yields compared to untreated CBV600 zeolite. Better hydrocracking activity is attributed to improved BAS accessibility after the removal of amorphous material. Low C14hydro yield in the Pt/CBV600-Choline catalyst is due to its high concentration of accessible BAS. BAS favor cracking or hydrocracking of hydrogenated products.

In summary, the choline chloride treatment improved BAS accessibility in the CBV600 USY zeolite by the removal of amorphous material. Choline Chloride treatment is not selective to silicon-amorphous material only. Choline chloride also removes the amorphous aluminum more efficiently than Na_2H_2EDTA. The above implies improved phenanthrene diffusion through the zeolite. The activity for phenanthrene hydrocracking reaction is improved but this could lead to the excessive formation of lighter products.

5.4 Conclusions

The effect of Brønsted Acid Sites (BAS) accessibility in the USY zeolite crystals on the phenanthrene hydrocracking reaction was investigated. Three bifunctional USY zeolite catalysts with different access to their BAS were tested. BAS accessibility was improved by treatment with choline chloride and Na_2H_2EDTA used to remove amorphous material inside USY zeolite. Choline chloride was selected due to its capacity to selectively remove amorphous silicon oxides. However, SEM-EDX analysis disproved this hypothesis. Choline chloride removed all amorphous oxides species, including aluminum oxides occluded inside zeolite crystals while preserving its crystalline structure. Both choline chloride and Na_2H_2EDTA treatments increased the microporous surface area of the USY zeolite with respect to their untreated analogs. Increased the microporous surface area together with the BAS accessibility enhanced catalytic phenanthrene hydrocracking. Accessibility of BAS promotes the cracking activity of previously hydrogenated species. This shifts the thermodynamic equilibrium of the phenanthrene hydrogenation reaction towards the right. The downside of accessible BAS and related hydrocracking reaction rate is the production of light hydrocarbons.

5.5 References

[1] British Petroleum Company, «Statistical Review of World Energy 2020,» 69, 2020.

[2] R. Sahu, B. Jin Song, J. S. Im, Y.-P. Jeon y C. W. Lee, «A review of recent advances in catalytic hydrocracking of heavy residues,» *Journal of Industrial and Engineering Chemistry,* 2015.

[3] A. Stanislaus y H. B. Cooper, «Aromatic Hydrogenation Catalysis: A Review,» *CATAL. REV.-SCI. ENG,* pp. 75-123, 1994..

[4] T. Tang, C. Yin, L. Wang, Y. Ji y F.-S. Xiao, «Superior performance in deep saturation of bulky aromatic pyrene over acidic mesoporous Beta zeolite-supported palladium catalyst,» *Journal of Catalysis,* vol. 249, p. 111–115, 2007.

[5] X. Meng, W. Yuxiu y Y. Li, «Tailoring the pore size of zeolite Y as the support of diesel aromatic saturation catalyst,» *J Porous Mater,,* vol. 13, p. 365–371, 2006.

[6] V. Calemma, M. Ferrari, S. Rabl y J. Weitkamp, «Selective ring opening of naphthenes: From mechanistic studies with a model feed to the upgrading of a hydrotreated light cycle oil,» *Fuel,* 2013.

[7] Q. Wang, Z.-G. Hou, B. Zhang, J. Liu, W.-Y. Song, D.-S. Xue, L.-Z. Liu, D. Wang y X.-G. Chen, «Preparation of a highly efficient Pt/USY catalyst for hydrogenation and selective ring-opening reaction of tetralin,» *Petroleum Science,* vol. 15, nº 2, pp. 605-612, 2018.

[8] M. A. Vicerich, V. M. Benitez, M. A. Sánchez y C. L. Pieck, «Influence of Support Material on the Activity and Selectivity of Pt–Ir Catalysts for Ring Opening Reactions,» *Catal Lett,* 2014.

[9] M. A. Arribas, P. Concepción y A. Martínez, «The role of metal sites during the coupled hydrogenation and ring opening of tetralin on bifunctional Pt(Ir)/USY catalysts,» *Applied Catalysis A: General,* vol. 267, p. 111–119, 2004.

[10] A. Martínez, M. A. Arribas y S. B. C. Pergher, «Bifunctional noble metal/zeolite catalysts for upgrading low quality diesel fractions via selective opening of naphthenic rings,» *Catalysis Science & Technology,* 2016.

[11] W. Vermeiren y J.-P. Gilson, «Impact of Zeolites on the Petroleum and Petrochemical Industry,» *Top Catal,* vol. 52, p. 1131–1161, 2009.

[12] D. Verboekend, N. Nuttens, R. Locus, V. J. Aelst, P. Verolme, J. C. Groen, J. Perez-Ramirez y B. F. Sels, «Synthesis, Characterization, and catalytic evaluation of

hierarchical faujasite zeolites: milestones, challenges and future directions,» *Chem. Soc. Rev.,* vol. 45, pp. 3331-3352, 2016.

[13] S. Mitchel, A. B. Pinar, J. Kenvin, K. J. Crivelli Paolo y J. Pérez Ramírez, «Structural analysis of hierarchically organized,» *Nature Communications,* nº 8633, 2014.

[14] D. Verboekend, G. Vilé y J. Pérez-Ramírez, «Hierarchical Y and USY Zeolites Designed by Post-Synthetic Strategies,» *Advanced Functional Materials,* vol. 22, nº 5, p. 916–928, 2011.

[15] W. Schwieger, A. G. Machoke, T. Weissenberger, A. Inayat, T. Selvam, M. Klumpp y A. Inayat, «Hierarchy concepts: classification and preparation strategies for zeolite containing materials with hierarchical porosity,» *Chem Soc Rev,* vol. 45, p. 3353, 2016.

[16] S. M. T. Almutairi, B. Mezari, G. A. Filonenko, P. Magusin, M. Rigutto S., E. A. Pidko y E. J. M. Hensen, «Influence of Extraframework Aluminum on the Brønsted Acidity and Catalytic Reactivity of Faujasite Zeolite,» *ChemCatChem,* vol. 5, nº 2.

[17] J. L. Agudelo, E. J. M. Hensen, S. A. Giraldo y L. J. Hoyos, «Influence of Steam-Calcination and Acid Leaching treatment on the VGO Hydrocracking Performance of Faujasite Zeolite,» *Fuel Processing Technology,* nº 133, pp. 89-96, 2015.

[18] C. S. Triantafillidis, A. G. Vlessidis y N. P. Evmiridis, «Dealuminated H-Y Zeolites: Influence of the Degree and the Type of Dealumination Method on the Structural and Acidic Characteristics of H-Y Zeolites,» *Ind. Eng. Chem. Res,* vol. 20, nº 20, pp. 307-319, 2000.

[19] R. A. Beyerlein, C. Choi-Feng, J. B. Hall, B. J. Huggins y G. J. Ray, «Effect of Steaming on the Defect Structure and Acid Catalysis of Protonated Zeolites.,» *Topics in Catalysis,* vol. 1, nº 4, pp. 227-42, 1997.

[20] B. A. Williams, S. M. Babitz, J. T. Miller, R. Q. Snurr y H. H. Kung, «The roles of acid strength and pore diffusion in the enhanced cracking activity of steamed Y zeolites,» *Applied Catalysis A: General,* vol. 177, p. 161–175, 1999.

[21] K. De Jong, J. Zecevic, H. Friedrich, P. E. De Jongh, M. Bulut, S. v. Donk, K. Régine, A. Finiels, V. Hulea y F. Fajula, «Zeolite Y crystals with trimodal porosity as ideal hydrocracking catalyst,» *Angew. Chem. Int,* nº 49, pp. 10074-10078, 2010.

[22] X.-w. Chang, L.-F. He, H.-n. Liang, X.-m. Liu y Z.-f. Yan, «Screening of optimum condition for combined modification of ultra-stable Y zeolites using multi-hydroxyl carboxylic acid and phosphate,» *Catalysis Today,* vol. 158, p. 198–204, 2010.

[23] A. Abramova, E. Slivinskii, Y. Goldfarb, A. Panin, E. Kulikova y G. Kliger, «Development of efficient zeolite-containing catalysts for petroleum refining and petrochemistry,» *Kinetics and Catalysis,* vol. 46, p. 758–769, 2005.

[24] D. Verboekend, G. Vilé y J. Pérez-Ramírez, «Mesopore Formation in USY and Beta Zeolites by Base Leaching: Selection Criteria and Optimization of Pore-Directing Agents,» *Cryst. Growth Des,* vol. 12, p. 3123−3132, 2012.

[25] J. L. Agudelo, B. Mezari, E. Hensen, S. A. Giraldo y L. J. Hoyos, «On the effect of EDTA treatment on the acidic properties of USY zeolite and its performance in vaccum gas oil hydrocracking,» *Applied Catalysis A: General,* nº 488, pp. 219-230, 2014.

[26] J. L. Agudelo, E. J. M. Hensen, S. A. Giraldo y L. J. Hoyos, «Effect of USY Zeolite Chemical Treatment with Ammonium Nitrate on Its VGO Hydrocracking Performance,» *Energy & Fuels,* vol. 30, nº 1, p. 616–625, 2015.

[27] J. Shi, Q. Yao, X. Li, G. Zhou y S. Fu, «Formation of Asymmetrical Structured Silica Controlled by a Phase Separation Process and Implication for Biosilicification,» *PLoS One,* vol. 8, nº 4, pp. 1-9, 2013.

[28] M. Z. Asunción, I. Hasegawa, J. W. Kampfa y R. M. Laine, «The selective dissolution of rice hull ash to form [OSiO1.5]8[R4N]8 (R 5 Me, CH2CH2OH) octasilicates. Basic nanobuilding blocks and possible models of intermediates formed during biosilicification processes,» *J. Matter. Chem,* vol. 15, pp. 2114-2121, 2005.

[29] A. P. Abbott, G. Capper, D. L. Davies, R. K. Rasheed y P. Shikotra, «Selective Extraction of Metals from Mixed Oxide Matrixes Using Choline-Based Ionic Liquids,» *Inorganic Chemistry,* vol. 44, nº 19, p. 6497–6499, 2005.

[30] J. A. Aragon Q, «*Extracción selectiva de material amorfo de zeolitas USY,* » Bogotá: Laboratorio de Catálisis Heterogénea (LCH), Universidad Nacional - Master Thesis, 2019.

[31] J. Zecevic, G. Vanbutsele, K. P. De Jong y J. A. Martens, «Nanoscale intimacy in bifunctional catalysts for selective conversion of hydrocarbons,» *Nature,* vol. 528, nº 7581, p. 245–254, 2015.

[32] F. Roessner y U. Roland, «Hydrogen spillover in bifunctional catalysis,» *J. Mol. Catal. A Chem,* vol. 112, nº 3, p. 401–412, 1996.

[33] U. Roland, T. Braunschweig y F. Roessner, «On the Nature of Split-over Hydrogen,» *J. Mol.Catal.,* vol. 127, pp. 61-84, 1997.

[34] E. Benazzi, L. Leite, N. Marchal-George, H. Toulhoat y P. Raybaud, «New insights into parameters controlling the selectivity in hydrocracking reactions,» *Journal of catalysis,* vol. 217, pp. 376-387, 2003.

[35] L. Leite, E. Benazzi, N. Marchal-George y H. Toulhoat, «Hydrocracking of Phenanthrene over Pt/SiO2-Al2O3, Pt/H-Y, Pt/H-B and Pt/H-ZSM5 Catalysts: Reaction Pathway and Products Distribution,» *Studies in Surface Science and Catalysis,* nº 130, 2495-2500.

[36] S. Al-Khattaf, J. A. Atias, K. Jarosch y H. De Lasa, «Diffusion and catalytic cracking of 1,3,5 tri-iso-propyl-benzene in FCC catalysts,» *Chem. Eng. Sci,* vol. 57, nº 22-23, pp. 4909-4920, 2002.

[37] L. Pine, P. Maher y W. Wacher, «Prediction of cracking catalyst behavior by a zeolite unit cell size model,» *Journal of Catalysis,* vol. 85, pp. 466-476, 1984.

6. Discussion

Hydrocracking is a complex reaction, which efficiency and selectivity are highly dependent on the catalyst properties [1] [2] [3]. When molecular size of hydrocarbon is superior to the micropore diameter of zeolite, most of the BAS inside the USY zeolites remain unavailable for reaction. Heavy hydrocarbons can pass through the zeolite microporous by increasing the reaction temperature, even if the molecular size is larger than the pore size. Hydrocarbon molecules improve mobility with the temperature increment [4][5]. Thus, the BAS inside the zeolite became accessible for hydrocarbon molecules, and BAS participation in catalytic hydrocracking intensifies.

Steaming of USY zeolites produce EFAl species inside the crystalline structure. EFAl material occluded into zeolite-framework obstruct the access of hydrocarbons molecules to the BAS. However, EFAl species do not have solely negative effect on hydrocracking [6] [7]. Firstly, EFAl species contain Lewis's acid sites (LAS) able to perform cracking reaction [8]. Chapters 3 and 4 show that cracking activity of hydrogenated species over γ-Al_2O_3 based catalysts is low compared to USY zeolites. Despite that, EFAl contributes to the yield to cracking reactions, and its contribution is not easy to differentiate from the USY zeolites. Besides, EFAl species close to BAS could be responsible for the additional acid strength of the zeolite [6]. Chapter 5 demonstrates that EFAl removal from the zeolites also resulted in a loss of SBAS, while BAS remained conserved well. It means that the absence of the EFAl species could be detrimental to the reaction. In Chapter 2, the direct correlation between SBAS and hydrocracking catalytic activity was measured by a calorimetric technique, supporting the aforementioned. Hydrogen spillover is more likely to occur on EFAl species than in the BAS of the zeolite [9]. This means increased hydrogenation rate in the presence of EFAl species [9]. These positive effects of the EFAl could mask the catalytic activity of BAS, causing misinterpretation of catalytic activity of catalysts based on dealuminated Y zeolites.

The variety of cracking acid sites (i.e., BAS, SBAS, LAS) requires consideration of several mechanisms of reaction to accurately interpret the role of the catalyst. Hydrogen spillover over mechanism can be monitored by FTIR spectrometry by the adsorption of deuterium atoms. This mechanism can be normally observed during hydrocracking reaction over USY zeolites [10] [11]. Although, theoretical calculations suggest that hydrogen spillover over non-reducible Y zeolite is unlikely, this process can be activated with the increasing of temperature. According to hydrogen spillover mechanism, hydrogen molecules are split on the platinum clusters and scattered over the USY surface as hydrogen atoms [12]. Dispersion of split-hydrogen atoms over the USY surface depends on the ability of BAS and LAS to stabilize the monoatomic hydrogen and the reaction temperature [9].

Many authors consider that hydrogen spillover is not thermodynamic feasible over non-reducible metal oxides such as zeolites or alumina [13]. However, Karim et. al. demonstrates that hydrogen spillover occurs over alumina at 70 °C achieving a coverage radius of 15 nm [9]. 15 nm seems a very short distance, but it is enough to cover many aluminum atoms. Since hydrogen spillover is activated by the high temperatures of hydrocracking, it should occur on zeolites, but probably reaching shorter coverage distance than in alumina. Even if the hydrogen spillover coverage distance is only 2 nm (the size of the unit cell of a Y zeolite), it should cover the aluminum per unit cell. Figure 6-1 shows an example of coverage distance using a TEM imaging of an impregnated Pt/CBV600 USY catalysts.

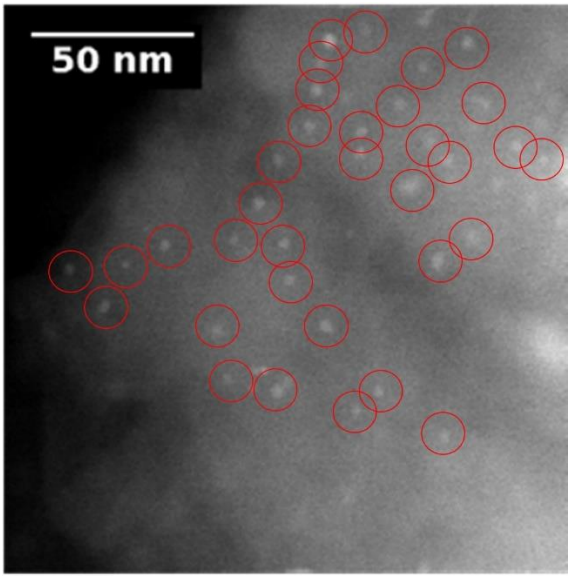

Figure 6-1 Hydrogen spillover over Pt/CVB600 USY zeolite. Red circles represent the areas covered by split hydrogen atoms if the coverage diameter is 2 nm. This TEM image is taken from chapter 2.

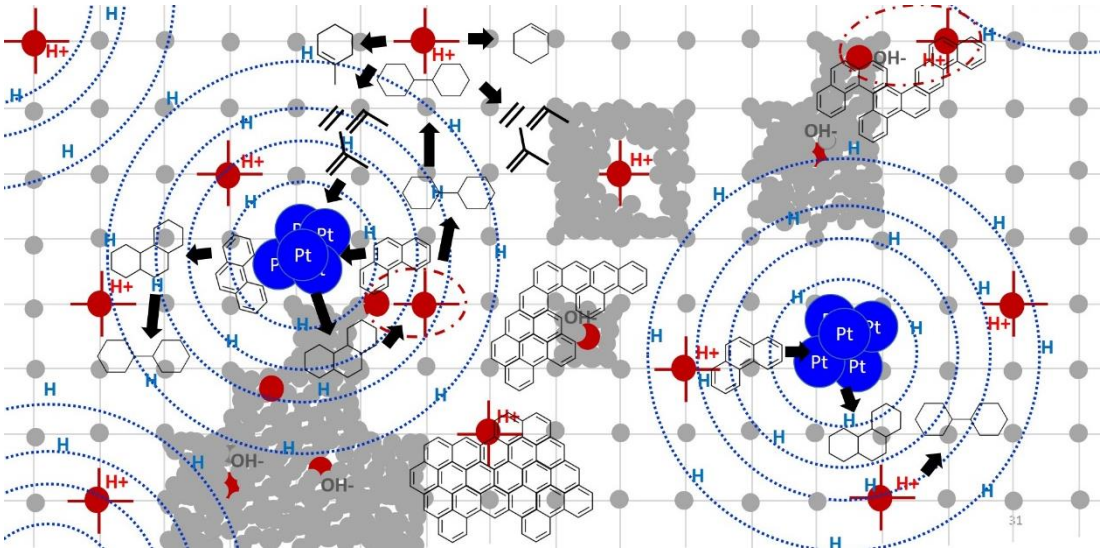

Figure 6-2 Graphical representation of different catalytic active sites and their role on the hydrocracking reaction.

Chapter 4 proposes that phenanthrene hydrocracking can occur via hydrogen spillover and classical mechanism simultaneously over a bifunctional platinum catalyst based on USY zeolites. Split hydrogen atoms on platinum clusters do not reach all aluminum atoms in the USY zeolite as represented in Figure 6-2. Dotted blue circles around platinum atoms only reach a portion of BAS (red dots). BAS together with the hydrogen atoms perform cracking and simultaneous hydrogenation of unsaturated carbon chains. In other words,

hydrocracking reactions. As is shown in Chapter 2, BAS do not catalyze hydrogenation of aromatics rings. Complete hydrogenation of unsaturated rings of fluorene occurs before hydrocracking reactions occur. In the situation where split-hydrogen does not reach BAS catalytic cracking or hydrocracking conducts via classical mechanism. This could explain the differences in selectivity between zeolites with different Si/Al ratios. Lack of BAS in zeolite means large distance between BAS and platinum clusters. Most of the BAS in zeolites with lack of BAS will perform catalytic cracking to overproduction of light hydrocarbons. In contrary, in zeolite with a relatively high BAS quantity, the probability of BAS closeness to the platinum clusters is higher. These BAS act as hydrocracking sites able to hydrogenate unsaturated carbon chains immediately after being cracked. Closeness of BAS and platinum leads to the production of desired middle distillates. The above agrees with the intimacy criterion of metal/acid sites, predicting that intimate proximity between acid and metal sites avoid over-cracking [14].

In Chapter 5, a way to obtain USY zeolites with high accessible BAS concentration was shown using choline chloride treatment. The activity of the resultant catalysts to phenanthrene hydrocracking presented high yields to light products. That pointed to most of the accessible BAS are not achieved for split-hydrogen. Therefore, for catalysts with a high amount of accessible BAS, it is needed to improve the metal deposition method to place clusters inside the zeolite, to improve BAS covered for the split-hydrogen. Furthermore, in this chapter, an EDTA treatment that partially removes the EFAl species demonstrates that it could present positive effects in activity and selectivity for phenanthrene hydrocracking. Interactions between EFAl species near to BAS could form SBAS. Catalysts with a high concentration of SBAS species hold elevated hydrocracking activity, without over cracking of products. Thus, catalyst with a high amount of accessible BAS is not always positive if SBAS are eliminated.

The selection of a suitable hydrocracking catalysts with enhanced catalytic activity and middle distillate selectivity should seek for the optimal concentration and ratio of the different centers of conversion (i.e., metal, LAS, BAS, and SBAS); Catalyst's accessibility is intimately related to its structural properties. That could require a techno-economical investment for the refinery to evaluate optimal alternatives.

6.1 References

[1] J. Weitkamp, «Catalytic Hydrocracking—Mechanisms and Versatility of the Process,» *ChemCatChem,* vol. 4, p. 292 – 306, 2012.

[2] J. L. Agudelo Valderrama, *Effect of modification on USY zeolite properties and its hydrocracking performance,* Bucaramanga: Universidad Industrial de Santander, 2015.

[3] J. L. Agudelo, B. Mezari, E. Hensen, S. A. Giraldo y L. J. Hoyos, «On the effect of EDTA treatment on the acidic properties of USY zeolite and its performance in vaccum gas oil hydrocracking,» *Applied Catalysis A: General,* nº 488, pp. 219-230, 2014.

[4] H. RAMANANS y M. AUERBACH, «MODELING JUMP DIFFUSION IN ZEOLITES: I. PRINCIPLES AND METHODS,» *Fluid Transport in Nanoporous Materials,* vol. 219, pp. 93-125, 2006.

[5] S. Al-Khattaf, J. A. Atias, K. Jarosch y H. De Lasa, «Diffusion and catalytic cracking of 1,3,5 tri-iso-propyl-benzene in FCC catalysts,» *Chem. Eng. Sci,* vol. 57, nº 22-23, pp. 4909-4920, 2002.

[6] R. A. Beyerlein, C. Choi-Feng, J. B. Hall, B. J. Huggins y G. J. Ray, «Effect of Steaming on the Defect Structure and Acid Catalysis of Protonated Zeolites.,» *Topics in Catalysis,* vol. 1, nº 4, pp. 227-42, 1997.

[7] L. Pine, P. Maher y W. Wacher, «Prediction of cracking catalyst behavior by a zeolite unit cell size model,» *Journal of Catalysis,* vol. 85, pp. 466-476, 1984.

[8] Corma, A., Grande, M. S., Gonzalez-Alfaro, V., & Orchilles, A. V. «Cracking Activity and Hydrothermal Stability of MCM-41 and Its Comparison with Amorphous Silica-Alumina and a USY Zeolite, » Journal of Catalysis, 159(2), (1996)

[9] W. Karim, «Catalyst support effects on hydrogen spillover,» *Nature,* vol. 541, nº 7635, p. 68–71, 2017.

[10] R. Ueda, T. Kusakari, K. Tomishige y K. Fujimoto, «Nature of Spilt over Hydrogen on Acid Sites in Zeolites: Observation of the Behavior of Adsorbed Pyridine on Zeolite Catalysts by Means of FTIR,» *Journal of Catalysis,* vol. 194, p. 14–22, 2000.

[11] P. Baeza, M. Villarroel, P. Ávila, A. López Agudo, B. Delmon y F. J. Gil-Llambías, «Spillover hydrogen mobility during Co-Mo catalyzed HDS in industrial-like conditions,» *Appl. Catal. A Gen.,* vol. 304, nº 1-2, p. 109–115, 2006.

[12] H. Shin, M. Choi y H. Kim, «A mechanistic model for hydrogen activation, spillover, and its chemical reaction in a zeolite-encapsulated Pt catalyst,» *Phys. Chem. Chem. Phys,* vol. 18, p. 7035–7041, 2016.

[13] R. Prins, «Hydrogen spillover. Facts and fiction,» *Chem. Rev.,* vol. 112, nº 5, p. 2714–2738, 2012.

[14] J. Zecevic, G. Vanbutsele, K. P. De Jong y J. A. Martens, «Nanoscale intimacy in bifunctional catalysts for selective conversion of hydrocarbons,» *Nature,* vol. 528, nº 7581, p. 245–254, 2015.

7. General Conclusions

This thesis studied the relationship between the properties of USY zeolites and relatively heavy hydrocarbons during catalytic hydrocracking process. The research question is the effect of USY zeolites accessibility for heavy hydrocarbons in the hydrocracking reaction. The structural and chemical properties of USY zeolites employed in this work were characterized using various analytical techniques. This characterization helps to support the observations regarding the effect of hydrocarbons accessibility into USY zeolites on the hydrocracking performance. Two systematic hydrocracking tests were developed and performed using USY zeolites with different Si/Al ratios and distinct structural properties. The first test aims to understand the role of acid sites in hydrocracking reaction. The second test studies the effect of structural properties of USY zeolites considering phenanthrene accessibility to the Brønsted Acid Site (BAS) inside USY zeolites.

The first test utilized an HP-STA to record the enthalpy of non-isothermal fluorene hydrocracking. DSC and TG signals show qualitative aspects of the fluorene hydrocracking pathways over bifunctional catalysts based on USY zeolites. The hydrocracking enthalpy over acidic USY catalysts and non-acidic catalysts demonstrated the important role of BAS to perform hydrocracking reaction. Catalysts based on USY zeolites decrease the hydrogenation temperature. Results suggest a catalytic role of BAS on a hydrogenation reaction although this requires more research. This test compares catalytic activity of regular BAS and strong BAS. Positive effect on hydrocracking enthalpy is observed in both cases but the effect was greater with strong BAS. In other words, catalysts with a high concentration of strong BAS presented the higher fluorene hydrocracking enthalpy.

The second test consisted of the phenanthrene hydrocracking over USY based catalysts at different temperatures utilizing a Trickle Bed Reactor (TBR). The relationship between phenanthrene conversion rate and the BAS concentration allow calculation of the Turn-

Over Frequency (TOF) of BAS. USY zeolites with high mesoporous volume reported better TOF of BAS than those with low mesoporous volume. This indicates that mesoporous contributes positively to the zeolite accessibility for phenanthrene molecules. The effect of zeolite accessibility in phenanthrene hydrocracking was confirmed by employing a USY zeolite with partial remotion of Extra-Framework Aluminum (EFAl). EFAl removal from USY zeolites increased the mesoporous volume of the USY zeolite and enhanced the TOF of BAS. This result indicates the positive effect of zeolite accessibility in the hydrocracking reaction.

The analysis of products detected by Mass spectrometry allows concluding that hydrocracking reaction occurs by two hydrocracking mechanisms: the classic mechanism and hydrogen spillover mechanism. USY zeolites with a low BAS concentration presented higher selectivity towards gas products compared to those with high BAS concentration. This is probably due to the fact that closeness of platinum clusters and BAS decrease in zeolites with low BAS concentration. BAS far from platinum clusters are not able to perform hydrocracking reactions by hydrogen spillover. Therefore, this BAS will perform classical cracking reactions which overproduce gas.

By analyzing the USY properties this thesis shows how the catalysts accessibility for heavy hydrocarbons (i.e., fluorene and phenanthrene) affects the hydrocracking yield and selectivity.